1-1-2002

Growth Increment Analysis of Marine Bivalves from the North

Stephen D. Houk

GROWTH INCREMENT ANALYSIS OF MARINE BIVALVES FROM THE NORTH COAST OF PERU

By

Stephen D. Houk, Jr.

B.A. Colorado State University, 1998

A THESIS

Submitted in Partial Fulfillment of the

Requirements for the Degree of

Master of Science

(in Quaternary and Climate Studies)

The Graduate School

The University of Maine

December, 2002

Advisory Committee:

Kirk Maasch, Associate Professor of Geological Sciences and Quaternary and Climate Studies, Co-Chair
Daniel H. Sandweiss, Associate Professor of Anthropology and Quaternary and Climate Studies, Co-Chair
Fei Chai, Associate Professor of Marine Sciences and Quaternary and Climate Studies
Harold B. Rollins, Professor Emeritus of Geology and Planetary Science, University of Pittsburgh

GROWTH INCREMENT ANALYSIS OF MARINE BIVALVES FROM THE NORTH COAST OF PERU

By Stephen Douglass Houk, Jr.

Thesis Co-Advisors: Dr. Kirk Maasch and Dr. Daniel H. Sandweiss

An Abstract of the Thesis Presented
in Partial Fulfillment of the Requirements for the
Degree of Master of Science
(in Quaternary and Climate Studies)
December, 2002

This study aids in developing a sea surface temperature (SST) proxy with monthly temporal resolution using a combination of growth increment and stable isotope analyses of marine bivalves from the north coast of Peru. Faunal assemblages from the Siches and Ostra Base Camp archaeological sites contain shells of warm-tropical mollusks that currently live farther north in Ecuador. The presence of warm-tropical species in these sites and others as far south as 10°S latitude and dating prior to 5730 cal yr B.P. indicates a stable warm-water regime in the eastern tropical Pacific which subsequently changes to a modern temperate-water regime after 5730 cal yr B.P. The presence of a warm-water regime may preclude the modern Walker Circulation and ENSO-scale (El Niño and Southern Oscillation) climate variability in the region. A high-temporal-resolution SST proxy can quantify interseasonal and interannual variability along the littoral of northern Peru in order to assess environmental conditions prior to 5730 cal yr B.P.

The intertidal species *Chione subrugosa* and *Protothaca ecuatoriana* exhibit daily growth periods, while the subtidal species *Trachycardium procerum* and the mangrove swamp species *A. tuberculosa* exhibit subdaily growth periods. Incremental growth in these species enabled a time correlation of stable oxygen isotope samples drilled from the shells. Modern specimens of *A. tuberculosa*, *C. subrugosa*, and *T. procerum* provided discrete time series (two to four years in duration) of stable oxygen isotope ratios that were correlated with recorded ocean temperature and salinity. Middle Holocene (7420 cal yr B.P. to 5650 cal yr B.P.) specimens of *A. tuberculosa*, *C. subrugosa*, *P. ecuatoriana*, and *T. procerum* recovered from shell middens at the Siches (4.5°S) and Ostra Base Camp (9°S) sites provided oxygen isotope ratio time series two to four years in duration. The oxygen isotope ratio time series constructed from the ancient shells float within the date range provided by radiocarbon-dated contexts from which the shells were excavated.

Results suggest that subtidal species, which lie beyond the influence of freshwater influx accurately record ambient water conditions. Furthermore, ancient specimens of *T. procerum* from the Ostra Base Camp (6660-6640 cal yr B.P.) have oxygen isotope ratios that differ from those of modern *T. procerum*. Some *C. subrugosa*, *A. tuberculosa*, and *P. ecuatoriana* from the Siches and Early Honda components (7420 cal yr B.P. to 5650 cal yr B.P.) of the Siches site indicate multiple freshening events (e.g. increased precipitation or river discharge) per annual cycle. These events imply a climate regime wetter than the modern climate regime at 4.5°S, which may result from a warmer mean SST.

TABLE OF CONTENTS

ACKNOWLEDGEMENTS.....ii

LIST OF TABLES.....vii

LIST OF FIGURES.....viii

Chapter

1. INTRODUCTION.....1

    1.1. Purpose of This Study.....1

    1.2. Thermally Anomalous Molluscan Assemblages as Evidence of Mid-Holocene Climate Change.....2

    1.3. ENSO and Ocean-Atmosphere Adjustments.....7

    1.4. The ENSO Record.....9

    1.5. Archaeomalacology and the ENSO Record.....14

2. THE SICHES MOLLUSCAN ASSEMBLAGE.....18

    2.1. Siches Site PV 7-19.....18

    2.2. Mangrove Swamp Habitat.....19

    2.3. Ecology of Molluscan Species.....20

        2.3.1. *Anadara tuberculosa*.....20

        2.3.2. *Chione subrugosa*.....23

        2.3.3. *Protothaca ecuatoriana*.....23

        2.3.4. *Trachycardium procerum*.....23

3. METHODS.....26

    3.1. Stable Isotopes in Archaeology.....26

3.2. Theory of Growth Line Formation....28

3.3. Growth Line Analysis....31

3.4. Method of Growth Increment Analysis in this Study....32

3.5. Correlation of Oxygen Isotope Data with Ocean Temperature and Salinity....35

3.6. Paleotemperature Determination....40

3.7. A Temperature Equation for *T. procerum*....42

4. RESULTS....45

4.1. Growth Increment and Stable Isotope Analyses of Modern *T. procerum*....45

4.1.1. *T. procerum* 3TP1-1b....45

4.1.2. *T. procerum* TP 1-12....47

4.2. Growth Increment and Stable Isotope Analyses of Modern *C. subrugosa*....54

4.2.1. *Chione subrugosa* PT1-14....56

4.2.2. *Chione subrugosa* 2PT1....59

4.3. Growth Increment and Stable Isotope Analyses of Modern *A. tuberculosa*....62

4.4. Growth Increment and Elemental Mole Ratio Analyses of Modern Shells....65

4.4.1. Elemental Mole Ratios in *T. procerum* TP 1-12....68

4.4.2. Elemental Mole Ratios in *C. subrugosa* 2PT1....74

4.5. Growth Increment and Stable Isotope Analyses of *C. subrugosa* from the Siches TAMA....86

4.5.1. *C. subrugosa* PV 7-19 IIB3(a) and PV 7-19 IIB3(b) (7420-7340 cal yr B.P.)....86

4.5.2. *C. subrugosa* PV 7-19 IB7 (55870-5750 cal yr B.P.) and *C. subrugosa* PV 7-19 IB4bi (5870-5750 to 5650 cal yr B.P.).....93

4.6. Growth Increment and Stable Isotope Analyses of *A. tuberculosa* from the Siches TAMA.....93

4.7. Growth Increment and Stable Isotope Analyses of *P. ecuatoriana* from the Siches TAMA.....93

4.7.1. *P. ecuatoriana* PV 7-19 IIB4(a) and PV 7-19 IIB4(b) (7470 cal yr B.P.).....98

4.7.2. *P. ecuatoriana* PV 7-19 IB7 (5870-5750 cal yr B.P.) and *P. ecuatoriana* PV 7-19 IB4bi and IB6b (5870-5750 to 5650 cal yr B.P.).....98

4.8. Growth Increment and Stable Isotope Analyses of *T. procerum* from the Ostra Base Camp.....104

4.8.1. Elemental Mole Ratios in *T. procerum* OBC V-1-C 2i-2ib, Elemento 2.....106

4.9. Estimated Temperatures for Middle Holocene *T. procerum* Analyzed by Perrier et al. (1994).....106

5. DISCUSSION.....109

5.1. Intertidal and Mangrove Swamp Bivalves as Sea Surface Temperature Proxies.....109

5.2. Subtidal Bivalves as Ocean Temperature Proxies.....112

5.3. Paleoenvironmental Conditions at the Siches Site PV 7-19.....113

5.3.1. From 7420 cal yr B.P. to 6890-6810 cal yr B.P.....113

5.3.2. 5880-5750 cal yr B.P.....115

5.3.3. From 5880-5750 cal yr B.P. to 5650 cal yr B.P.....116

5.4. Paleoenvironmental Conditions at Ostra Base Camp (6660 cal yr B.P.).....117

5.5. Conclusions.....119

BIBLIOGRAPHY.....123

APPENDICES.....129

Appendix A. Growth Increment Analysis and Correlation of Temperature and Stable Isotope Data.....129

Appendix B. Data Time Series and Digital Images for All Modern Specimens.....In Pocket

Appendix C. Data Time Series and Digital Images for All Archaeological Specimens.....In Pocket

Appendix D. ICP-OES and Mass Spectrometry Results for All Shells Sampled during This Study.....In Pocket

BIOGRAPHY OF THE AUTHOR.....133

LIST OF TABLES

Table 1. Shells utilized for growth increment analysis in this study.....21

Table B1. Growth increment counts and oxygen isotope data for modern *Chione subrugosa* and *Anadara tuberculosa*.....In Pocket

Table B2. Growth increment counts and oxygen isotope data for modern *Trachycardium procerum*.....In Pocket

Table B3. Elemental mole ratios for *Chione subrugosa* 2PT1 and *Trachycardium procerum* TP 1-12.....In Pocket

Table C1. Growth increment counts and oxygen isotope data for *Trachycardium procerum* from Ostra Base Camp.....In Pocket

Table C2. Growth increment counts and oxygen isotope data for all shells from Siches PV 7-19.....In Pocket

Table C3. Elemental mole ratios for *Trachycardium procerum* OBC V-1-C 2i-2ib, Elemento 2.....In Pocket

Table D1. Inductively-coupled-plasma optical emission spectrometry results for *Chione subrugosa* 2PT1, *Trachycardium procerum* TP 1-12, and *Trachycardium procerum* OBC V-1-C 2i-2ib, Elemento 2.....In Pocket

Table D2. Mass spectrometry results for *Chione subrugosa* 2PT1, *Trachycardium procerum* TP 1-12, and *Trachycardium procerum* OBC V-1-C 2i-2ib, Elemento 2.....In Pocket

LIST OF FIGURES

Figure 1. Location of major municipalities and important sites mentioned in the text.....4

Figure 2. *Anadara tuberculosa* and *Protothaca ecuatoriana* utilized in stable oxygen isotope and growth increment analyses.....22

Figure 3. *Chione subrugosa* and *Trachycardium procerum* utilized in stable oxygen isotope and growth increment analyses.....24

Figure 4. Daily growth in *C. subrugosa* 2PT1.....36

Figure 5. Daily growth in *P. ecuatoriana* PV 7-19 IIB4(a).....37

Figure 6. Subdaily growth in *A. tuberculosa* PV 7-19 IIB3(a).....38

Figure 7. Subdaily growth in *T. procerum* TP 1-12.....39

Figure 8. Results of the Model II linear regression of a pooled sample containing all modern *Trachycardium procerum* utilized in this study.....43

Figure 9. Presumed onset of environmental stress in *T. procerum* TP 1-12.....46

Figure 10. NCEP ocean temperature versus $\delta\ ^{18}O_{shell}$ in all modern *T. procerum* specimens.....48

Figure 11. Time series of $\delta^{18}O_{shell}$ values in *T. procerum* 3TP1-1b and ocean temperatures estimated by the Model II regression line.....49

Figure 12. Time series of $\delta^{18}O_{shell}$ values in *T. procerum* TP 1-12 and ocean temperatures estimated by the Model II regression line.....51

Figure 13. Time series of $\delta^{18}O_{shell}$ values in *T. procerum* TP 1-12 (Houk)* and ocean temperatures estimated by the Model II regression line.....52

Figure 14. Comparison of $\delta^{18}O_{shell}$ time series from *T. procerum* TP 1-12 (Houk)* and *T. procerum* TP 1-12. 53

Figure 15. Area of growth perturbation in *C. subrugosa* 2PT1.....55

Figure 16. NCEP SST versus $\delta^{18}O_{shell}$ in all modern *C. subrugosa* specimens.....57

Figure 17. Time series of $\delta^{18}O_{shell}$ values in *C. subrugosa* PT1-14.....58

Figure 18. Time series of $\delta^{18}O_{shell}$ values in *C. subrugosa* 2PT1.....60

Figure 19. Time series of $\delta^{18}O_{shell}$ values in *C. subrugosa* 2PT1 (Houk)*.....61

Figure 20. Comparison of the $\delta^{18}O_{shell}$ time series from *C. subrugosa* 2PT1 and *C. subrugosa* 2PT1 (Houk)*.....63

Figure 21. NCEP SST versus $\delta^{18}O_{shell}$ in all modern *A. tuberculosa* specimens.....64

Figure 22. Time series of $\delta^{18}O_{shell}$ values in *A. tuberculosa* AT 5-1.....66

Figure 23. Time series of $\delta^{18}O_{shell}$ values in *A. tuberculosa* AT 5-2.....67

Figure 24. NCEP ocean temperature (-15 m) versus elemental mole ratios in *T. procerum* TP 1-12.....69

Figure 25. Comparative time series of (Mg/Na X 1000) in *T. procerum* TP 1-12 and NCEP ocean temperature (-15 m).....70

Figure 26. Comparative time series of (Sr/Na X 1000) in *T. procerum* TP 1-12 and NCEP ocean temperature (-15 m).....71

Figure 27. Comparative time series of (Mg/Ca X 1000) in *T. procerum* TP 1-12 and NCEP ocean temperature (-15 m).....72

Figure 28. Comparative time series of (Sr/Ca X 1000) in *T. procerum* TP 1-12 and NCEP ocean temperature (-15 m).....73

Figure 29. NCEP salinity versus elemental mole ratios in *T. procerum* TP 1-12.....75

Figure 30. Comparative time series of (Mg/Na X 1000) in *T. procerum* TP 1-12 and NCEP salinity.....76

Figure 31 Comparative time series of (Sr/Na X 1000) in *T. procerum* TP 1-12 and NCEP salinity.....77

Figure 32. Comparative time series of (Mg/Ca X 1000) in *T. procerum* TP 1-12 and NCEP salinity.....78

Figure 33. Comparative time series of (Sr/Ca X 1000) in *T. procerum* TP 1-12 and NCEP salinity.....79

Figure 34. NCEP SST versus elemental mole ratios in *C. subrugosa* 2PT1.....80

Figure 35. Comparative time series of (Mg/Na X 1000) in *C. subrugosa* 2PT1 and NCEP SST.....81

Figure 36. Comparative time series of (Sr/Na X 1000) in *C. subrugosa* 2PT1 and NCEP SST 82

Figure 37. Comparative time series of (Mg/Ca X 1000) in *C. subrugosa* 2PT1 and NCEP SST 83

Figure 38. Comparative time series of (Sr/Ca X 1000) in *C. subrugosa* 2PT1 and NCEP SST.....84

Figure 39. NCEP salinity versus elemental mole ratios in *C. subrugosa* 2PT1.....85

Figure 40. Comparative time series of (Mg/Na X 1000) in *C. subrugosa* 2PT1 and NCEP salinity.....87

Figure 41. Comparative time series of (Sr/Na X 1000) in *C. subrugosa* 2PT1 and NCEP salinity.....88

Figure 42. Comparative time series of (Mg/Ca X 1000) in *C. subrugosa* 2PT1 and NCEP salinity 89

Figure 43. Comparative time series of (Sr/Ca X 1000) in *C. subrugosa* 2PT1 and NCEP salinity.....90

Figure 44. Time series of $\delta^{18}O_{shell}$ values in *C. subrugosa* PV 7-19 IIB3(a).....91

Figure 45. Time series of $\delta^{18}O_{shell}$ values in *C. subrugosa* PV 7-19 IIB3(b).....92

Figure 46. Time series of $\delta^{18}O_{shell}$ values in *C. subrugosa* PV 7-19 IB7.....94

Figure 47. Time series of $\delta^{18}O_{shell}$ values in *C. subrugosa* PV 7-19 IB4bi.....95

Figure 48. Time series of $\delta^{18}O_{shell}$ values in *A. tuberculosa* PV 7-19 IIB3(a).....96

Figure 49. Time series of $\delta^{18}O_{shell}$ values in *A. tuberculosa* PV 7-19 IIB3(b).....97

Figure 50. Time series of $\delta^{18}O_{shell}$ values in *P. ecuatoriana* PV 7-19 IIB4(a).....99

Figure 51. Time series of $\delta^{18}O_{shell}$ values in *P. ecuatoriana* PV 7-19 IIB4(b).....100

Figure 52. Time series of $\delta^{18}O_{shell}$ values in *P. ecuatoriana* PV 7-19 IB7.....101

Figure 53. Time series of $\delta^{18}O_{shell}$ values in *P. ecuatoriana* PV 7-19 IB4bi.....102

Figure 54. Time series of $\delta^{18}O_{shell}$ values in *P. ecuatoriana* PV 7-19 IB6b.....103

Figure 55. Time series of $\delta^{18}O_{shell}$ values in *T. procerum* OBC V-1-C 2i-2ib, Elemento 2.....105

Figure 56. Time series of elemental mole ratios in *T. procerum* OBC V-1-C 2i-2ib, Elemento 2.....107

Figure B1. *Chione subrugosa* PT1-14.....In Pocket

Figure B2. *Chione subrugosa* 2PT1.....In Pocket

Figure B3. *Chione subrugosa* 2PT1 (Houk)*.....In Pocket

Figure B4. *Anadara tuberculosa* AT 5-1.....In Pocket

Figure B5. *Anadara tuberculosa* AT 5-2.....In Pocket

Figure B6. *Trachycardium procerum* 3TP1-1b.....In Pocket

Figure B7. *Trachycardium procerum* TP 1-12 .....In Pocket

Figure C1. *Trachycardium procerum* OBC V-1-C 2i-2ib, Elemento 2.....In Pocket

Figure C2. *Chione subrugosa* PV 7-19 IB4bi.....In Pocket

Figure C3. *Chione subrugosa* PV 7-19 IB7.....In Pocket

Figure C4. *Chione subrugosa* PV 7-19 IIB3(a).....In Pocket

Figure C5. *Chione subrugosa* PV 7-19 IIB3(b).....In Pocket

Figure C6. *Anadara tuberculosa* PV 7-19 IIB3(a).....In Pocket

Figure C7. *Anadara tuberculosa* PV 7-19 IIB3(b).....In Pocket

Figure C8. *Protothaca ecuatoriana* PV 7-19 IB4bi.....In Pocket

Figure C9. *Protothaca ecuatoriana* PV 7-19 IB6b.....In Pocket

Figure C10. *Protothaca ecuatoriana* PV 7-19 IB7.....In Pocket

Figure C11. *Protothaca ecuatoriana* PV 7-19 IIB4(a).....In Pocket

Figure C12. *Protothaca ecuatoriana* PV 7-19 IIB4(b).....In Pocket

ACKNOWLEDGEMENTS

I express my appreciation to the faculty, staff, and graduate students in the Department of Geological Sciences and the Institute for Quaternary and Climate Studies. Also, I would like to thank Michael Handley and Tiffany Wilson at the Mitchell Center, Karl Kreutz and Doug "Cap" Introne at the Stable Isotope Laboratory, Dr. Scott Johnson for the use of his microscope, all members of my Graduate Committee (Dr. Dan Sandweiss, Dr. Kirk Maasch, Dr. Fei Chai, and Dr. Harold "Bud" Rollins), the Foundation for the Exploration and Research of Cultural Origins (FERCO), and my best friend and wife, Rachel Turner Houk. Furthermore, I am eternally grateful to a dear friend, Mr. Glen Fiddich, for his encouragement during the final stage of this thesis.

CHAPTER 1

INTRODUCTION

1.1. Purpose of This Study

The purpose of this study is to aid in developing a high-temporal-resolution sea surface temperature (SST) proxy in order to test the hypothesis that climate conditions along the north Peruvian littoral were warmer (wetter) prior to 5730 cal yr B.P. Faunal assemblages consisting of both tropical and temperate species in mid-Holocene archaeological sites on the north coast of Peru qualitatively suggest the presence of a stable warm-water regime as far south as 10°S prior to 5730 cal yr B.P. (Richardson III 1981, 1978, 1973; Reitz and Sandweiss 2001; Rollins et al. 1986; Sandweiss et al. 2001,1997, 1996). In order to facilitate future resolution of variations that result from a stable warm-water regime, this study will analyze growth increments of molluscan species present on the north Peruvian littoral during the mid-Holocene.

Previous analysis of the stable isotope ratios (Nicholas 1996) in mollusk shells from the Middle Preceramic Siches (7420 cal yr B.P. to 5650 cal yr B.P.) and Ostra Base Camp (6660 cal yr B.P.) sites was unable to constrain $\delta^{18}O$ data in the time domain. Little can be assessed regarding annual and interseasonal SST oscillations during the mid-Holocene without a corresponding time component for the data. A synthesis of growth increment and stable isotope analyses can constrain isotope data in the time domain. Unfortunately, errors in the Nicholas (1996) $\delta^{18}O$ data do not permit measurement of mid-Holocene SST at this time; nevertheless, this study sets the stage for such measurement once stable isotope ratios in the sample shells have been reanalyzed.

Further, this study will advance knowledge of mid-Holocene climate conditions along the north coast of Peru by establishing $\delta^{18}O$ time series for specimens of *Chione subrugosa*, *Protothaca ecuatoriana*, *Anadara tuberculosa*, and *Trachycardium procerum* collected from the Thermally Anomalous Molluscan Assemblages (TAMA) at Siches and Ostra Base Camp.

1.2. Thermally Anomalous Molluscan Assemblages as Evidence of Mid-Holocene Climate Change

Controversy surrounds the mid-Holocene climate record inferred from geomorphological and geoarchaeological evidence (Markgraf and Diaz 2000; Sandweiss et al. 1996; DeVries and Wells 1996). Archaeological shell middens excavated on the coast of Peru contain Thermally Anomalous Molluscan Assemblages (TAMA) that consist of both warm-temperate and tropical mollusk species. The presence of tropical species in dated archaeological contexts as far south as 10°S suggests that between 8990-8820 cal yr B.P. and 5730 cal yr B.P., a stable warm-water regime with SST warmer than those of today influenced climate in the eastern tropical Pacific. The presence of a stable warm-water regime between 8990-8820 cal yr B.P. and 5730 cal yr B.P. may preclude or suppress the modern Walker Circulation regime of the tropical Pacific and climate variability induced by El Niño/Southern Oscillation (ENSO) (Richardson III 1981, 1978, 1973; Rollins et al. 1986; Sandweiss et al. 2001,1997, 1996; Schulmeister and Lees 1995). Today, the climate of the Peruvian coast south of 4°S is influenced by the northward flowing, warm-temperate waters of the Humboldt Current. Seasonal SST variation is minimal except during ENSO. During these periodic events, SST range from

2°C to 10°C warmer than the mean annual temperature of the Humboldt Current (Sandweiss et al., 1996).

During ENSO events, tropical species of fish, crustaceans, and mollusks from Ecuador and extreme northern Peru migrate south and survive either for the duration of the warm event or the lifespan of the migrant organism. Furthermore, in response to the warm event, temperate species retreat southward or suffer high mortality (Sandweiss et al. 2001, 1996). Prior to the 1982-83 ENSO, the warm-temperature sensitive clam *Mesodesma donacium* occupied the littoral of Chile and Peru as far north as Lima (12°S). During the 1982-83 event, *M. donacium* declined sharply in waters less than 4m deep (Arntz and Valdivia 1985). Following the event, *M. donacium* was present only south of Lomas, Peru at 15° 30'S. By the time of the 1997-98 ENSO, the species still had not recovered to its former range and was pushed even farther south by the 1997-98 event (Sandweiss et al. 2001).

Faunal collections from coastal Peruvian archaeological sites dating from approximately 13,000 cal yr B.P. to 5700 cal yr B.P. suggest that warmer water persisted north of 10°S during the Early and Middle Preceramic periods (Reitz and Sandweiss 2001; Sandweiss et al. 1996). Early Preceramic occupations (13,160 cal yr B.P.) at the Amotape Camp (4°40'S) contain tropical molluscan assemblages. Middle Preceramic occupations at Siches (4°30'S) (**FIGURE 1**), Quebrada Chorrillos (6°00'S), Ostra (8°55'S, Santa Valley), and Almejas (9°30'S, Casma Valley) also contain tropical faunal assemblages. The archaeological record for this time period is complicated by interactions between sea-level rise and the width of the continental shelf (Richardson III

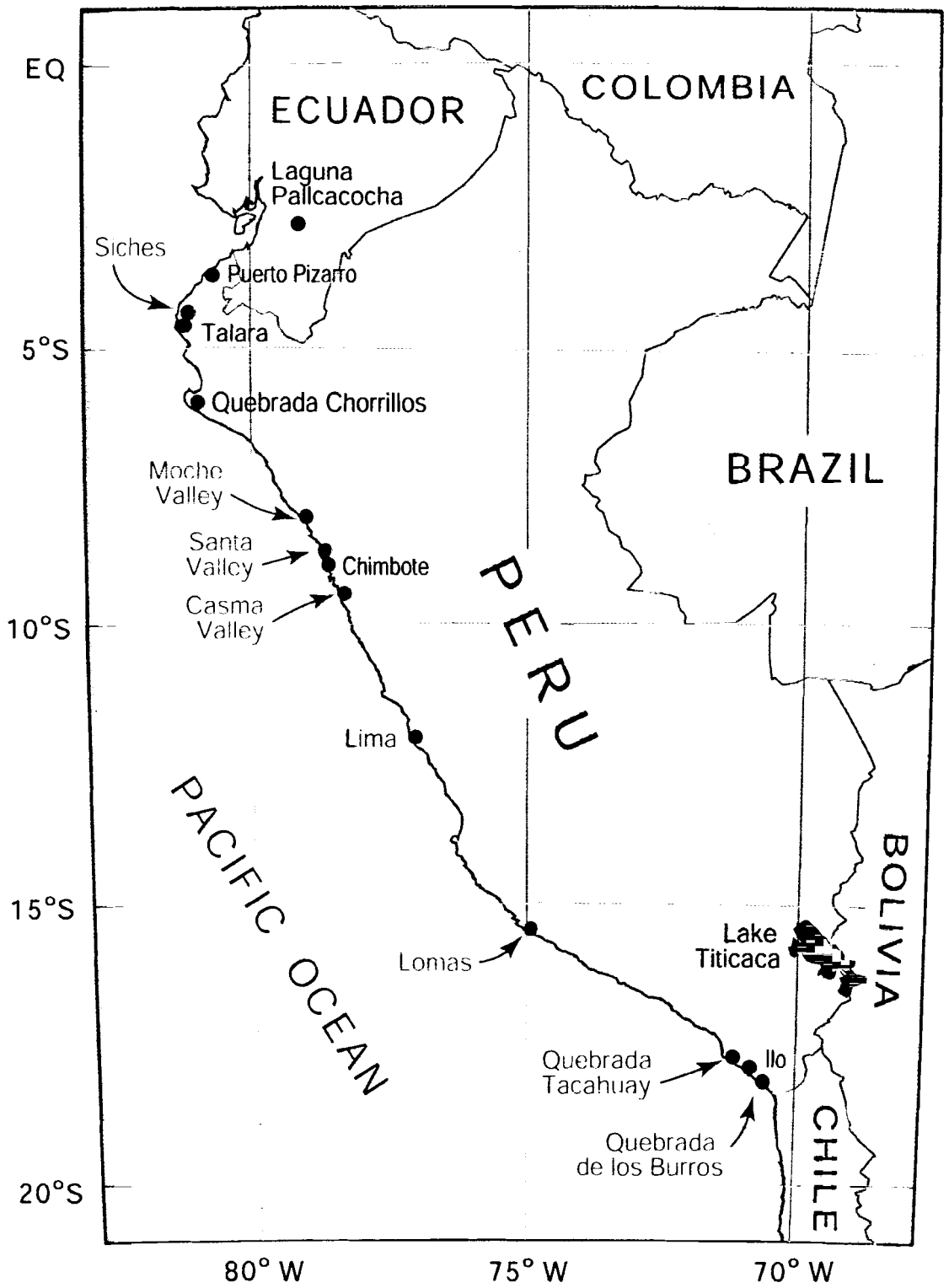

FIGURE 1: Location of major municipalities and important sites mentioned in the text. Adapted from (Sandweiss et al. 2001).

1981). Early maritime sites have been discovered where the continental shelf is narrow and shoreline transgression has been minimal. Sea level approached its modern value around 7000 cal yr B.P., and maritime sites located where the continental shelf is wide do not appear until that time. Thus, records for the Early Preceramic are limited to the north coast near Talara (4°30'S) and south of the Paracas peninsula at 14°S (Sandweiss et al. 1996, Richardson III 1981).

The presence of TAMA in northern Peru is interpreted to indicate tropical oceanic conditions along the north coast in the Early and Middle Holocene (Sandweiss et al. 1996, Rollins et al. 1986, Richardson III 1981). Evidence for a stable tropical water regime comes from the sites of Pampa Las Salinas and Ostra Base Camp (OBC), which lie to the north of Chimbote, Peru (9°S) in the Santa river valley (**FIGURE 1**). At Pampa Las Salinas, a Preceramic base camp (OBC) at the southern edge of a stranded sea cliff overlooks an uplifted embayment. Extractive camps are spread out 10 km along the top of the sea cliff. Test pits revealed 70 cm of shell material at the largest extractive camp. Shell material at the bottom of the pit dated at 5400 +/- 60 ^{14}C yr B.P. (5470 cal yr B.P.). Material at 35 cm depth dated at 5160 +/- 60 ^{14}C yr B.P. (5240 cal yr B.P.). Radiocarbon dates on charcoal from OBC confirm exploitation of marine resources in the embayment between 6250 +/- 250 ^{14}C yr B.P. (7200 cal yr B.P.) and 5450 +/- 110 ^{14}C yr B.P. (6280 cal yr B.P.) (Sandweiss 1996a).

The molluscan assemblages from Pampa Las Salinas and OBC contain species found today north of 5°S in the Panamic Biogeographic Province. The assemblages include a diversity of species from the province, which provided a resource base for the Preceramic inhabitants over multiple occupations. Periodic ENSO events may produce a

short-lived TAMA by southward migration of tropical species; however, at Pampa Las Salinas tropical species persist through decades of multiple occupations that outweigh the lifespan of a single organism. Also at Pampa Las Salinas, multiple age classes of tropical mollusks are located *in situ* along an uplifted beach proximal to the midden (Rollins et al. 1986). These characteristics of the sites suggest a consistent and stable ecological regime capable of supporting a diversity of tropical species.

Fronting the ancient shoreline at Pampa Las Salinas is a series of nine beach ridges extending up to 5 km to the west. The ridges originate at the mouth of the Santa River and consist of marine sand and river cobbles deposited by long shore transport. The configuration of the ridges may indicate a combination of episodic flooding and sediment pulses associated with major ENSO events, tectonic uplift, and relative sea level lowering (Sandweiss 1986; Sandweiss et al. 1983). The first beach ridge west of Pampa Las Salinas exhibits the highest amplitude of the nine-ridge sequence. The high amplitude may indicate a prolonged period of arid weathering resulting in the formation of transportable colluvium prior to the initiation of the earliest major ENSO event.

Radiocarbon dating of a coldwater gastropod species (*Prisogaster niger*) provided a date of 4235 +/- 115 B.P. (3930 cal yr B.P.) for the first ridge west of the stranded shoreline. *P. niger* occurs with other coldwater intertidal species in the ridge. The stable occurrence of coldwater species at 3930 cal yr B.P. in conjunction with the Santa TAMA at 5240 cal yr B.P. suggests that sometime between 5240 cal yr B.P. and 3930 cal yr B.P. a major change occurred in tropical eastern Pacific Ocean circulation. The replacement of a warm-water regime with a cold-water regime created conditions acceptable for the occurrence of ENSO (Rollins et al. 1986).

Contrary to the idea of a stable tropical climate regime as far south as the Santa river valley (9°S), DeVries and Wells (1990) and DeVries et al. (1997) contend that the Santa TAMA developed because of changes in coastal morphology. These authors argue that the tropical species developed in a warm narrow embayment open to the ocean and existed coevally with temperate species occupying the open coast. The coeval occurrence of tropical and temperate species is further documented by TAMA from the lower and upper Pleistocene deposits near Loma (15°S) and Ilo (18°S). These Pleistocene occurrences may be comparable to modern occurrences of tropical mollusk species in suitable habitats of central and southern Peru immediately following ENSO events. This explanation, however, does not account for the occurrence of TAMA at other mid-Holocene sites in northern Peru (Sandweiss et al. 1997).

1.3. ENSO and Ocean-Atmosphere Adjustments

The eastern equatorial Pacific along the coast of Peru is relatively cool. The normal cool conditions of the region result from a balance of heat transfer between the ocean and the atmosphere. ENSO results when this balance is upset (Barber and Chavez 1983). Cool SST and reduced heat storage in the surface layers of the ocean in this region correlate with a low sea level, a shallow surface mixed-layer, and a shallow thermocline (Cane 1983). Trade winds blowing across the Pacific from east to west set a tilt in the thermocline that brings its middle (20°C isotherm) to a depth of 40 m or less in the eastern boundary (Barber and Chavez 1983, Busalacchi et al. 1983). Meridional long-shore winds blowing north toward the equator induce upwelling of nutrient-rich water from depths of 40 to 80 m. Enhanced nutrient supply and enhanced capture of light due

to the shallow surface mixed layer increase biological productivity of the region at all trophic levels (Barber and Chavez 1983).

The cool SST of the eastern Pacific are in strong contrast to the warm SST of the western Pacific and result in a strong east-west temperature gradient. This temperature gradient results in the thermally directed Walker circulation in the equatorial plane. The Walker circulation is characterized by sinking motion in the eastern Pacific, westward low level flow (trade winds), rising motion and cumulus convection over the western Pacific and Indonesia, and eastward return flow at the cirrus cloud level (10-15 km). Large-scale subsidence associated with the Walker circulation results in little or no rainfall east of the date line (Rasmusson and Wallace 1983).

During ENSO episodes, equatorial waters in the eastern half of the Pacific are warmer than normal while the waters in the western Pacific warm pool are near or slightly below normal. The east-west temperature gradient is diminished and the region of heavy precipitation shifts eastward. Desert islands in the equatorial central Pacific may experience torrential rainfall. To the west of the dateline, the easterly surface winds weaken or shift to westerly and strong easterlies may occur at cirrus cloud level (Rasmusson and Wallace 1983). This dynamic coupling between the ocean and the atmosphere results in a positive feedback loop among surface winds, SST gradients, and ocean upwelling. Surface winds over the tropical Pacific are driven by SST gradients (Lindzen and Nigam 1987), and changes in the SST gradients affect the strength of surface winds. Furthermore, changes in the strength of surface winds affect the strength of upwelling, which affects SST gradients (De-Zheng Sun 2000).

1.4. The ENSO Record

The ENSO record may be inferred from various paleoclimate data proxies in South America and Australia. Some proxies show increased SST and precipitation in the tropical Pacific (Gagan et al. 1998; Schulmeister and Lees 1995), as well as increased aridity in the Andean highlands and littoral of southern Peru and Chile (Fontugne et al. 1999; Valero-Garcés et al. 1996), during the mid-Holocene. Interpretations of proxy data suggest that the frequency of ENSO events increases after 7000-5700 cal yr B.P. (Sandweiss et al. 2001; Wells 1990; Rodbell et al. 1999) following sea-level adjustments to modern values. Results of tropical Pacific modeling experiments indicate that both changes in Holocene orbital forcing (Clement et al. 2000,1999) and thermal structure of the mixed-layer (Sun 2000) determine the stability of the climate regime during the mid-Holocene.

Few mid-Holocene terrestrial records from the littoral of southern Peru and Chile are preserved for paleoclimate analysis (Sandwiess et al. 1996,1997; DeVries et al. 1997; Wells and Noller 1997; Rodbell et al. 1999). This coastal region is one of the most arid in the world. Fontugne et al. (1999) were able to construct a continuous 5000-year record from sediments at Quebrada de los Burros (Figure 1). The authors sampled fourteen organic rich layers resulting from decomposition of aquatic plants fed by ENSO rains at mid-latitude or fog drip from the upslope Pampa de Lintay to the north. The deposition of fine-grained sediments between 8060 cal yr B.P. and 3380 cal yr B.P. implies low energy sedimentation; however, a fine gravel layer (<1cm) implies higher energy deposition between 5390 cal yr B.P. and 4555 cal yr B.P. This period of higher energy sedimentation correlates with an ENSO event at Quebrada Tacahuay dated at 4550 ^{14}C yr

B.P. (5300 cal yr B.P.) (Keefer et al. 1998). Two debris flow deposits, believed to result from ENSO events, occur after 3380 cal yr B.P. and also around 8980 cal yr B.P., but do not occur between 8060 cal yr B.P. and 3380 cal yr B.P. (Keefer et al. 1998, Fontugne et al. 1999). The authors interpret the organic-rich sediments in Quebrada de Los Burros to indicate a difference between modern and mid-Holocene climates. Sediment cores suggest an extremely dry mid-Holocene climate interrupted by short high soil moisture events related to an increase in coastal upwelling between 8060 cal yr B.P. and 3380 cal yr B.P. Low energy sedimentation during the period of increased upwelling suggests that the southern coast of Peru was not affected by ENSO events of discernible magnitude or periodicity (Fontugne et al. 1999; Rodbell et al. 1999).

Valero-Garcés et al. (1996) employed high-resolution seismic profiles in conjunction with sediment cores from Laguna Miscanti, Chile (23° 44'S, 67° 46W) in the Atacama Altiplano in order to document environmental change during the mid and late Holocene. In agreement with the terrestrial record at Quebrada de Los Burros, the authors interpreted an arid period during the mid-Holocene (8990-8820 cal yr B.P. to 4500-4440 cal yr B.P.) with a progressive increase in lake level rise beginning at 4500-4440 cal yr B.P. An increase in lake level is consistent with a change over from warm environments without ENSO to the present cooler background interrupted by ENSO every few years. A rise in Lake Titicaca at 4400-4300 cal yr B.P. is coeval with the rise at Laguna Miscanti. Both increases are linked to increasing frequencies in ENSO (Martin et al. 1993; Enfield 1992).

Proxy data in the western tropical Pacific indicate increased precipitation and SST during the mid-Holocene. Gagan et al. (1998) collected stable isotope data from mid-

Holocene Great Barrier Reef corals in the warm pool of the Western Pacific. The authors interpreted these data to suggest that areas near the present-day warm pool exhibited mid-Holocene SST which were warmer by as much as 1.2°C during the period 8000 cal yr B.P. to 5000 cal yr B.P. The increase in temperature was accompanied by lower interannual SST variability for the western warm pool prior to 5000 cal yr B.P. Moreover, Schulmeister and Lees (1995) interpreted pollen records from northern Australia to suggest increased precipitation in the region from the terminal Pleistocene until 5730 cal yr B.P. and a precipitation maximum from 5730 cal yr B.P. to 4500-4440 cal yr B.P. After 4500-4440 cal yr B.P., interannual variability in precipitation increases, and the climate regime becomes unstable. The authors suggest that this increase in interannual variability and instability in the climate regime result from the establishment of the Walker Circulation-dominated climate with an ENSO-scale variability.

Sun (2000) suggests that orbital forcing is responsible for changes in the thermal structure of the equatorial Pacific. The author constructed a simple analytical model of the coupled ocean-atmosphere system over the equatorial Pacific. The model predicts that the climate of the Eastern tropical Pacific has two regimes; one is warm and stable, the other is cold and oscillating. The transition from the steady regime to the oscillating regime occurs when the temperature difference between the surface warm pool and the deep ocean exceeds a critical value. The author shows that the stable warm water regime exists as a result of thermal forcing without ENSO-scale oscillations.

If the eastern equatorial Pacific in the early and middle Holocene consisted of a stable warm-water regime, then the coastal regions of the South America should experience strong seasonal rains every year. Clement et al. (2000) imposed orbitally

induced changes on a coupled ocean-atmosphere model and concluded that the mid-Holocene orbital configuration altered the seasonal cycle of the ocean–atmosphere system. This alteration suppressed warm events in the mid-Holocene. Currently, the earth passes through perihelion at the beginning of the calendar year; however, during the Early and Middle Holocene perihelion occurred during the middle of the calendar year. The thermodynamic response of the ocean to mid-Holocene solar forcing resulted in decreased variability in the seasonal cycle. Decreased variability is due to cooling in the Boreal winter and spring and warming in the Boreal summer and fall when SST are seasonally cold. Warming in the Boreal summer and fall increases SST in the cold season by 0.5°C. Cooling in the Boreal winter explains a weak Early and Middle Holocene ENSO variability due to smaller event amplitudes. Parts of the tropics may have been warmer in the Early and Middle Holocene, but the eastern Pacific was colder and similar to the modern climate regime (Clement et al. 2000).

Analysis of otoliths from Peruvian sea catfish (*Galeichthys peruvianus*) of Mid-Holocene age conflict with the results of Clement et al. (2000). Stable oxygen isotope values in otoliths recovered from Ostra (6860-6800 cal yr B.P.) and Siches (7420-7340 cal yr B.P.) suggest that mean sea surface temperatures in the eastern tropical Pacific were approximately 2-3°C higher than modern values. Furthermore, the oxygen isotope profiles of the mid-Holocene otoliths suggest that seasonal temperature variation was increased by approximately 3-4°C at the Ostra site (8°45'S). It was determined that fresh water influx could not be responsible for increasingly negative $\delta^{18}O$ values in the mid-Holocene otoliths due to the open coastal waters preferred by *G. peruvianus*. Thus, SST variation accounted for the observed values.

Betancourt et al. (2000) combined data from fossil rodent middens and wetland deposits in the central Atacama Desert (22°S to 24°S) in order to examine monsoonal circulation and tropical rainfall since the last glacial maximum. A history of vegetation change and groundwater fluctuation suggests a wet phase between 8000 cal yr B.P. and 3000 cal yr B.P. The authors infer that the record of increased precipitation happened during a time of strengthened Pacific trade winds and persistent La Niña-like conditions that favored convection and precipitation. According to coupled ocean-atmosphere models, the strengthening of the Pacific trade winds occurs as a result of reduction in austral summer insolation, increase in boreal summer insolation (Liu et al. 1999), and differential cooling of the eastern relative to the western Pacific (Clement et al. 1999, 2000). These factors decrease the intensity of ENSO events during the Early and Middle Holocene (Liu et al. 1999).

A core obtained from Laguna Pallcacocha (Figure 1) in southwestern Ecuador suggests that the frequency of clastic depositional events has increased progressively since the terminal Pleistocene. The periodicity of clastic sedimentation has changed from greater than or equal to 15 years during the late glacial and early Holocene to 2-8.5 years after 5000 cal yr B.P. This 2-8.5 year periodicity is consistent with the periodicity of modern ENSO events (Rodbell et al. 1999).

Further evidence for an increasing frequency of Middle Holocene to Late Holocene ENSO events comes from the Casma river valley (**FIGURE 1**). Wells (1990) studied overbank flood sediments resulting from the 1982-83 ENSO in order to characterize an ENSO deposit. The author then described and sampled Holocene overbank deposits from Rio Casma, Rio Sechin, and Quebrada Rio Seco in order to develop a proxy record of

ENSO events in the Holocene. The flood-plain stratigraphy indicated that a minimum of 18 flood events occurred during the Holocene with 13 of the events occurring since 3200 cal yr B.P. Flooding appears to become greatly enhanced during the Holocene with a marked increase after 3200 cal yr B.P.

1.5. Archaeomalacology and the ENSO Record

Sandweiss et al. (2001) analyzed mollusks from archaeological sites on the north and central coast of Peru and interpreted an increase in the frequency of ENSO between 3200 cal yr B.P. and 2800 cal yr B.P. Tropical molluscan species found in sites north of 10°S and dating before 5800 cal yr B.P. indicate a warm climate regime. These tropical taxa are now found only north of 4°S. After 5800 cal yr B.P., the tropical species were replaced by a temperate species in assemblages characteristic of modern southern Peru and northern Chile. By 2800 cal yr B.P., the temperature-sensitive temperate species (i.e. *Choromytilus chorus*, *M. donacium*) disappeared from middens north of 9°S. The sensitivity of these two species to temperature and the period required for recolonization after ENSO-induced mass mortality suggest an increase in the frequency of ENSO events.

Marine mollusks excavated from archaeological shell middens serve as both environmental and cultural indicators. Mollusks function as environmental indicators due to dynamic physiological and anatomical factors or inherent characteristics that provide information on habitat and climate (Sandweiss 1996b). Subsequently, habitat and climate information supply indirect clues by which to interpret cultural behavior. In addition to habitat and climate information, archaeological contexts and forms of shells may also provide important insights for the interpretation of cultural behavior (e.g. the

shell functions as food, raw material, or a symbol) (Rollins et al. 1990, Sandweiss and Rodriguez 1991).

Rollins et al. (1987) used the 1982-83 ENSO in order to develop criteria for recognizing ancient ENSO events using mollusks from archaeological shell middens along the coast of Peru. A combination of stable isotope and growth increment analyses in selected specimens of *C. subrugosa* and *T. procerum* indicated elevated SST during the 1982-83 event. The authors concluded that these techniques could be employed to recognize culturally disruptive events in the geoarchaeological record. The chances of discovery of a major ENSO event in the geoarchaeological record is enhanced by both the catastrophic nature of the events and the probability of ENSO events being closely spaced in time.

Perrier et al. (1994) also sampled stable oxygen and carbon isotopes in modern and archaeological specimens of mollusks at Pampa Las Salinas and Salinas de Chao in order to document oceanographic changes between 7430 cal yr B.P. and 4500-4440 cal yr B.P. Among the sampled shells were four ancient specimens of *T. procerum* radiocarbon dated at 5500 +/- 150 B.P. (5600 cal yr B.P.), 5500 +/- 150 B.P. (5600 cal yr B.P.), 5800 +/- 150 B.P. (5920 cal yr B.P.), and 6100 +/- 150 B.P. (6280 cal yr B.P.). The authors applied the calcite temperature equation of Epstein et al. (1953) to the isotopic data from aragonitic species and isolated a single temperature anomaly at 5600 cal yr B.P. which deviated from the interannual, interseasonal temperature variation by as much as 8°C. Samples from the two *T. procerum* specimens dated at 5920 cal yr B.P. and 6280 cal yr B.P. indicated that seasonal and interannual SST for the life of the shells varied within ranges of 3.5°C and 5°C respectively. Unfortunately, because the calcite temperature

equation of Epstein et al. (1953) was used inappropriately with data from aragonitic species, estimated temperature anomalies are unreliable.

Nicholas (1996) analyzed the stable oxygen and carbon isotope ratios of modern and ancient mollusk shells (*Anadara tuberculosa, Chione subrugosa, Protothaca ecuatoriana, Trachycardium procerum*) in order to examine mid-Holocene hydrographic conditions along the north coast of Peru. In 1984, modern *T. procerum* and *C. subrugosa* were collected from Chimbote and Puerto Pizarro, respectively, to study the growth increment and stable isotope evidence of environmental change associated with the 1982-83 ENSO (Rollins et al. 1987, Nicholas 1996). The changes associated with this ENSO provided the opportunity to test these species as recorders of hydrographic changes as well as to describe the attributes of an ENSO event in the shell chemistry. Modern specimens of *T. procerum* and *A. tuberculosa* were collected again in 1995 and in order to examine the isotope signals of non-ENSO years (Nicholas 1996). The modern *A. tuberculosa* collected in 1995 were from Puerto Pizarro, the local habitat that is closest to the Siches site. Isotopic values of shells from the mid-Holocene sites of Siches and Ostra Base Camp were compared with the isotopic values of modern shells collected at Puerto Pizarro and Chimbote.

Nicholas interpreted her isotopic data in terms of absolute temperature by applying them to the Horibe and Oba (1972) temperature equation. The author interpreted the oxygen isotope values in *T. procerum* excavated from the Ostra Base Camp site to indicate SST 3-4°C cooler than modern conditions at 5730 cal yr B.P. The isotope values in *C. subrugosa* and *A. tuberculosa* at the Siches site were interpreted to indicate periodic rainfall in the region prior to 5730 B.P. Nicholas designated *C. subrugosa* and *A.*

tuberculosa as indicators of both temperature and salinity. The author pointed out that freshening in the Tumbes estuary, where modern *C. subrugosa* and *A. tuberculosa* specimens were collected, might have affected mean $\delta^{18}O$ values. If the same freshening events occurred in a paleoestuary near the Siches site, $\delta^{18}O$ values of the ancient shells would indicate mid-Holocene SST 4-5°C cooler than modern values (Nicholas 1996). Unfortunately, recent analysis of $\delta^{18}O$ and ^{14}C in shells studied by Nicholas indicate unexplained errors in her measurements, suggesting that her results and interpretations are unreliable. Furthermore, a paleoestuary in the vicinity of Siches would require a significant increase in precipitation, which could only occur with warmer SST (Sandweiss, personal communication).

CHAPTER 2

THE SICHES MOLLUSCAN ASSEMBLAGE

2.1. Siches Site PV 7-19

The Siches site PV7-19 is a shell midden with multiple occupations ranging from 8990-8820 cal yr B.P. to 3830-3730 cal yr B.P. The site contains two preceramic phases: the Siches phase dates between 8990-8820 cal yr B.P. and 5730 cal yr B.P., and the later Honda phase dates between 5730 cal yr B.P. and 3830-3730 cal yr B.P. This site is located north of the present-day town of Talara at 4°20'S, 81°13'W. It covers approximately 20 ha on a marine tablazo approximately 16 km from the terminal Pleistocene shoreline (Richardson III et al. 1996; Richardson III 1973).

PV7-19 is the type-site of the Siches phase. This phase is characterized by unifacially worked quartzite flakes, ground stone, and T-shaped stone axes similar to those of the El Estero site in the nearby Amotape Mountains. Also found in the Siches phase is the gourd *Lagenaria siceraria*, which may represent incipient agriculture. The later Honda phase is characterized by unifacially worked flakes preferentially made from flint, ground stone, the gourd *L. siceraria*, shell beads, and bead blanks (Richardson III et al. 1996; Richardson III 1973). The unspecialized unifacial toolkits of the Siches phase provided adaptations to a wide range of changing environments and occurred as terrestrial hunters in the Amotape highlands were forced to adapt to changing ecological conditions during the terminal Pleistocene (Richardson III 1992, 1978).

Middle Preceramic occupations at PV7-19 and other Siches sites as well as Early Preceramic occupations at Amotape Camp mark the exploitation of the mangrove

mollusk *A. tuberculosa*. Late Preceramic Honda and El Estero middens (5730 cal yr B.P. to 4500-4440 cal yr B.P.) do not contain mangrove mollusks. The disappearance of the mangrove mollusk probably results from rapid coastal cooling and a precipitation decrease after 5730 cal yr B.P. (Sandweiss et al. 1996a).

2.2. Mangrove Swamp Habitat

The mangrove species *Rhizophora mangle* is one of the most abundant species of mangrove in the world. Its southernmost limit in South America is the southern part of the Gulf of Guayaquil (3.4°S) at the Peru and Ecuador border (Tomlinson 1986). Mangroves develop extensively where there is a large tidal range and adequate shelter from the wave action of the open ocean (Hutchings and Saenger 1987). The species occupies the intertidal zone between mean sea level and mean high water (Tomlinson 1986). Mangroves can develop in substrates of peat, sand, or coral, but the preferred habitats are muddy soils with a low pH found near river outlets in estuaries, deltas, or lagoons (Hutchings and Saenger 1987; Tomlinson 1986). Mangroves are not tolerant to freezing and will not develop in areas where the seasonal air temperature drops below 16°C or fluctuates within a range of less than 10°C. The same is true if the seasonal air temperature never rises above 24°C (Hutchings and Saenger 1987).

Nicholas (1996) analyzed the stable oxygen and carbon isotopes of three molluscan species from the Siches TAMA: *C. subrugosa*, *A. tuberculosa*, and *P. ecuatoriana*. Dates were obtained for the specimens by their position in a radiocarbon-dated stratigraphic sequence. In addition to the specimens from the Siches TAMA, Nicholas also analyzed *T. procerum* from OBC. No specimens of *T. procerum* were

available in the Siches assemblage, which probably results from that organism's ecological niche.

2.3. Ecology of Molluscan Species

The four molluscan species (**TABLE 1**; *Chione subrugosa*, *Anadara tuberculosa*, and *Protothaca ecuatoriana* from Siches; *Trachycardium procerum* from OBC) analyzed by Nicholas (1996) are the subjects of little ecological study, and the literature pertaining to them is thin. The available data come from biogeographical surveys that describe the temperature tolerances and substrates of the species in their current geographical ranges. The absolute temperature ranges for all of these species are unknown (Nicholas 1996).

2.3.1. *Anadara tuberculosa*

A. tuberculosa (**FIGURE 2**) lives among the roots of *R. mangle* in mangrove swamps along the coastal zones of the eastern Pacific Ocean. The species can be found at depths ranging from the intertidal zone to 5 m below the water surface (Olsson 1961). The absolute temperature tolerance of the species is not known (Nicholas 1996), but it tends to inhabit water with temperatures ranging from 19°C to 27°C (Bernard 1983). The northern most point in the geographic range of *A. tuberculosa* is Baja, California at 27°N. (Olsson 1961; Bernard 1983; Alamo and Valdivieso 1987). The southern most extent of the geographic range is listed by Bernard (1983) and Olsson (1961) as Tumbes, Peru at 3.4°S; however, Alamo and Valdivieso (1987) list Piura, Peru at 5.1°S. An isolated group of mangroves (*Avicenia germinans*) inhabits the estuary at the mouth of the Piura River (Peña and Vásquez 1985). *A. germinans* may provide appropriate habitat for *A. tuberculosa*, resulting in a discrepancy among Alamo and Valdivieso (1987), Bernard (1983), and Olsson (1961). Another mangrove species, *Rhizophora samoensis*, is

Species	Context	Site	Time of Death
Trachycardium procerum	TP 1-12	Chimbote (9°S)	April 1984
Trachycardium procerum	TP 1-12 (Houk)*	Chimbote (9°S)	April 1984
Trachycardium procerum	3TP1-1b	Chimbote (9°S)	July 1995
Trachycardium procerum	OBC V-1-C 2i-2ib Elemento 2**	Ostra Base Camp (9°S)	5830 ± 90 B.P.
Chione subrugosa	PT 1-14	Puerto Pizarro (3.3°S)	April 1984
Chione subrugosa	2PT1	Puerto Pizarro (3.3°S)	December 1984
Chione subrugosa	2PT1 (Houk)*	Puerto Pizarro (3.3°S)	December 1984
Chione subrugosa	PV 7-19 IB4bi	Siches (4.5°S)	> 4930 ± 80 B.P. < 5060 ± 80 B.P.
Chione subrugosa	PV 7-19 IB7	Siches (4.5°S)	5060 ± 80 B.P.
Chione subrugosa	PV 7-19 IIB3(a)	Siches (4.5°S)	6040 ± 80 B.P.
Chione subrugosa	PV 7-19 IIB3(b)	Siches (4.5°S)	6040 ± 80 B.P.
Anadara tuberculosa	AT 5-1	Puerto Pizarro (3.3°S)	July 1995
Anadara tuberculosa	AT 5-2	Puerto Pizarro (3.3°S)	July 1995
Anadara tuberculosa	PV 7-19 IIB3(a)	Siches (4.5°S)	6450 ± 80 B.P.
Anadara tuberculosa	PV 7-19 IIB3(b)	Siches (4.5°S)	6450 ± 80 B.P.
Protothaca ecuatoriana	PV 7-19 IB4bi	Siches (4.5°S)	> 4930 ± 80 B.P. < 5060 ± 80 B.P.
Protothaca ecuatoriana	PV 7-19 IB6b	Siches (4.5°S)	> 4930 ± 80 B.P. < 5060 ± 80 B.P.
Protothaca ecuatoriana	PV 7-19 IB7	Siches (4.5°S)	5060 ± 80 B.P.
Protothaca ecuatoriana	PV 7-19 IIB4(a)	Siches (4.5°S)	6490 ± 90 B.P.
Protothaca ecuatoriana	PV 7-19 IIB4(b)	Siches (4.5°S)	6490 ± 90 B.P.

TABLE 1: Shells utilized for growth increment analysis in this study. Unless indicated, stable isotope data were collected by Nicholas (1996). (Houk)* indicates a stable isotope data set collected during this study from a shell previously analyzed by Nicholas. ** indicates a specimen sampled for stable isotopes and analyzed only by this author.

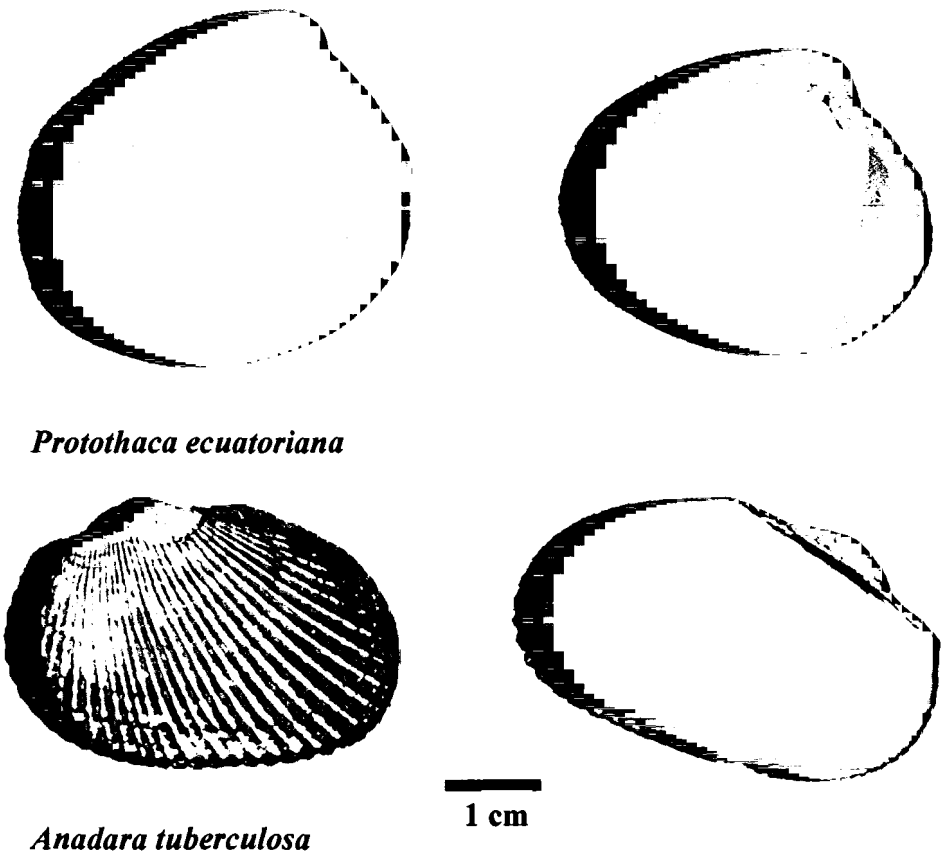

FIGURE 2: *Anadara tuberculosa* and *Protothaca ecuatoriana* utilized in stable oxygen isotope and growth increment analyses. Specimens shown are modern.

morphologically similar to *R. mangle* and may represent a variety of that species (Tomlinson 1986). *R. samoensis* habitat exists from northern Peru to northern Chile; however, the organism is not found in the region today.

2.3.2. *Chione subrugosa*

C. subrugosa (**FIGURE 3**) is an intertidal species found mainly in lagoon and mudflat environments on the Pacific coast of the Americas (Olsson 1961). The absolute temperature tolerance is unknown, but it prefers a temperature range of 17°C to 31°C (Bernard 1983). Today, the species ranges from the Gulf of California (29°N) to Cabo Blanco, Peru (4.25°S) (Olsson 1961, Bernard 1983). At Cabo Blanco, *C. subrugosa* is replaced by a similar species, *Chione broggi*, which prefers a temperature range of 13°C to 30°C. The range of this species is from 4.25°S to 33°S (Bernard 1983). Other authors (Alamo and Valdivieso 1987) suggest that *C. subrugosa* ranges from Baja California, Mexico to Valparaiso, Chile (33°S), and *C. broggi* is restricted to the Peruvian coast between Cabo Blanco and Bayóvar (5.5°S).

2.3.3. *Protothaca ecuatoriana*

P. ecuatoriana (**FIGURE 2**) is an intertidal species that inhabits the Pacific coast of South America where water temperatures range from 18°C to 32°C (Bernard 1983). The species ranges from 2°N in Colombia to Puerto Pizarro, Peru (3.3°S) and prefers sandy substrates (Bernard 1983; Alamo and Valdivieso 1987).

2.3.4. *Trachycardium procerum*

T. procerum (**FIGURE 3**) is a subtidal species that lives in sandy or muddy substrates at water depths from 5 to 15 meters (Alamo and Valdivieso 1987; Bernard

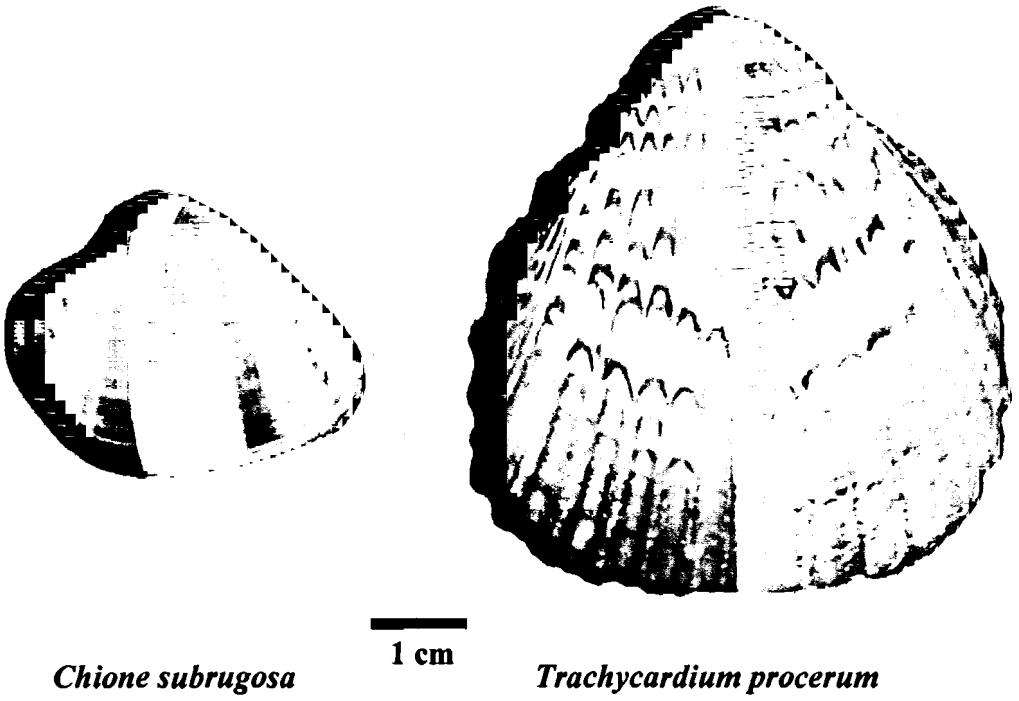

FIGURE 3: *Chione subrugosa* and *Trachycardium procerum* utilized in stable oxygen isotope and growth increment analyses. Specimens shown are modern.

(1983). Its geographic range is from 24°N to 14°S on the Pacific coast of the Americas where water temperatures range from 19°C to 30°C (Bernard 1983; Olsson 1961) As mentioned above, no *T. procerum* were present in the Siches assemblage; however, this species was present in other archaeological assemblages (Ostra Base Camp). *T. procerum* functions well as a recorder of SST changes due to its subtidal habitat beyond the influence of freshwater influx. It is important as an environmental indicator (Nicholas 1996). This study analyzes oxygen isotope data from two modern specimens and two archaeological specimens (Ostra Base Camp) of *T. procerum*.

CHAPTER 3

METHODS

3.1. Stable Isotopes in Archaeology

Stable isotopes have been used in archaeology not only to determine seasonality of shellfish harvesting and site occupation, but also changing environmental conditions which affect human behavior. Shackleton (1973) applied stable isotope analysis to modern and archaeological shells from South Africa. He analyzed the oxygen isotope content of *Patella tabularis* and *Perna perna* in order to conclude that there is no difference in the isotopic composition of carbonates precipitated in species living at spring low tide and mean low tide, respectively. Further analysis of archaeological *P. tabularis* from the Wilton cultural period (10,190 cal yr B.P. to 5730 cal yr B.P.) midden on the Robberg Peninsula, South Africa suggested that the shellfish were harvested in winter due to isotopic values on the growing margin similar to winter in the modern shells.

Killingley and Berger (1979) used oxygen and carbon stable isotopes to assess variances in seasonal upwelling along the California coast. Results of their analysis suggest that stable carbon isotope values in *Mytilus californianus* reflect changes in marine upwelling and stable oxygen isotopes record temperature. Results from fossil shells were similar to modern shells and suggest that an upwelling system was present along the California coast during the last interglacial at 120,000 cal yr B.P. Killingley (1981) applied the same techniques to shells from the Hubb's site shell midden near Punta Minitas, Baja California, Mexico. Though the sample was too small to be used as

an indicator of seasonality of site occupation, analysis of the $\delta^{18}O$ values of modern and archaeological California mussels suggested that the ocean near the site might have been a few degrees cooler 3000 to 2000 years ago.

Bailey et al. (1983) criticized Killingley (1981) for his use of some species without modern controls. The authors collected *Monodonta lineata* and *Patella vulgata* from the north coast of Spain. Differences in isotope ratios showed that different species provide different estimates of the same environmental conditions. They argued that the environmental tolerances and the degree of disequilibria between ambient water and mineral phases are unique to individual species. For this reason, it is important to sample modern individuals of the same species and compare modern isotope values based on instrumental data with estimated ancient values.

Glassow et al. (1994) used oxygen isotopes from *Mytilus californianus* to assess mid-Holocene ocean cooling. They compared the oxygen and carbon values of modern mussels with those excavated from site CA-SCRI-333, a midden near Forney's Cove on Santa Cruz Island. The authors concluded that the mean annual water temperature was 2.5°C cooler and annual variability was greater than present for the period 6720-6690 cal yr B.P. to 5280-5050 cal yr B.P. The annual range of oxygen isotope values from archaeological shells was greater than that of the modern shells with oxygen isotope values from archaeological shells enriched 0.5 per mil relative to modern shells. Carbon isotope values suggested that upwelling occurred during the colder months when the site was occupied. Today, upwelling occurs during the warmer months.

Kennett and Voorhies (1995) used oxygen and carbon stable isotopes to gauge changes in estuarine conditions and precipitation regimes at the Tlacuachero site along

the Acapethua estuary in southern Mexico. The authors analyzed isotopes in modern and archaeological marsh clams *Polymesoda radiata*. The range and mean oxygen isotope values measured in the modern and archaeological shells were similar, but shells from the uppermost Archaic component of the site (4500-4440 cal yr B.P.) recorded lower values than other archaeological and modern shells. The lower values indicated increased precipitation.

3.2. Theory of Growth Line Formation

Microscopic, periodic structures within molluscan shells reflect variations in the relative proportions of organic material (conchiolin) and calcium carbonate (aragonite, calcite, or vaterite). The deposition of these structures correlates well with shell movements (Pannella and MacClintock 1968). The valves of many species are closed during low tide and open during high tide. Opening and closing of the valve contributes to a high correlation between the number of increments and the number of tides to which an organism is exposed. Valve movement periodicity is most pronounced in intertidal individuals; however, subtidal species also exhibit biological rhythms with the tidal cycle (Whyte 1975).

When the valves are open (aerobic metabolism) and actively pumping, a layer is deposited that is richer in calcium carbonate relative to the adjacent shell material (Lutz and Rhoads 1977). This process is usually correlated with periods of high tide in well-oxygenated water. As the concentration of dissolved oxygen falls in the microenvironment created by closed valves (exposure at low tide), anaerobic respiratory pathways are employed, and the level of succinic acid within the extrapallial fluid rises. The acid is gradually neutralized by the dissolution of calcium carbonate in the shell

leading to increased levels of calcium cations and succinate in the extrapallial and mantle fluids. Because of decalcification, the ratio of relatively acid-insoluble organic material to calcium carbonate increases at the mantle-shell interface. With the return of oxygenated conditions and resumption of aerobic metabolism, the deposition of calcium carbonate in a region already containing organic material results in an increase in the ratio of calcium carbonate to organic material. The product of this process is one growth increment (Lutz and Rhoads 1975).

Gordon and Carriker (1978) experimented with the subtidal clam *Merceneria merceneria* and present data in support of the Lutz and Rhoads (1975) hypothesis. The authors suggest that subdaily growth increments are a result of continuous and simultaneous secretion of organic matrix and calcium carbonate during the aerobic shell-building part of the growth cycle. Decalcification during anaerobiosis affects only a portion of the newly deposited shell and the associated organic matrix. The remaining insoluble matrix resists attack by metabolic acids and remains as a residue. The new layer of calcified material secreted during aerobiosis covers the residue. At this point, the matrix is hardened by polymerization of the protein. It maintains its integrity during and after decalcification. The width of residual matrix indicates the length of time the shell was exposed to metabolic acids (e.g. the duration of valve closure).

Pannella and MacClintock (1968) provided convincing evidence of diurnal periodicities within the molluscan shell. Their study of *Merceneria merceneria* counted between 360 and 370 lines for a growth period of 368 days and between 720 and 725 lines for a growth period of 723 days. These results suggested that the growth increments were formed with a solar periodicity. Kennish (1980), in his study of *M. mercenaria*,

documents that alternating periods of shell deposition and decalcification result in growth increments indicative of a circadian rhythm. A subdaily microgrowth pattern consists of one or more diffuse organic-rich lines within a daily growth increment. The subdaily pattern is commonly encountered in intertidal clams but has also been found in subtidal specimens. Kennish and Olson (1975) suggest that the formation of subdaily patterns may be related to semidiurnal low tides as a result of valve closure during low tide exposure to light or heat.

Research on transplanted and natural populations of *M. merceneria* indicates that extremes or rapid changes in environmental conditions and other physiological stresses can preclude shell secretion for a period of 24 hours or more (Kennish 1980). During this period, decalcification takes place due to valve closure and anaerobic respiration (Crenshaw and Neff 1969, Lutz and Rhoads 1977, Gordon and Carriker 1978). Some organisms may withdraw their mantle when stressed, producing v-shaped notches (growth breaks) in the outer shell layer (Kennish and Olsson 1975, Kennish 1978). Extensive growth breaks may appear in the external shell surface as concentric growth lines, linear depressions, or rings. In cross-section, crossed lamellar structure and an increased concentration of shell organic material are associated with the region of the breaks. Other kinds of depositional breaks may appear on the exterior of the shell, but represent only a few microns of change in microstructure. These are generally not associated with crossed lamellar structure or a high organic content.

The origin of a growth break may be identified due to a unique pattern of growth increments and microstructural changes preceding and following the break (Kennish 1980). Kennish and Olsson (1975) identified seven types of growth breaks in *M.*

merceneria. Four are associated with periodic events (i.e. freeze shock, heat shock, spawning, and neap tide). The remaining three are associated with semi periodic or random events (i.e. thermal shock, abrasion, and storms). By counting daily growth increments backward from the valve margin of freshly killed specimens, it is possible to accurately date the time of formation of growth breaks (Kennish 1980, Rollins et al. 1987).

3.3. Growth Line Analysis

Deith (1983) employed growth line analysis to determine the season of shellfish collection at the shell midden in the Mesolithic site of Morton, Fife. Analysis of modern specimens of the cockle *Cerastoderma edule* suggested that increments are created with a tidal periodicity for the main growing season between 22 April and 25 September. Seasonal resolution was good for the five months of the main growing season. Winter growth of the organism was not sufficient to allow internal classification such as early or late winter. Archaeological shells that demonstrated clear records of complete annual growth cycles were used to determine similarity in growing season between modern and Mesolithic shells. Dieth determined the season of collection and season of occupation by the arrangement of growth increments at the growing margin. Results suggested a predominately winter collection (78.6%) with a brief episode of collection around June or July.

Studies of the environmental effects on microgrowth structure suggest that shell midden analyses may estimate variations in marine temperature, storm events, and the length of seasons. Microgrowth analysis of individuals excavated from shell middens which accurately record changes in microenvironment conditions can be used to

determine the season a mollusk is harvested, age of the harvested mollusk, season of site occupation, and whether or not the clam was harvested while alive for food or dead for the use of its shell as jewelry (Koike 1980). Rollins et al. (1987) incorporated stable isotope analysis and growth increment analysis of modern *T. procerum* from Chimbote, Peru and *C. subrugosa* from Tumbes, Peru collected in 1984 following the 1982-83 ENSO. The authors concluded that the stable isotope values of *T. procerum* and the growth perturbations of *T. procerum* and *C. subrugosa* track environmental changes associated with ENSO.

3.4. Method of Growth Increment Analysis in this Study

Growth increment counts of *C. subrugosa*, *A. tuberculosa*, *P. ecuatoriana*, and *T. procerum* were completed on digital photo mosaics constructed from acetate peels. The preparation of acetate peels is outlined in Kennish et al. (1980). Individual valves were cut with a water-cooled Felker rock saw using a 6" MK-1000 Saber diamond lapidary blade with a rim width of .012. Valves were cut along the transect (axis of maximum growth) established by Nicholas (1996) during her collection of the stable isotope data. The objective was to maximize the number of stable isotope samples visible in the cross-section.

After cutting, the cross-sections were ground using 220, 320, and 600 grit silicon-carbide paper adhered to a glass plate. Following grinding, the shell cross-sections were polished with 5.0 micron Buehler Aluminum Oxide powder, Mager Scientific 1.0 micron Alpha C alumina powder, and 0.3 micron Buehler Micropolish II Deagglomerated Alpha alumina powder. The powders were mixed with water in order to create a thick paste. The shells were then wiped clean and placed in a beaker of acetone. The beaker was

placed in a Fisher Scientific FS5 dual action ultrasonic cleaner for 1.5 minutes in order to remove any remaining alumina paste. Shells were allowed to dry at room temperature and humidity for two days.

After polishing and drying, cross-sections were etched by immersing them in 5% HCl. Etching times varied according to species. Laboratory trials with modern specimens of *T. procerum*, *C. subrugosa*, and *A. tuberculosa* determined that the optimum etching times for *T. procerum* and *C. subrugosa* were two minutes with an optimum etching time of two minutes and thirty seconds for *A. tuberculosa*. No modern *P. ecuatoriana* were available for laboratory trials. After etching ancient *P. ecuatoriana* for 2 minutes, acetate peels suggested that the shells were over-etched. Therefore, all specimens of *P. ecuatoriana* were ground, polished, and etched again for duration of one minute. One minute etching time provided the greatest clarity in the *P. ecuatoriana* acetate peels. Immediately following the etching process, all shells were rinsed with deionized water and allowed to dry for two days.

Acetate peels were produced by flooding the etched shell surface with acetone and applying the flooded surface to a sheet of acetate. Acetone is quite volatile and quickly vaporizes so the process must be done quickly. The acetate used in this study was purchased at Structure Probe, Inc. Combinations of both thick (#1857) and thin (#1856) sheets were used. There was no difference in the optical quality of the peel; however, thin replicating sheets tended to wrinkle upon contact with the acetone and in some cases, the acetone completely dissolved the acetate. While applying the flooded shell surface to the acetone, the shell was slowly rolled onto the acetate sheet with firm pressure in order

to reduce air bubbles. Care was taken to avoid movement because movement will destroy the replication of shell microstructure.

Completed acetate peels were mounted between two glass microscope slides and viewed with a Nikon SMZ-U microscope with conventional photographic capabilities at 56X magnification. Photographing of the acetate peel cross-sections began at the ventral margin and progressed toward the umbo while using Kodachrome ISO 64 color slide film. Color slides were digitized using a slide scanner. Digital photomosaics were constructed with Adobe Photoshop 6.0 software. All growth increment counts were completed on the digital photomosaic soft copies.

Growth line counts on high intertidal bivalves stress daily periodicities whereas counts on low intertidal and subtidal bivalves stress semi-daily periodicities. (Rollins et al. 1987). Daily lines have been recognized in venerids such as *M. merceneria*, *Meretrix lusoria*, and *Chione* spp. (Koike 1973, Pannella and MacClintock 1968). Growth line counts in *Chione subrugosa* and *Trachycardium procerum* suggest that *C. subrugosa* exhibits prominent daily lines and *T. procerum* exhibits subdaily lines of equal strength (Rollins et al. 1987). In order to obtain growth increment counts from *P. ecuatoriana* this intertidal species is presumed to exhibit daily growth periods similar to *C. subrugosa.*

Periodic growth (i.e. daily or subdaily) of *A. tuberculosa* is unknown and literature pertaining to the species is thin. Nevertheless, a synthesis of some commercial fisheries research may give an indication. In their study of *A. tuberculosa* populations in Sierpe-Térraba, Costa Rica, Campos M. et al. (1990) suggest a minimum capture length of 4.4 cm for commercially harvested *A. tuberculosa.* Rapid growth of the species results in a commercial length within 18-24 months of birth (Campos et al.1990, Martín 1988).

If the commercially acceptable length is 4.4 cm and this length is reached in 18-24 months, then modern *A. tuberculosa* specimens of 4.4 cm in length should provide a growth increment count of approximately 2 years.

Assuming prominent subdaily growth lines, an increment count of the last 4.4 cm of growth in *A. tuberculosa* AT 5-1 provides a chronology from July 7, 1995 to December 27, 1994. Assuming daily growth lines in the same shell, an increment count of the last 4.4 cm of growth provided a chronology from July 7, 1995 to July 12, 1992. Assuming subdaily growth lines indicates that 4.4 cm of growth in AT 5-1 occurred in approximately 18 months, rather than 36 months if daily growth lines are assumed. Furthermore, if growth lines are assumed subdaily, growth increment counts of the last 30 mm of specimen AT 5-2 provide a chronology from July 7, 1995 to June 15, 1994. The last 30 mm of growth occurred in approximately 11 months. These growth rates agree with those derived from Campos et al. (1990) and Martín (1988). The agreement indicates prominent subdaily growth lines in *A. tuberculosa*.

3.5. Correlation of Oxygen Isotope Data with Ocean Temperature and Salinity

Growth increment counts from the ventral margin (time of death) to the umbo in modern specimens of *C. subrugosa* PT 1-14 (death = 4/16/84) and 2PT1 (death = 4/16/84), *A. tuberculosa* AT 5-1 (death = 7/7/95) and AT 5-2 (death = 7/7/95), and *T. procerum* TP1-12 (death = 4/18/84) and 3TP1-1b (death = 7/7/95) provided a time correlation for oxygen isotope ratios. This correlation was accomplished by counting the number of growth increments between the ventral margin and the first isotope sample, the number of increments contained in the first isotope sample, and the number of increments between and contained within each subsequent sample (**FIGURES 4-7**).

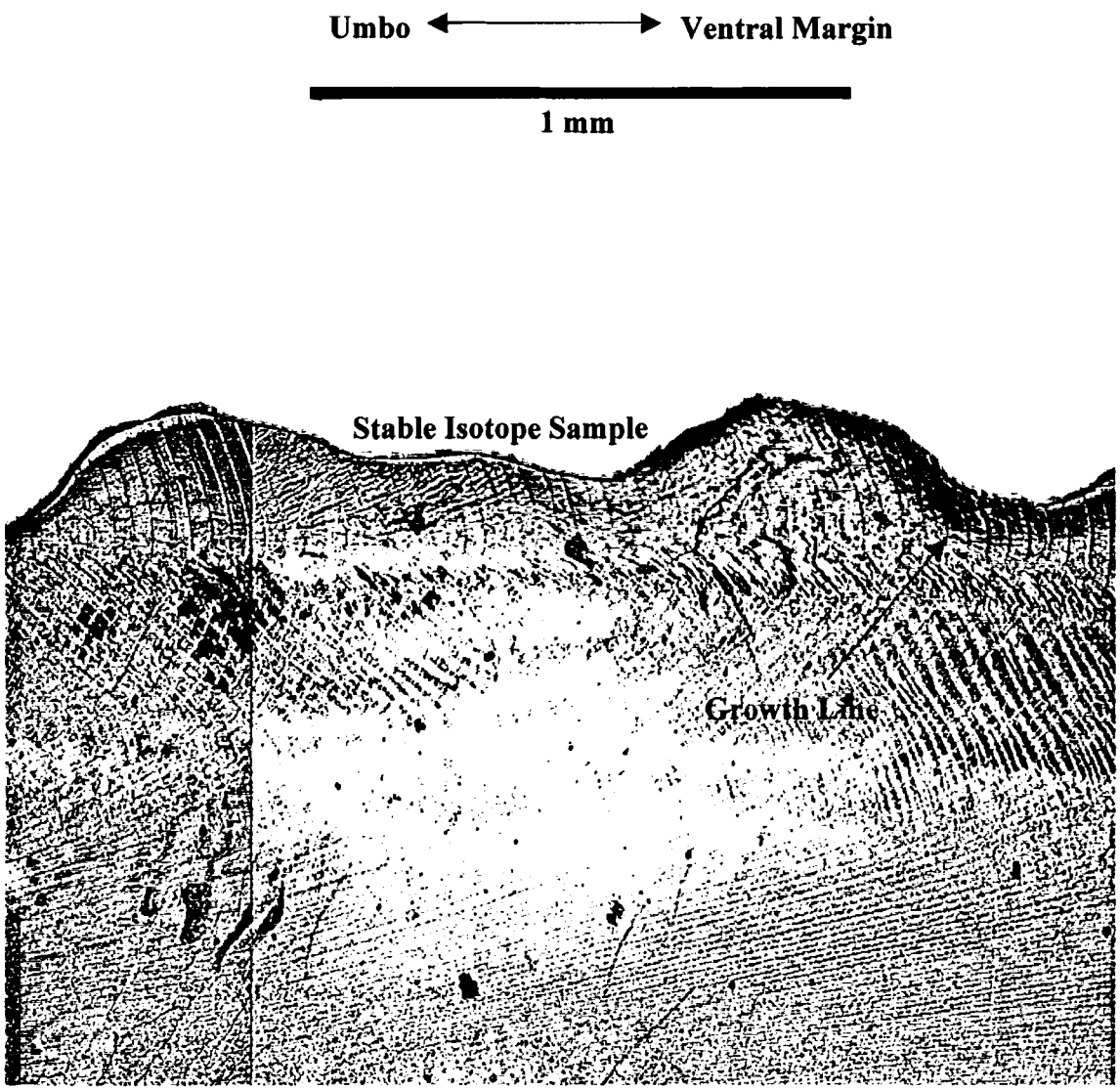

FIGURE 4: Daily growth in *C. subrugosa* 2PT1. One daily growth increment consists of one dark organic-rich band and one light carbonate-rich band. Subdaily growth structures exist as faint organic-rich lines within a larger carbonate-rich band.

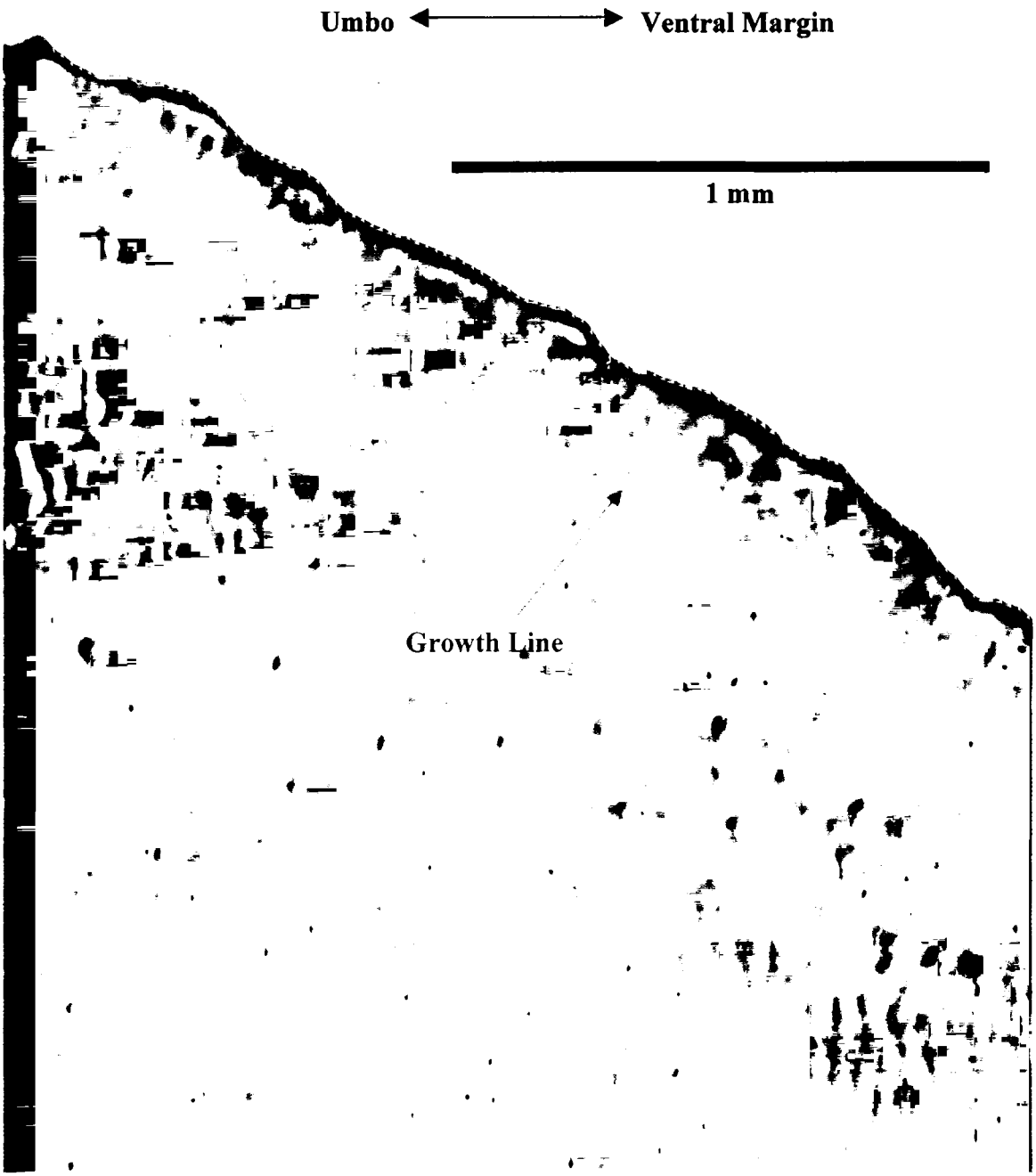

FIGURE 5: Daily growth in *P. ecuatoriana* PV 7-19 IIB4(a). One daily growth increment consists of one dark organic-rich band and one light carbonate-rich band.

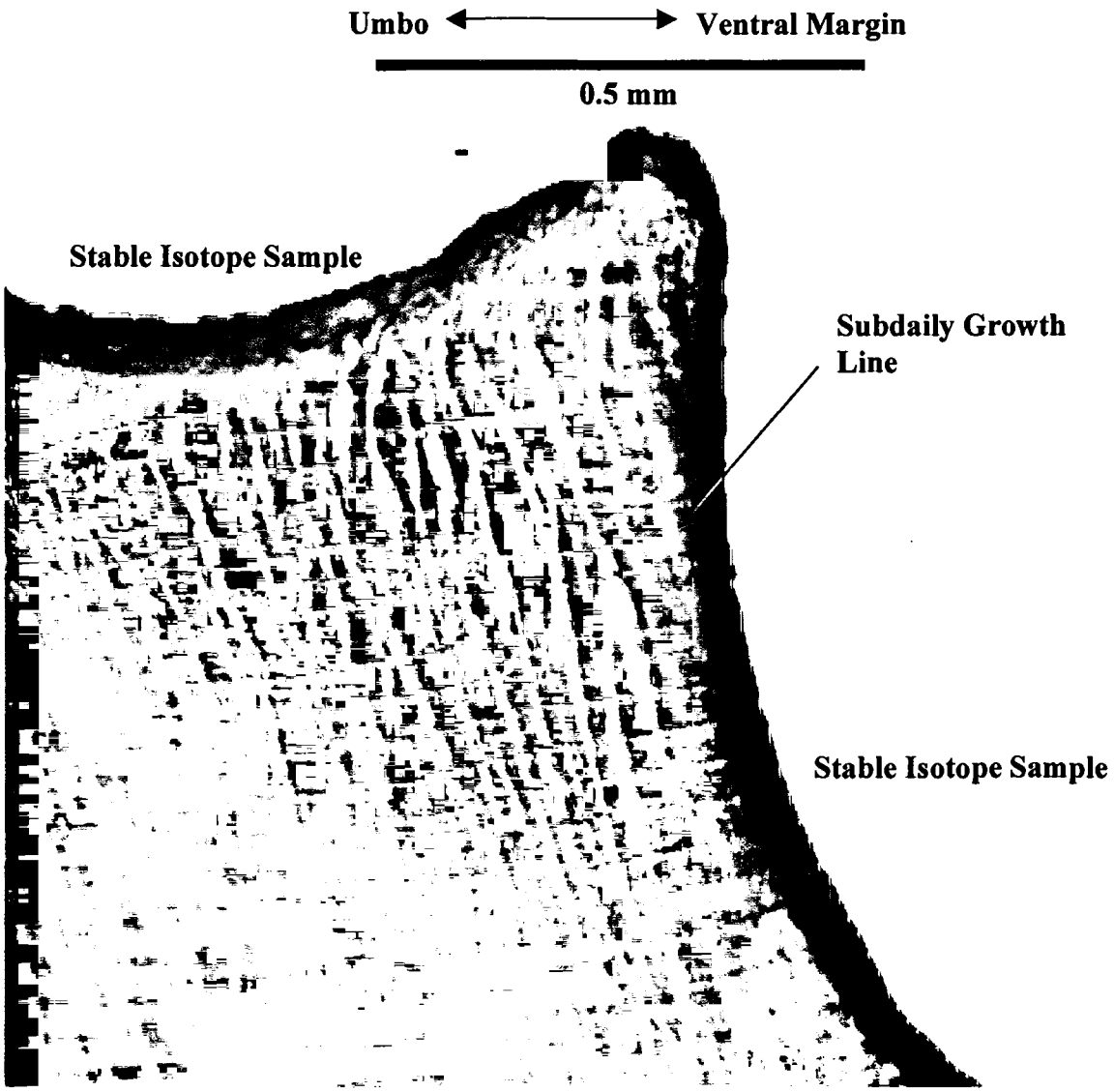

FIGURE 6: Subdaily growth in *A. tuberculosa* PV 7-19 IIB3(a). One daily growth increment consists of two dark organic-rich bands and two light carbonate-rich bands.

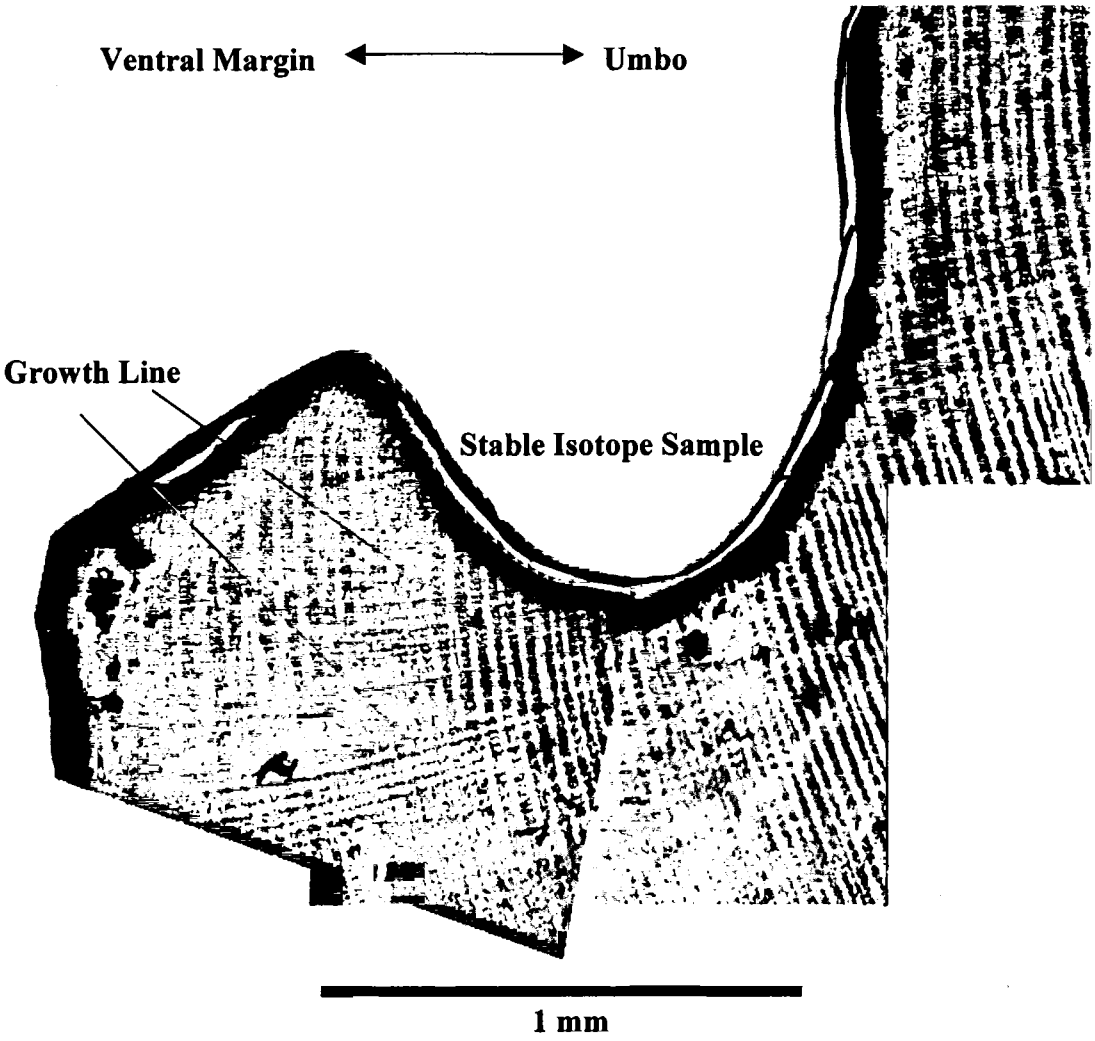

FIGURE 7: Subdaily growth in *T. procerum* TP 1-12. One daily growth increment consists of two dark organic-rich bands and two light carbonate-rich bands.

Once dates for the stable isotope samples were established, the values were correlated with observed ocean temperature and salinity data provided by the NOAA-CIRES Climate Diagnostics Center, Boulder, Colorado, USA. Ocean temperature data associated with modern specimens are based on the NCEP Pacific Ocean Analysis at the grid coordinates 9°S 80°W (Chimbote, Peru) and 3.5°S 81.5°W (Puerto Pizarro, Peru) for the years 1980-1995. Salinity data for both sites are NOAA-NCEP CMB Pacific monthly salinities. Additionally, comparative precipitation data for 3.75°S 81.25°W (Puerto Pizarro, Peru) are monthly means from the CPC Merged Analysis of Precipitation for the years 1980-1995. The complete process of time correlation for temperature and salinity data is outlined in **Appendix A**.

3.6. Paleotemperature Determination

Salinity and $\delta^{18}O$ data can be used to calculate temperature of the water in which biogenic calcium carbonate is secreted. Perrier et al. (1994) used the temperature equation developed by Epstein et al. (1953) in order to evaluate temperature variation at Pampa Las Salinas and Salinas de Chao. Nicholas (1996) used the equation of Horibe and Oba (1972) to evaluate temperature variation at Siches and Ostra. Rollins et al. (1987) used Grossman and Ku's (1981) equation to evaluate the relationship between SST and $\delta^{18}O$ in modern *C. subrugosa* and *T. procerum*.

The oxygen isotope composition of calcium carbonate differs from that of water when precipitated under equilibrium conditions. The equilibrium constant for the isotope exchange reaction can be written as:

$$\text{(Eq. 1)}\quad K = \frac{[CaC^{18}O_3][H_2{}^{16}O]^3}{[CaC^{16}O_3][H_2{}^{18}O]^3} \quad \text{or} \quad \text{(Eq.2)}\quad K = \frac{(CaC^{18}O_3/CaC^{16}O_3)}{(H_2{}^{18}O/H_2{}^{16}O)^3}.$$

Equation 2 of the equilibrium constant is equal to the $^{18}O/^{16}O$ ratio in the carbonate phase divided by the $^{18}O/^{16}O$ ratio in the water, which is α. The fractionation factor α is given by:

$$\alpha_{CaCO_3\text{-}H_2O} = \frac{(^{18}O/^{16}O)_{CaCO_3}}{(^{18}O/^{16}O)_{H_2O}}$$

Thus, K = α. Since the fractionation factor (α) is temperature-dependent, the isotopic composition of oxygen in equilibrium with calcium carbonate is also temperature-dependent. The isotopic composition of seawater is not affected because the amount of water is quite large relative to the amount of carbonate equilibrated with it (Faure 1987).

Craig (1965) modified the temperature equations of Epstein et al. (1953), which expressed a relationship between temperature of the water and δ-values of calcite and water at equilibrium. Craig established the equation: $T(°C) = 16.9 - 4.2\ (\delta_{calcite} - \delta_{water}) + 0.13(\delta_{calcite}-\delta_{water})^2$, where $\delta_{calcite}$ is the value of CO2 gas evolved from calcite by treating with 100% phosphoric acid at 25°C, and δ_{water} is the δ-value of CO_2 equilibrated with water at the same temperature. The isotopic compositions of both calcite and water are expressed as variables in this equation. It is necessary to subtract the oxygen isotope value of the ambient water (a function of salinity) from the oxygen isotope value of the biogenic carbonate in order to obtain $\delta^{18}O_c$, a salinity-corrected value (Faure 1987).

Paleotemperature determination is limited by the fact that the calcium carbonate secreted by some organisms is not in isotopic equilibrium with water. In cases such as this, $\delta^{18}O$ is not a function of temperature alone (Wilber 1972). The disequilibria may be due to the influence of respiratory CO_2 which exchanges oxygen with bicarbonate in solution (Faure 1987). These influences can produce inconsistencies in $\delta^{18}O$ data (McConnaughey 1986). For example, the foram *H. elegans* varies perhaps 1-2 per mil at

a given temperature (Grossman 1984). A similar effect occurs in corals, which usually precipitate aragonite skeletons far from isotope equilibrium with seawater (McConnaughey 1986).

3.7. A Temperature Equation for *T. procerum*

A species-specific temperature equation for *T. procerum* was developed by Model II linear regression of a pooled sample of all modern *T. procerum* used in this study. The pooled sample consisted of oxygen isotope samples from 3TP1-1b, TP 1-12, TP 1-12 (Houk)* correlated with NCEP ocean temperatures and salinities by growth increment counts. The 1982-83 ENSO temperature maximum probably forced *T. procerum* to their lowest depth tolerance, reported to be –15 m (Sandweiss, personal communication). Because of this, $\delta^{18}O_{shell}$ values from modern *T. procerum* collected in both 1984 and 1995 were correlated with NCEP temperatures at –15 m depth. Stable oxygen isotope ratios were corrected for salinity and the oxygen isotope content of the water in which the specimens reportedly lived ($\delta^{18}O_c = \delta^{18}O_{shell} - \delta^{18}O_{water}$). The equation of the Model II regression line (**FIGURE 8**) is $T(^{o}C) = 14.67 - 4.76(\delta^{18}O_c)$. The estimate (r) of the product-moment correlation coefficient for the pooled sample equals –0.86.

The error bounds of the Model II regression contain inherent uncertainty; therefore, only a conservative estimate of the true functional relationship is possible (Laws 1997:69). The true slope of the functional relationship between NCEP ocean temperature and $\delta^{18}O_c$ lies somewhere between the expectation values (E(B) and 1/E(D)) of the slopes of the two Model I regression lines at least 95% of the time. This geometric mean method of Model II linear regression does not give an unbiased estimate of the true

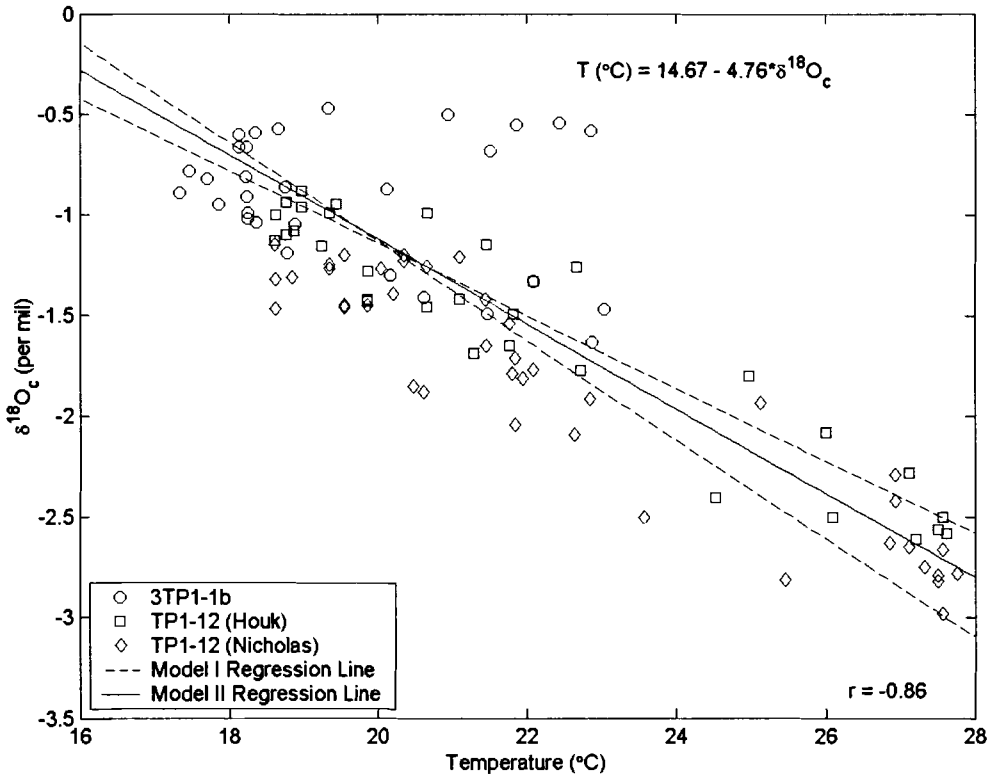

FIGURE 8: Results of the Model II linear regression of a pooled sample containing all modern *Trachycardium procerum* utilized in this study. The equation of the Model II regression line is: $T(°C) = 14.67 - 4.76(\delta^{18}O_c)$. The true slope of the relationship between temperature and $\delta^{18}O_c$ lies between the expectation values E(B) and 1/E(D) of the slopes of the two Model I regression lines 95% of the time.

slope, and the magnitude of error in both the ocean temperature data (due to differences between open ocean conditions and microenvironments) and the $\delta^{18}O_c$ values (due to differences in open ocean salinity and microenvironments) cannot be ascertained.

Chapter 4

RESULTS

4.1. Growth Increment and Stable Isotope Analyses of Modern *T. procerum*

Growth increment and stable isotope (Nicholas 1996) analyses of *T. procerum* specimens 3TP1-1b and TP 1-12 provided chronologies from July 7, 1995 to July 30, 1993 and from April 18, 1984, to April 10, 1982, respectively. An additional chronology constructed for a set of isotope samples extracted from specimen TP 1-12 during this study ranged from April 18, 1984 to May 10, 1982. This new dataset is denoted TP 1-12 (Houk)*. Specimen TP 1-12 exhibited a growth perturbation (**FIGURE 9**), which occurred approximately February 14, 1983. Similar perturbations were observed by Rollins et al. (1987) in specimens of *T. procerum* collected from Chimbote, Peru in April of 1984. The growth perturbations result from changes in water temperature, salinity, and nutrient levels associated with the 1982-83 ENSO. The perturbation in TP 1-12 did not result in a complete growth hiatus and does not appear to affect the accuracy of the count, which is supported by the high correlation between NCEP ocean temperature data and $\delta^{18}O_{shell}$.

4.1.1. *T. procerum* 3TP1-1b

T. procerum 3TP1-1b was collected in July 1995 at Chimbote, Peru (9°S) (Nicholas 1996). Monthly NCEP ocean temperature and salinity data (-15 m) for the grid coordinate 9°S 80°W show the mean monthly ocean temperature in 1995 to be 19.64°C with a minimum of 17.33°C, and a maximum of 23.05°C. The correlation between

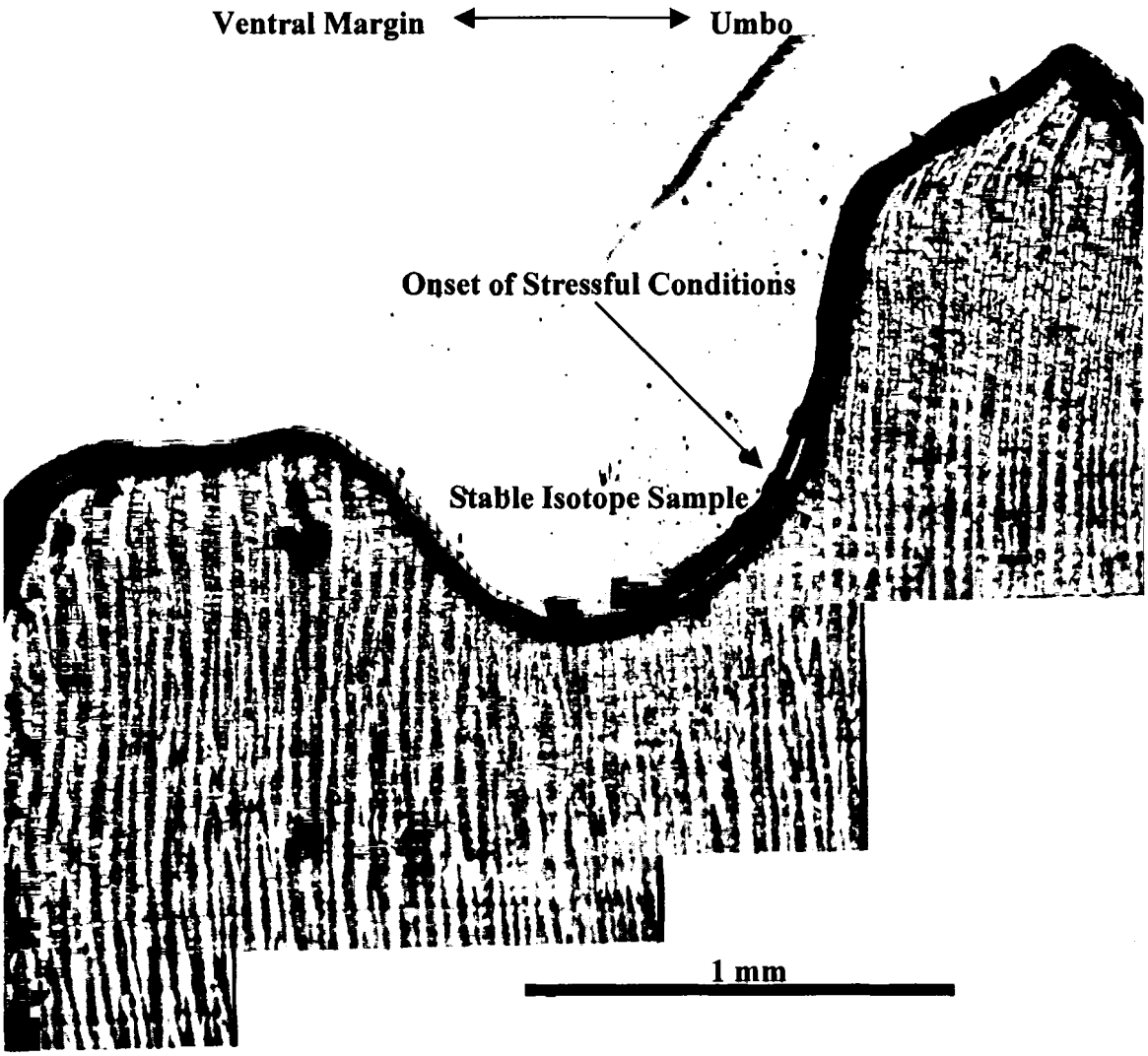

FIGURE 9: Presumed onset of environmental stress in *T. procerum* TP 1-12. Onset of environmental stress is approximately February 14, 1983. Growth increments become nearly horizontal. Rollins et al. (1987) provided a similar description for growth perturbations in *T. procerum* from the same collection made in 1984 at Chimbote, Peru.

$\delta^{18}O_{shell}$ and NCEP ocean temperature at –15 m is shown in **FIGURE 10,** Panel A. The estimate (r) of the product-moment correlation coefficient equals –0.29. Unfortunately, the correlation is not significant at the 90% confidence interval (df = 28) (Laws 1997, Appendix C).

The time series of the stable oxygen isotope ratios in the shell ($\delta^{18}O_{shell}$) and temperatures predicted by the Model II regression line are shown in **FIGURE 11**. $\delta^{18}O_{shell}$ values range from 0.11 per mil to –1.05 per mil. The temperature equation determined by Model II linear regression underestimates NCEP ocean temperature maxima and overestimates NCEP ocean temperature minima. Temperatures predicted by the regression line during the seasonal maxima of February 1994 and January 1995 are underestimated by 5.76°C and 1.62°C, respectively. This same equation overestimates the seasonal minimum in August 1994 by 1.51°C.

The positive covariance of $\delta^{18}O_{shell}$ and NCEP ocean temperature between November 1993 and April 1994 conflicts with expected results. It is apparent that an event occurs during this time range that affects the oxygen isotope content of the shell and cannot be corrected by the $\delta^{18}O_c$ term in the Model II regression equation. Furthermore, there is no visible evidence of growth perturbation due to storms, spawning events, or temperature shock.

4.1.2. *T. procerum* TP 1-12

T. procerum specimen TP 1-12 was collected at Chimbote, Peru (9°S) in April 1984. NCEP temperature and salinity data (-15 m) for grid coordinate 9°S 80°W show the mean monthly temperature in 1984 to be 20.10°C with a minimum of 18.10°C and a maximum of 22.44°C. The relationship between $\delta^{18}O_{shell}$ and NCEP ocean temperature

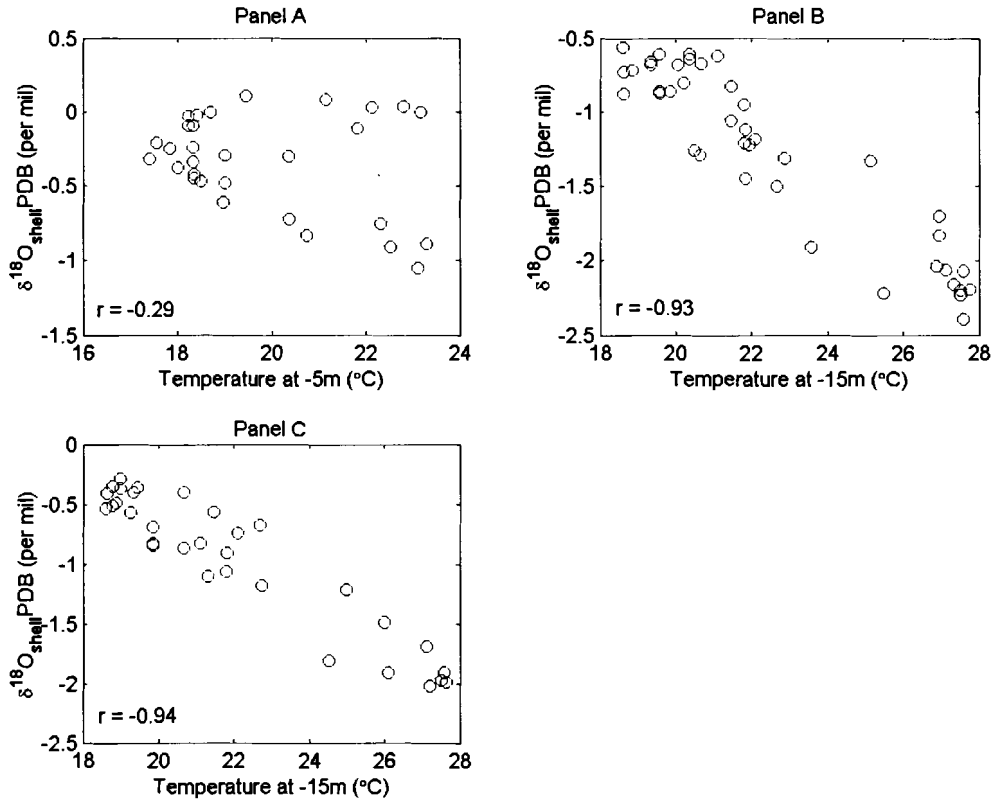

FIGURE 10: NCEP ocean temperature versus $\delta^{18}O_{shell}$ in all modern *T. procerum* specimens. Panel A: NCEP ocean temperature (-15 m) versus $\delta^{18}O_{shell}$ in *T. procerum* 3TP1-1b. Panel B: NCEP ocean temperature (-15 m) versus $\delta^{18}O_{shell}$ in *T. procerum* TP 1-12. Panel C: NCEP ocean temperature (-15 m) versus $\delta^{18}O_{shell}$ in *T. procerum* TP 1-12 (Houk)*.

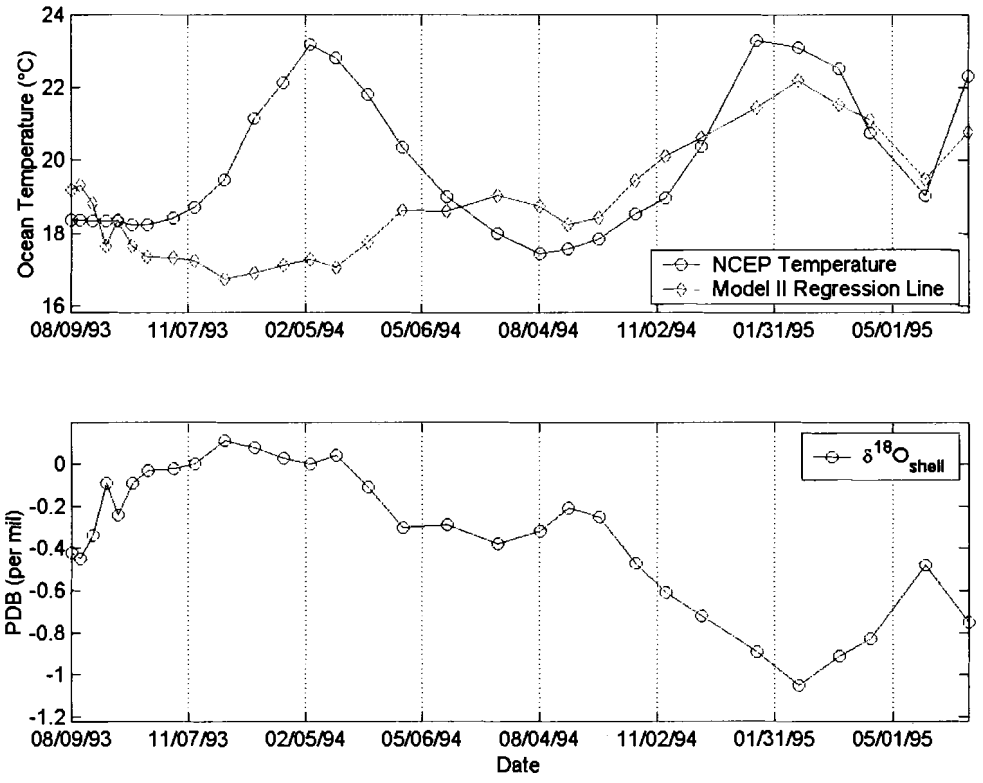

FIGURE 11: Time series of $\delta^{18}O_{shell}$ values in *T. procerum* 3TP1-1b and ocean temperatures estimated by the Model II regression line. Time scale is identical for both panels. NCEP ocean temperatures at –15 m are included for comparison.

at –15 m is shown in **FIGURE 10**, Panel B. The estimate (r) of the product-moment correlation coefficient equals –0.93. The correlation is significant at the 99% confidence level (df = 39) (Laws 1997, Appendix C). The predicted values of the Model II regression temperature equation (**FIGURE 12**) closely approximate NCEP ocean temperatures. The Model II regression line equation overestimates the NCEP temperature maximum during the 1982-83 ENSO by 0.14°C. During the minima of July 1982 and October 1983, the regression line equation overestimates NCEP temperature by 1.55°C and 2.98°C, respectively. $\delta^{18}O_{shell}$ values range from –0.56 per mil to –2.39 per mil (**FIGURE 12**).

The time series developed by growth increment analysis of the most recent set of samples extracted from this specimen, denoted TP 1-12 (Houk)* ranges from May 10, 1982 to April 18, 1984. The relationship between $\delta^{18}O_{shell}$ and NCEP ocean temperature at –15 m is shown in **FIGURE 10**, Panel C. The estimate (r) of the product-moment correlation coefficient equals –0.94. The correlation is significant at the 99% confidence level (df = 30) (Laws 1997, Appendix C). $\delta^{18}O_{shell}$ values range from –0.29 to –2.02. Temperatures estimated by the Model II regression equation (**FIGURE 13**) approximate NCEP ocean temperatures. The Model II regression equation underestimates the 1982-83 ENSO maximum by 0.67°C. The minima in July 1982 and October 1983 are overestimated by 0.82°C and 0.94°C, respectively.

The two oxygen isotope analyses of *T. procerum* TP 1-12 by Nicholas (1996) and this author provide data curves of similar shapes, but they differ quantitatively. **FIGURE 14** compares the time series of the oxygen isotope ratios from both analyses. The mean $\delta^{18}O_{shell}$ value of the Nicholas (1996) analysis is –1.27 per mil whereas the mean value of

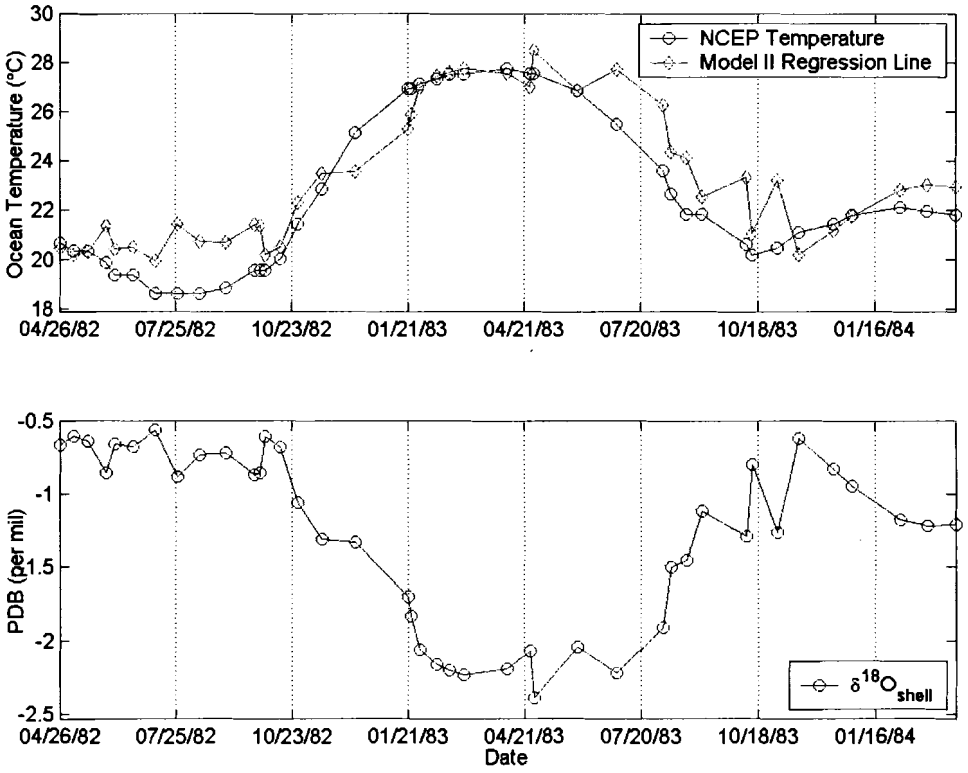

FIGURE 12: Time series of $\delta^{18}O_{shell}$ values in *T. procerum* TP 1-12 and ocean temperatures estimated by the Model II regression line. Time scale is identical for both panels. NCEP ocean temperatures at –15 m are included for comparison.

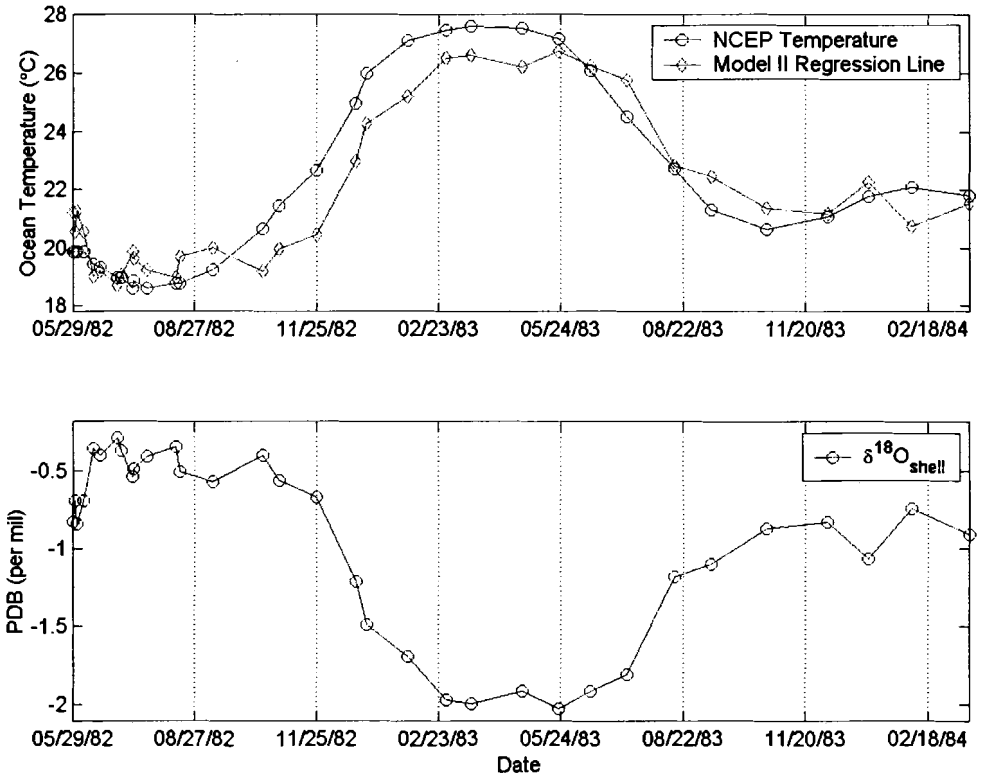

FIGURE 13: Time series of $\delta^{18}O_{shell}$ values in *T. procerum* TP 1-12 (Houk)* and ocean temperatures estimated by the Model II regression line. Time scale is identical for both panels. NCEP ocean temperatures at –15 m are included for comparison.

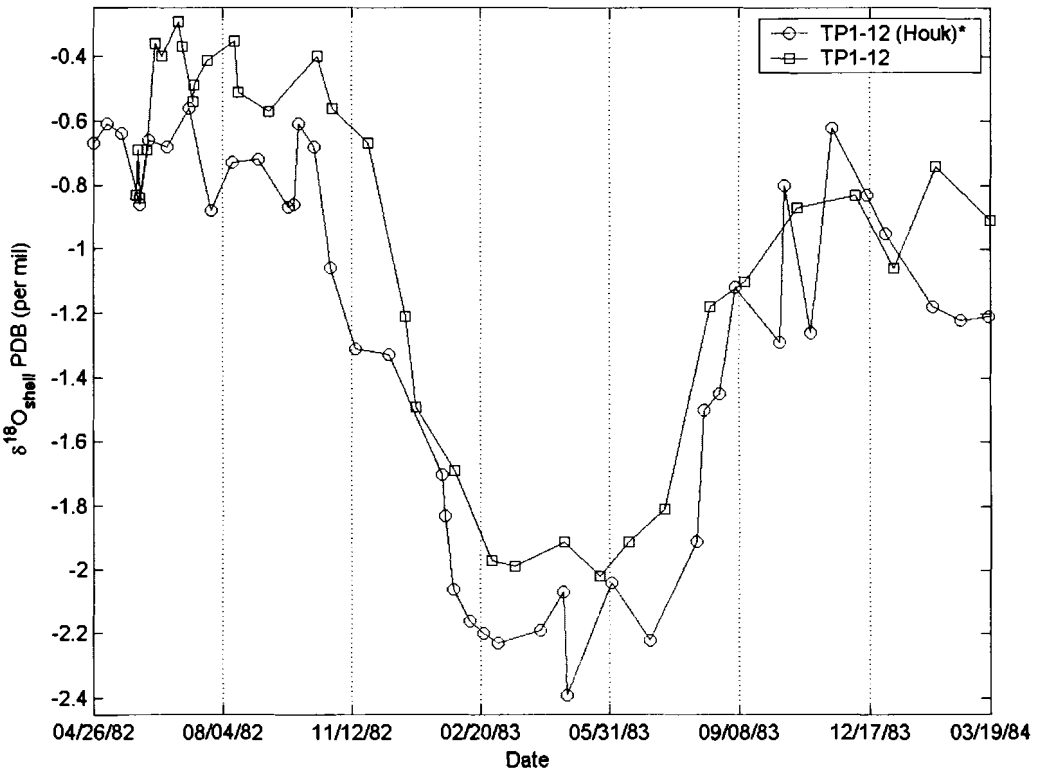

FIGURE 14: Comparison of $\delta^{18}O_{shell}$ time series from *T. procerum* TP 1-12 (Houk)* and *T. procerum* TP 1-12.

the analysis performed by this author is –0.96 per mil. Grossman (1984) identified variations in oxygen isotope ratios in biogenic carbonates of +/- 0.2 per mil. These variations are due to isotopic disequilibria induced by living organisms. The differences in the mean values of the two analyses might be attributed to such disequilibria. Regardless of the differences in the mean values, the oxygen isotope values of both analyses are strongly correlated with NCEP ocean temperature.

4.2. Growth Increment and Stable Isotope Analyses of Modern *C. subrugosa*

Two modern specimens of *C. subrugosa*, PT 1-14 and 2PT1, were used in this study. Both 2PT1 and PT1-14 were sampled by Nicholas in 1996, and 2PT1 was sampled a second time by this author in 2001. Both shells were collected in 1984 from Puerto Pizarro, Peru (3.3°S). Puerto Pizarro lies near the Tumbes River estuary in the Panamic Biogeographic Province (Nicholas 1996). The location and intertidal habitat of *C. subrugosa* specimens suggest that the organisms are not only subjected to periods of anaerobic respiration during exposure at low tide, but also freshwater discharge in the Tumbes River estuary.

Specimen PT1-14 lacks a growth break indicative of environmental perturbations accompanying the 1982-83 ENSO; however, specimen 2PT1 exhibits a growth break with an onset of approximately July 3, 1983 (**FIGURE 15**). The perturbation is characterized by blunting of the shell and an increase in cross-lamellar density. Growth lines are closely spaced and have equal strength. These characteristics agree with ENSO growth breaks described in analyses of *Chione subrugosa* in the same collection from Tumbes, Peru (Rollins et al. 1987). Subdaily growth lines, characterized by faint organic

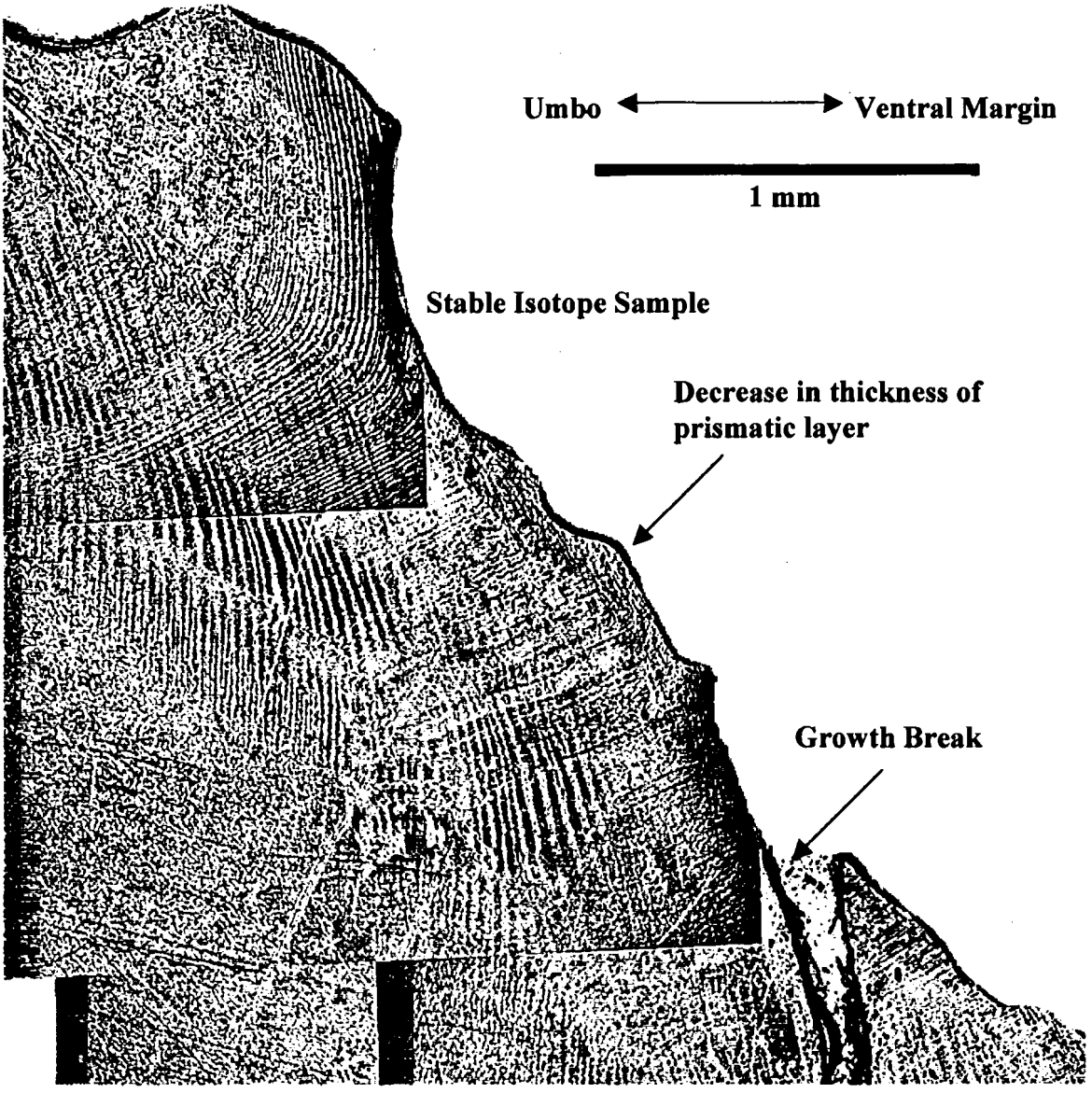

FIGURE 15: Area of growth perturbation in *C. subrugosa* 2PT1.

layers, are often evident near the umbo region where growth is rapid during youth and daily increments are thickest (Pallant 1990; Rollins et al. 1987).

4.2.1. *Chione subrugosa* PT1-14

C. subrugosa specimen PT1-14 provides a chronology from January 22, 1984 to June 29,1980. The maximum NCEP ocean temperature (-5 m) associated with the 1982-83 ENSO (29.26°C) occurs on the week of April 12,1983. The minimum NCEP ocean temperature for the range of the time series is 19.34°C with a monthly mean temperature of 23.74°C. The correlation between NCEP temperature and $\delta^{18}O_{shell}$ is shown in **FIGURE 16,** Panel C. The estimate (r) of the product-moment correlation coefficient equals -0.19. This value is insignificant at the 90 % confidence interval (df = 28) (Laws 1997, Appendix C).

The time series of $\delta^{18}O_{shell}$ values as well as comparative NCEP ocean temperature and CPC Merged Analysis precipitation data are shown in **FIGURE 17.** $\delta^{18}O_{shell}$ values range from –1.27 per mil to –2.48 per mil. $\delta^{18}O_{shell}$ values negatively covary with the NCEP SST maximum associated with the 1982-83 ENSO. This negative covariance is regardless of an increase in precipitation. Alternatively, $\delta^{18}O_{shell}$ positively covaries with NCEP SST during the seasonal maximum of February 1982. The positive covariance probably results from an increased level of precipitation and freshwater discharge in the Gulf of Guayaqil. Thus, the 1982-83 ENSO temperature change was great enough to overwhelm precipitation effects, whereas precipitation effects during the seasonal SST maximum of February 1982 overwhelmed the temperature signal.

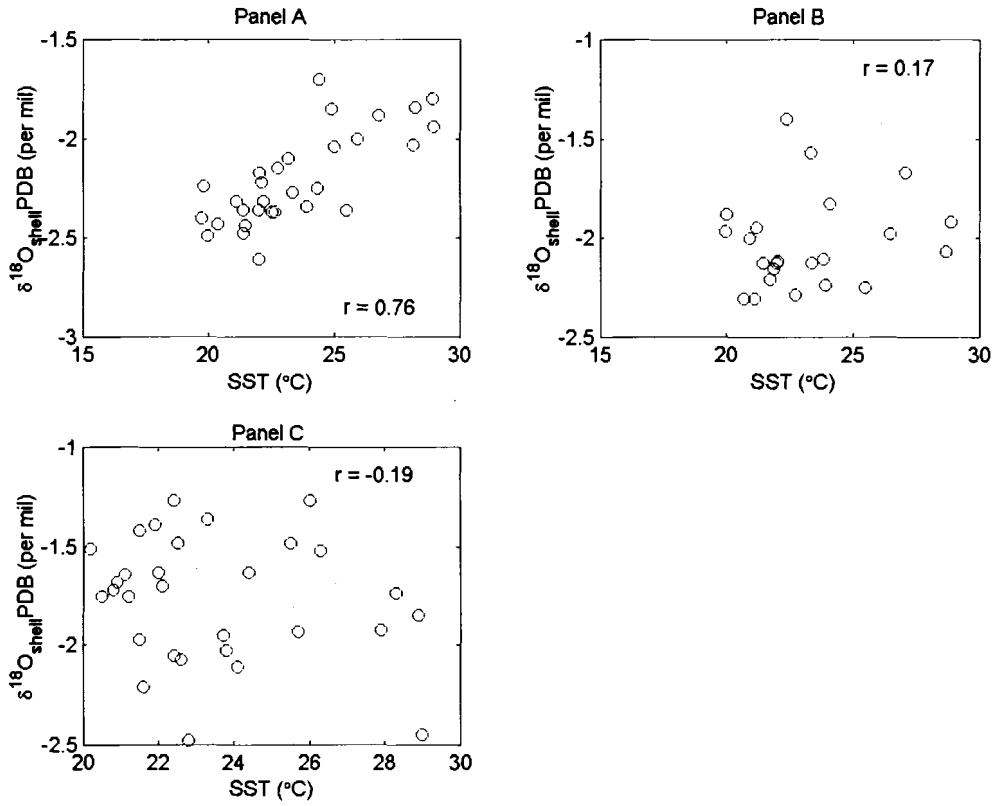

FIGURE 16: NCEP SST versus $\delta^{18}O_{shell}$ in all modern *C. subrugosa* specimens. Panel A: NCEP SST versus $\delta^{18}O_{shell}$ in *C. subrugosa* 2PT1. Panel B: NCEP SST versus $\delta^{18}O_{shell}$ in *C. subrugosa* 2PT1 (Houk)*. Panel C: NCEP SST versus $\delta^{18}O_{shell}$ in *C. subrugosa* PT1-14.

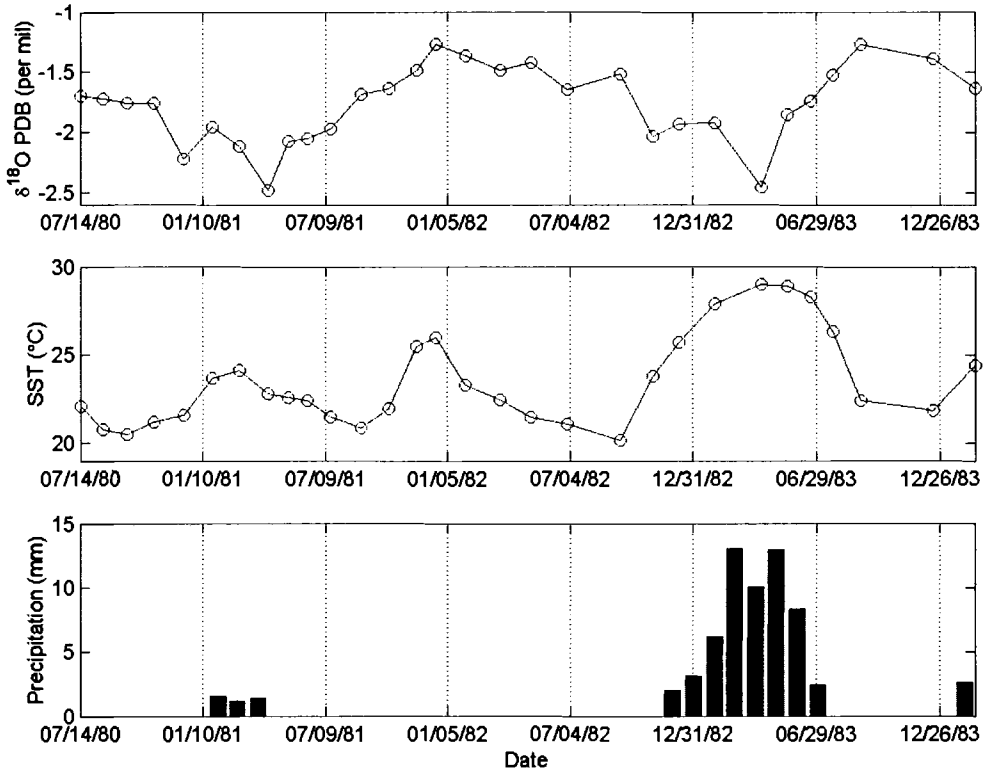

FIGURE 17: Time series of $\delta^{18}O_{shell}$ values in *C. subrugosa* PT1-14. Time scale is identical for all panels. NCEP SST and CPC precipitation data are included for comparison.

4.2.2. *Chione subrugosa* 2PT1

The chronology constructed for *C. subrugosa* 2PT1 ranges from November 7, 1984 to October 14, 1981. The mean NCEP SST for this period is 23.27°C. The maximum NCEP SST (29.26°C) occurs on the week of April 12,1983. The minimum NCEP SST for the time series is 19.34°C. The correlation between NCEP SST and $\delta^{18}O_{shell}$ is shown in **FIGURE 16**, Panel A. The estimate (r) of the product-moment correlation coefficient equals 0.76. This value is significant at the 99% confidence level (df = 28) (Laws 1997,Appendix C). The significant positive correlation is apparent in the $\delta^{18}O_{shell}$, NCEP SST, and CPC precipitation time series (**FIGURE 18**). $\delta^{18}O_{shell}$ values range from –1.70 per mil to –2.61 per mil. In general, $\delta^{18}O_{shell}$ values become more positive as NCEP SST increases. This positive covariance suggests that increasing levels of precipitation and a concomitant increase of freshwater flux into the Gulf of Guayaquil affect oxygen isotope values in *C. subrugosa* 2PT1.

The chronology of the second set of stable isotope samples extracted from *C. subrugosa* 2PT1 (denoted 2PT1 (Houk)*) for this study ranges from July 16, 1984 to March 31, 1981. The average NCEP SST for this time period is 23.60°C with the maximum (29.26 °C) occurring during the week of April 12, 1983. The relationship between $\delta^{18}O_{shell}$ and NCEP SST is shown in **FIGURE 16**, Panel B. The estimate (r) of the product-moment correlation coefficient equals 0.17. This value is insignificant at the 90% confidence level (df = 21) (Laws 1997, Appendix C). The time series of the $\delta^{18}O_{shell}$ values and NCEP SST show the insignificant correlation (**FIGURE 19**). $\delta^{18}O_{shell}$ values range from –1.4 per mil to –2.31 per mil. The positive covariance between $\delta^{18}O_{shell}$ and

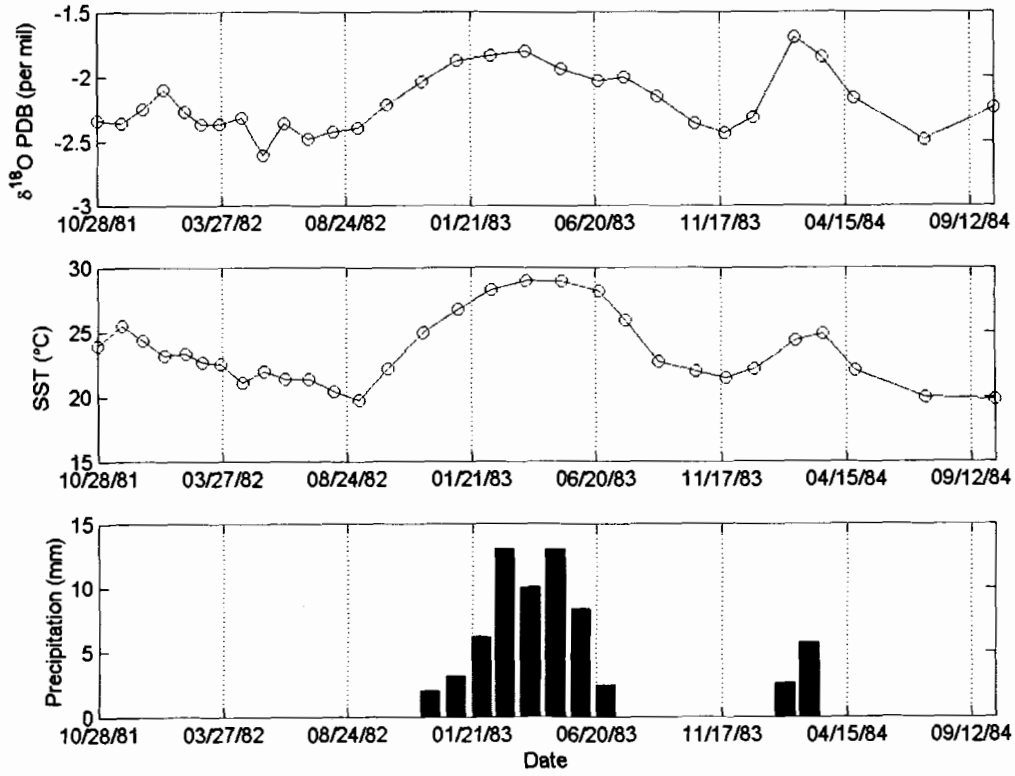

FIGURE 18: Time series of $\delta^{18}O_{shell}$ values in *C. subrugosa* 2PT1. Time scale is identical for all panels. NCEP SST and CPC precipitation data are included for comparison.

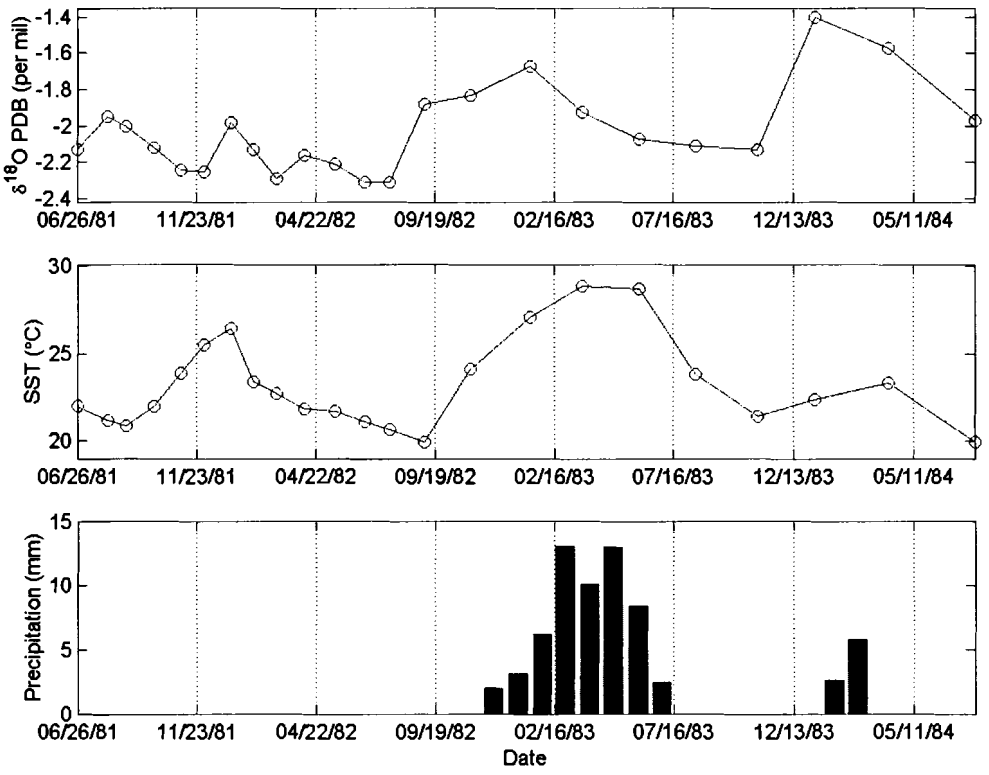

FIGURE 19: Time series of $\delta^{18}O_{shell}$ values in *C. subrugosa* 2PT1 (Houk)*. Time scale is identical for all panels. NCEP SST and CPC precipitation data are included for comparison.

NCEP SST during February to March 1984 and the 1982-83 ENSO is due once again to the increased precipitation and freshwater flux in the Gulf of Guayaquil.

The two oxygen isotope analyses of *C. subrugosa* 2PT1 by Nicholas (1996) and this author provide data curves of similar shapes; however, they differ quantitatively. **FIGURE 20** compares the time series of the oxygen isotope ratios from both analyses. The mean $\delta^{18}O_{shell}$ value of the Nicholas (1996) analysis is –2.20 per mil while the mean value of the analysis performed by this author is –2.03 per mil. The differences in these values are within the range of isotopic disequilibria described by Grossman (1984). The difference between the NCEP SST - $\delta^{18}O_{shell}$ correlation coefficients of the two sets is puzzling and suggests that errors may exist in the data due to either instrumentation, laboratory methods, environmental conditions unseen in the precipitation and temperature data, a physiological process, or miscounting of growth increments.

4.3. Growth Increment and Stable Isotope Analyses of Modern *A. tuberculosa*

A. tuberculosa AT 5-1 provides a chronology from June 21, 1995 to December 27, 1993. The NCEP SST data for grid coordinate 3°S 81°W show a mean weekly SST of 22.10°C. The maximum weekly temperature (26.53°C) occurs during the week ending February 7, 1995, and the minimum weekly temperature (17.76°C) occurs during the week of August 9, 1994. The correlation between $\delta^{18}O_{shell}$ and NCEP SST is shown in **FIGURE 21**, Panel A. $\delta^{18}O_{shell}$ values range from –1.13 per mil to –2.77 per mil. The estimate (r) of the product-moment correlation coefficient equals 0.62. This value is significant at the 99% confidence level (df = 42) (Laws 1997, Appendix C). The significant positive correlation between $\delta^{18}O_{shell}$ and NCEP SST is apparent in the

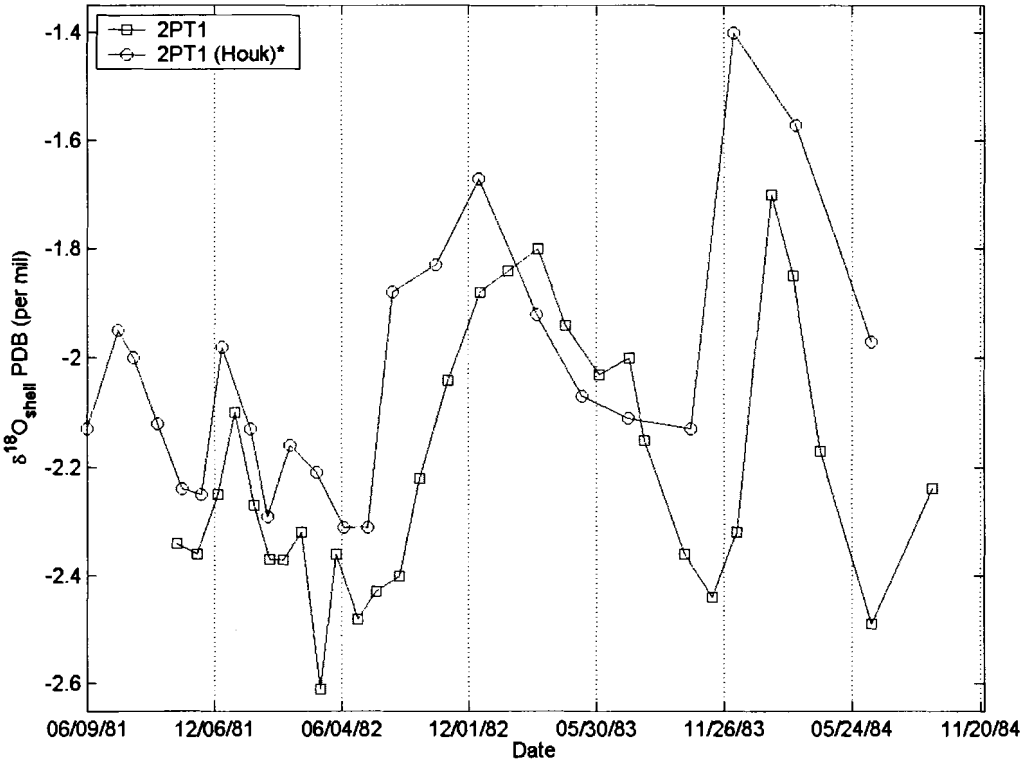

FIGURE 20: Comparison of the $\delta^{18}O_{shell}$ time series from *C. subrugosa* 2PT1 and *C. subrugosa* 2PT1 (Houk)*.

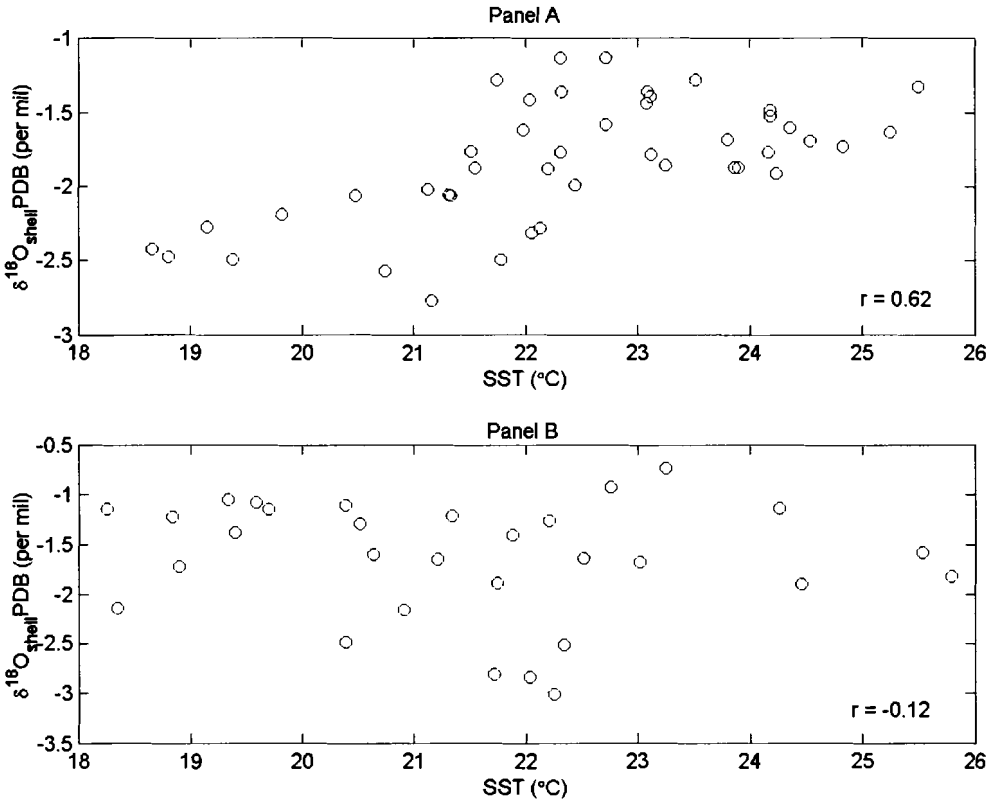

FIGURE 21: NCEP SST versus $\delta^{18}O_{shell}$ in all modern *A. tuberculosa* specimens. Panel A: NCEP SST versus $\delta^{18}O_{shell}$ in *A. tuberculosa* AT 5-1. Panel B: NCEP SST versus $\delta^{18}O_{shell}$ in *A. tuberculosa* AT 5-2.

$\delta^{18}O_{shell}$, and NCEP SST time series (**FIGURE 22**). A comparison of these time series with a CPC Merged Analysis precipitation time series indicates that precipitation levels and a concomitant increase in freshwater flux into the Gulf of Guayaquil probably affect $\delta^{18}O_{shell}$ values in AT 5-1.

Alternatively, the results for *A. tuberculosa* AT 5-2 are not similar. This shell provides a chronology from June 24, 1995 to June 15,1994. The NCEP SST data for grid coordinate 3°S 81°W show a mean weekly SST of 21.88°C for the range of the time series. The maximum weekly temperature (26.53°C) occurs during the week ending February 7, 1995, and the minimum (17.76°C) occurs during the week of August 9, 1994. The correlation between $\delta^{18}O_{shell}$ and NCEP SST is shown in **FIGURE 21**, Panel B. $\delta^{18}O_{shell}$ values range from –0.73 per mil to –3.01 per mil. The estimate (r) of the product-moment correlation coefficient equals –0.12. This value is insignificant at the 90% confidence level (df = 28) (Laws 1997, Appendix C). A comparison of the $\delta^{18}O_{shell}$, NCEP SST, and CPC Merged Analysis precipitation time series (**FIGURE 23**) suggests that $\delta^{18}O_{shell}$ values in this shell may covary both positively and negatively with temperature. Increased precipitation levels in February 1995 might cause $\delta^{18}O_{shell}$ values to become more positive. If so, then there appears to be a lag between the NCEP SST temperature maximum (and concomitant precipitation increase) in February of 1995 and a positive change in $\delta^{18}O_{shell}$ values.

4.4. Growth Increment and Elemental Mole Ratio Analyses of Modern Shells

Two modern shells were chosen to evaluate the relationship among elemental mole ratios, ocean temperature, and salinity. The magnesium/calcium (Mg/Ca), strontium/calcium (Sr/Ca), magnesium/sodium (Mg/Na), and strontium/sodium (Sr/Na)

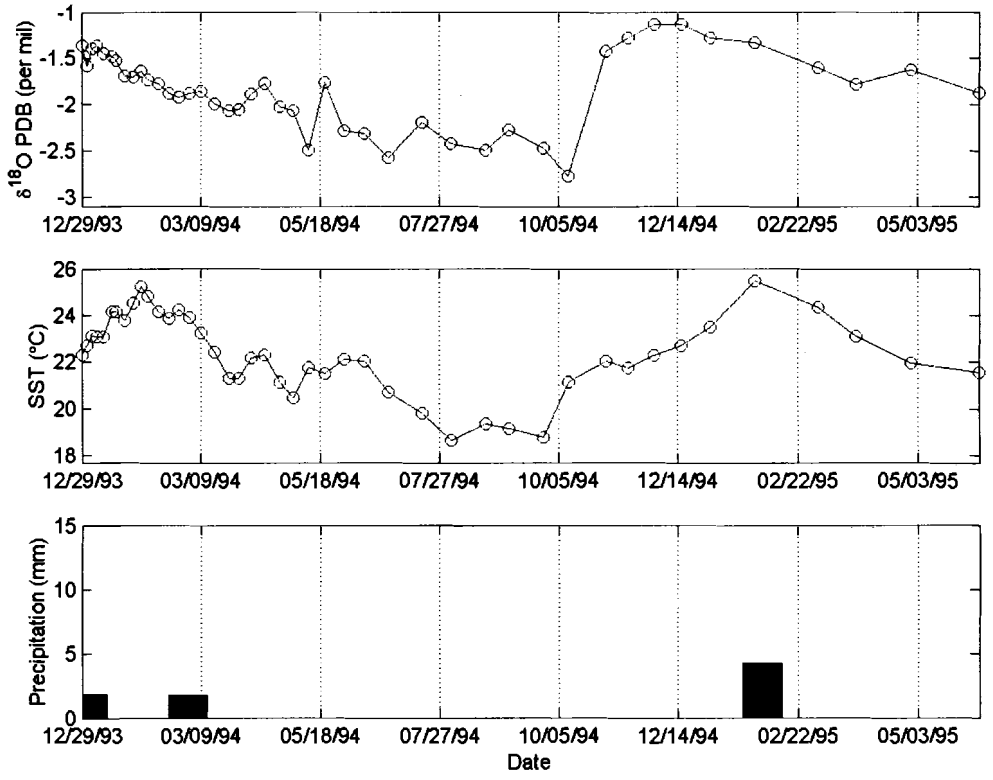

FIGURE 22: Time series of $\delta^{18}O_{shell}$ values in *A. tuberculosa* AT 5-1. Time scale is identical for all panels. NCEP SST and CPC precipitation data are included for comparison.

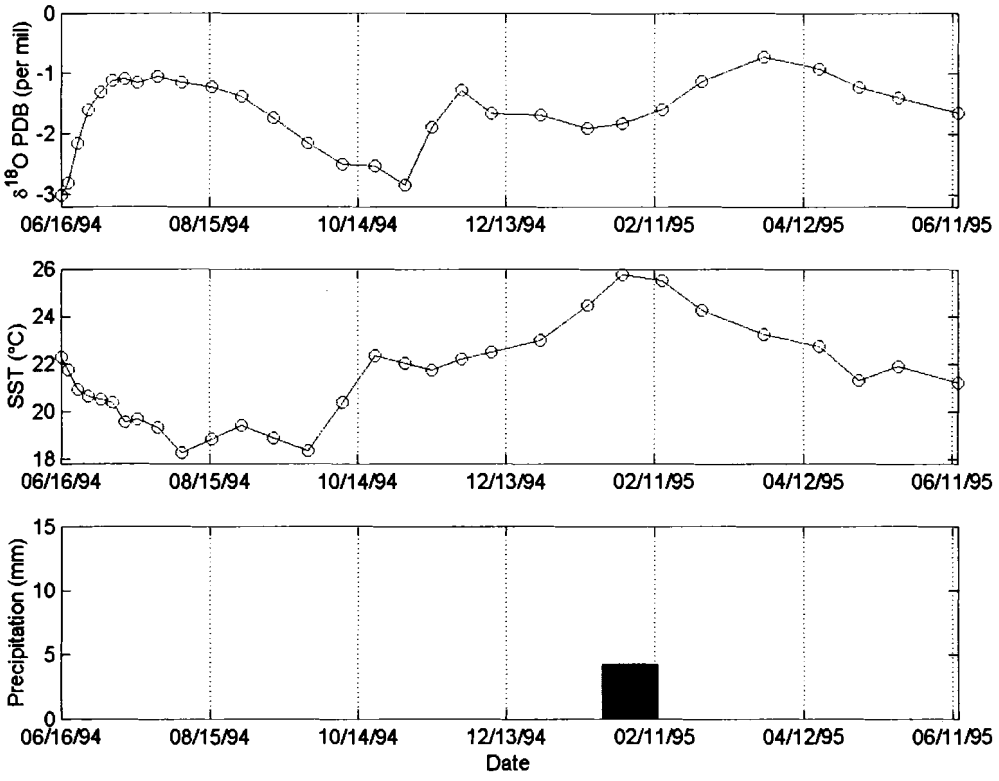

FIGURE 23: Time series of $\delta^{18}O_{shell}$ values in *A. tuberculosa* AT 5-2. Time scale is identical for all panels. NCEP SST and CPC precipitation data are included for comparison.

mole ratios of *T. procerum* TP 1-12 and *C. subrugosa* 2PT1 were correlated with NCEP ocean temperature and NCEP salinity by growth increment counts. Mole ratio values were obtained by converting ICP-OES results (ug/L) to molar concentrations. The mole ratios were multiplied by a scalar (mole ratio x 1000) in order to make the values more robust. It was assumed that all Mg, Sr, Na, and Ca were present as carbonate-bound cations.

4.4.1. Elemental Mole Ratios in *T. procerum* TP 1-12

The correlations among Mg/Na, Sr/Na, Mg/Ca, and Sr/Ca mole ratios and NCEP ocean temperature (-15m) are shown in **FIGURE 24**. The estimate (r) of the product-moment correlation coefficient for the covariance between Mg/Na and NCEP temperature equals –0.06. This value is insignificant at the 90% confidence level (df = 33) (Laws 1997, Appendix C). Alternatively, the estimated values of the correlation coefficient for Sr/Na and NCEP temperature, Mg/Ca and NCEP temperature, and Sr/Ca and NCEP temperature are –0.78, 0.56, and –0.68, respectively. These correlation coefficients are significant at the 99% confidence level (df = 33) (Laws 1997, Appendix C). The significant correlations of these elemental mole ratios and NCEP temperature are evident in the time series of the elemental mole ratios (**FIGURES 25-28**), which were developed by growth increment counts.

The covariance among Mg/Na, Sr/Na, Mg/Ca, and Sr/Ca mole ratios and NCEP salinity show opposite results. Ratios that negatively covary with ocean temperature show positive covariance with salinity. The estimate (r) of the product-moment correlation coefficient for the relationship between the Mg/Ca mole ratio and NCEP

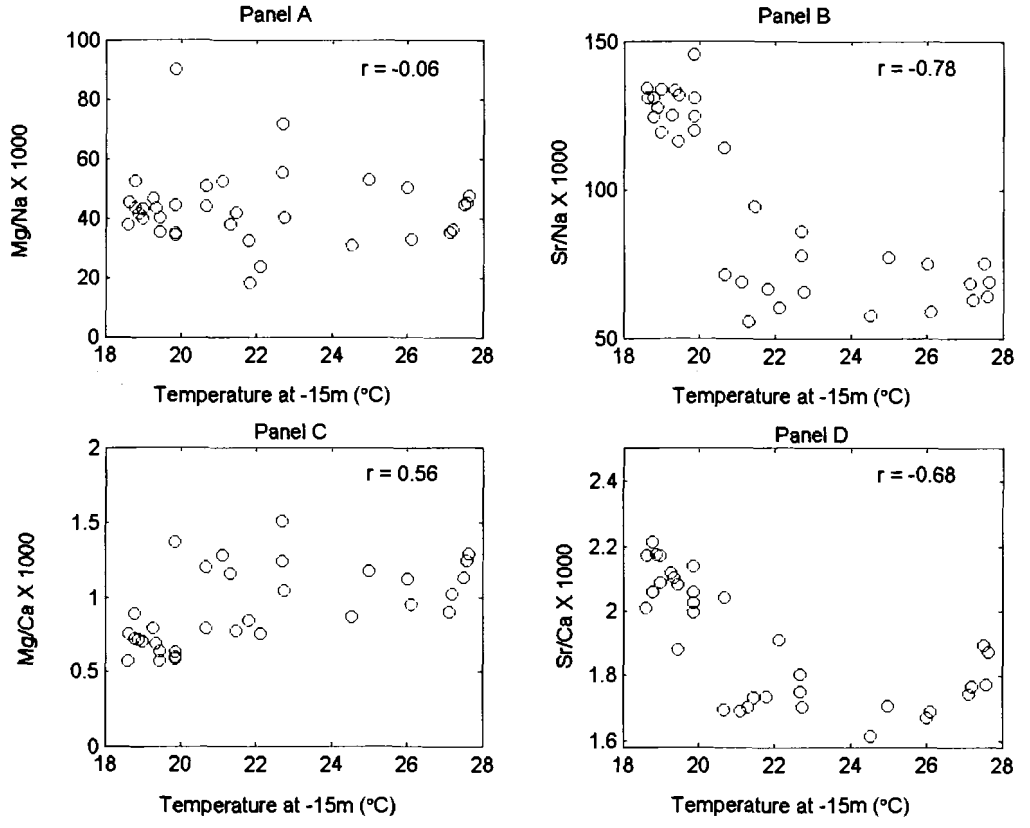

FIGURE 24: NCEP ocean temperature (-15 m) versus elemental mole ratios in *T. procerum* TP 1-12. Panel A: NCEP temperature versus (Mg/Na X 1000). Panel B: NCEP temperature versus (Sr/Na X 1000). Panel C: NCEP temperature versus (Mg/Ca X 1000). Panel D: NCEP temperature versus (Sr/Ca X 1000).

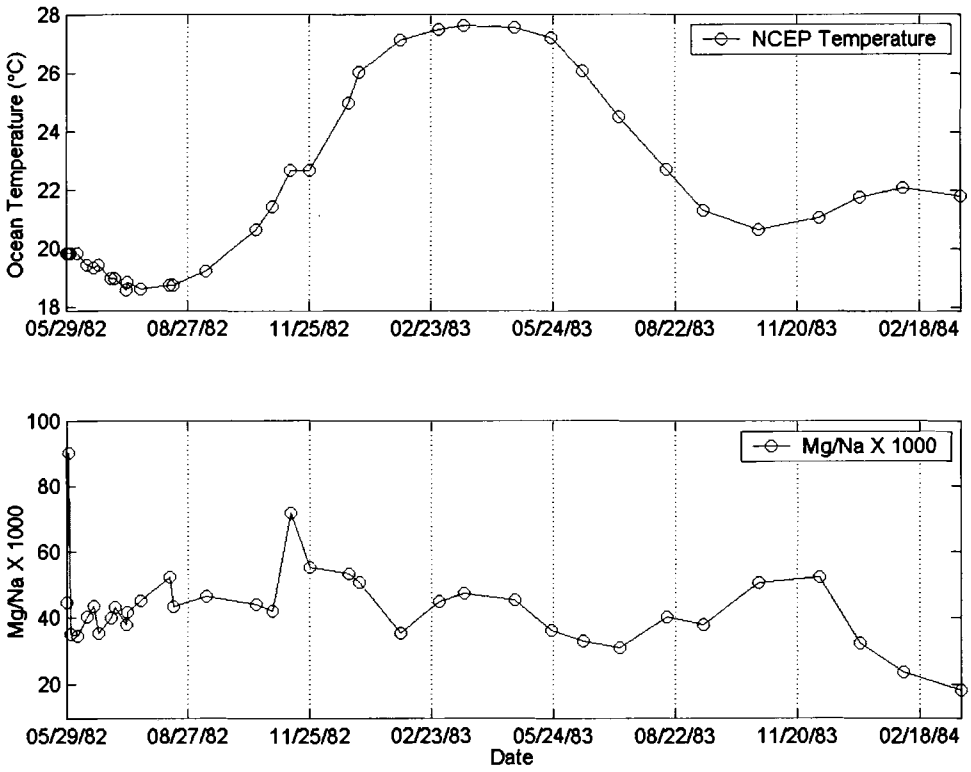

FIGURE 25: Comparative time series of (Mg/Na X 1000) in *T. procerum* TP 1-12 and NCEP ocean temperature (-15 m). Panel A: NCEP temperature time series. Panel B: (Mg/Na X 1000) time series derived from growth increment counts. Time scales are identical.

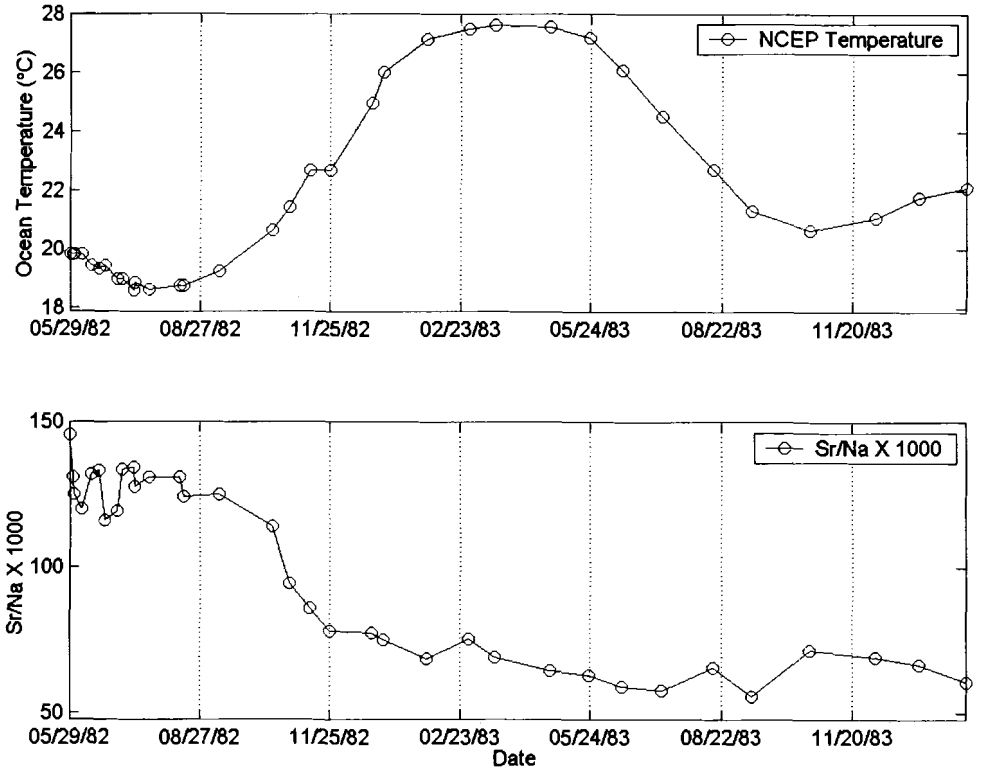

FIGURE 26: Comparative time series of (Sr/Na X 1000) in *T. procerum* TP 1-12 and NCEP ocean temperature (-15 m). Panel A: NCEP temperature time series. Panel B: (Sr/Na X 1000) time series derived from growth increment counts. Time scales are identical.

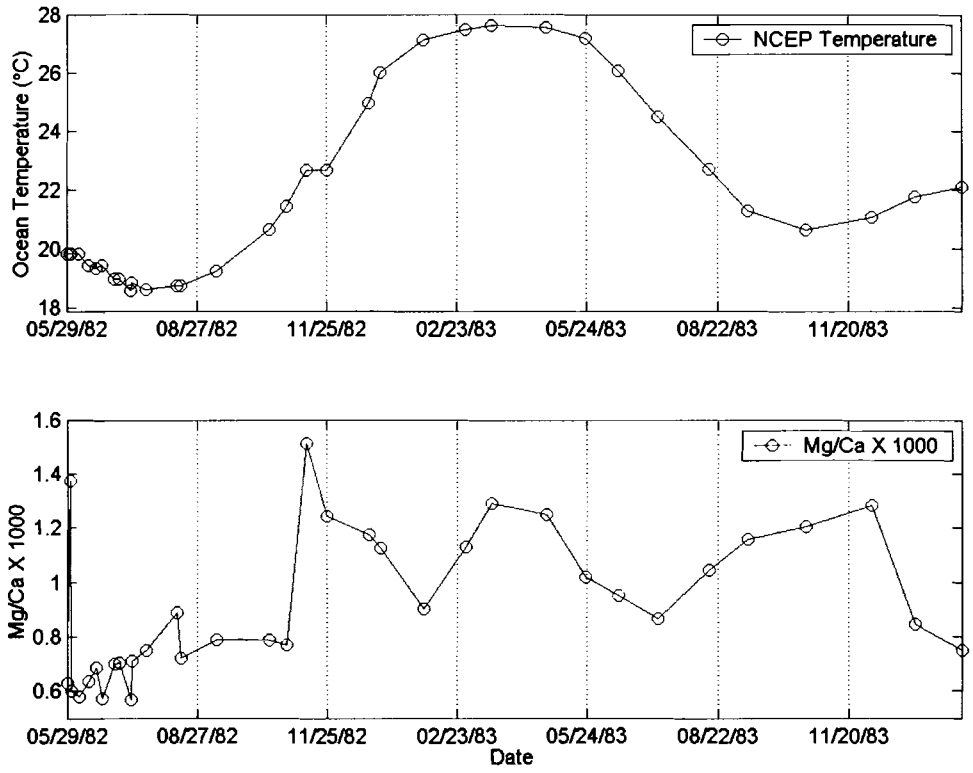

FIGURE 27: Comparative time series of (Mg/Ca X 1000) in *T. procerum* TP 1-12 and NCEP ocean temperature (-15 m). Panel A: NCEP temperature time series. Panel B: (Mg/Ca X 1000) time series derived from growth increment counts. Time scales are identical.

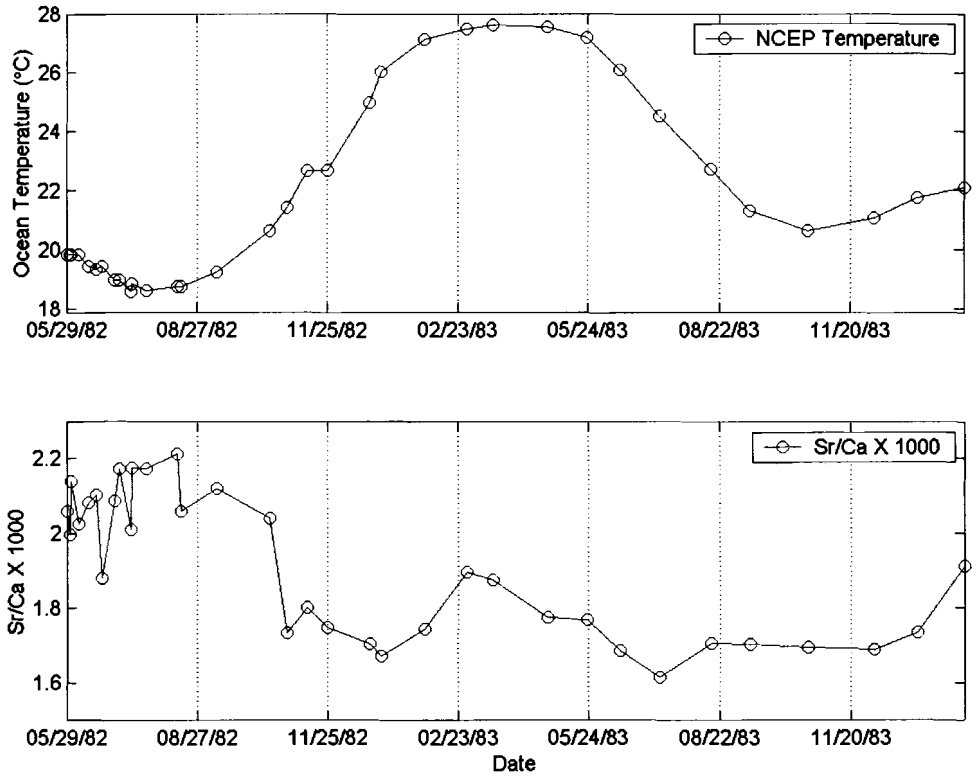

FIGURE 28: Comparative time series of (Sr/Ca X 1000) in *T. procerum* TP 1-12 and NCEP ocean temperature (-15 m). Panel A: NCEP temperature time series. Panel B: (Sr/Ca X 1000) time series derived from growth increment counts. Time scales are identical.

salinity is –0.32. This value is significant at the 90% confidence interval (df = 33) (Laws 1997, Appendix C). Estimates of the product-moment correlation coefficients among Mg/Na, Sr/Na, and Sr/Ca mole ratios and NCEP salinity are 0.44, 0.76, and 0.56, respectively (**FIGURE 29**). These correlation coefficients are significant at the 99% confidence level (df = 33) (Laws 1997, Appendix C). The time series of elemental mole ratios and NCEP salinity (**FIGURES 30-33**) show the significant covariance among these variables.

4.4.2. Elemental Mole Ratios in *C. subrugosa* 2PT1

The covariance among Mg/Na, Sr/Na, Mg/Ca, and Sr/Ca mole ratios from 2PT1 and NCEP SST (-5m) are shown in FIGURE 34. The estimates (r) of the product-moment correlation coefficients among these elemental mole ratios and NCEP SST are insignificant at the 90% confidence level (df = 21). The estimated values of the correlation coefficient for Mg/Na and NCEP SST, Sr/Na and NCEP SST, Mg/Ca and NCEP SST, and Sr/Ca and NCEP SST are –0.19, -0.25, -0.05, and –0.16, respectively. The insignificant correlations of these elemental mole ratios and NCEP SST are apparent in the time series of the elemental mole ratios, which were developed by growth increment counts (**FIGURES 35-38**).

The covariance among Mg/Na, Sr/Na, Mg/Ca, and Sr/Ca mole ratios and NCEP salinity show similar results (**FIGURE 39**). The estimates (r) of the product-moment correlation coefficients among Mg/Na mole ratios, Sr/Na mole ratios, Mg/Ca mole ratios, Sr/Ca mole ratios and NCEP salinity are –0.14, -0.03, -0.30, and –0.21, respectively.

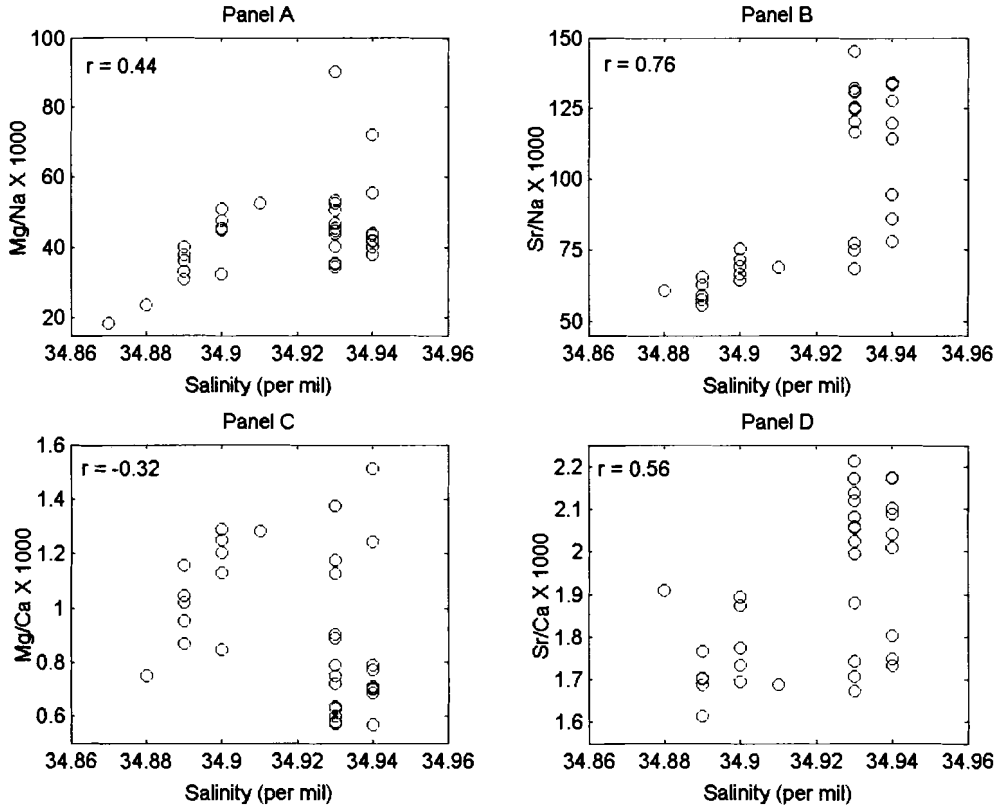

FIGURE 29: NCEP salinity versus elemental mole ratios in *T. procerum* TP 1-12. Panel A: NCEP salinity versus (Mg/Na X 1000). Panel B: NCEP salinity versus (Sr/Na X 1000). Panel C: NCEP salinity versus (Mg/Ca X 1000). Panel D: NCEP salinity versus (Sr/Ca X 1000).

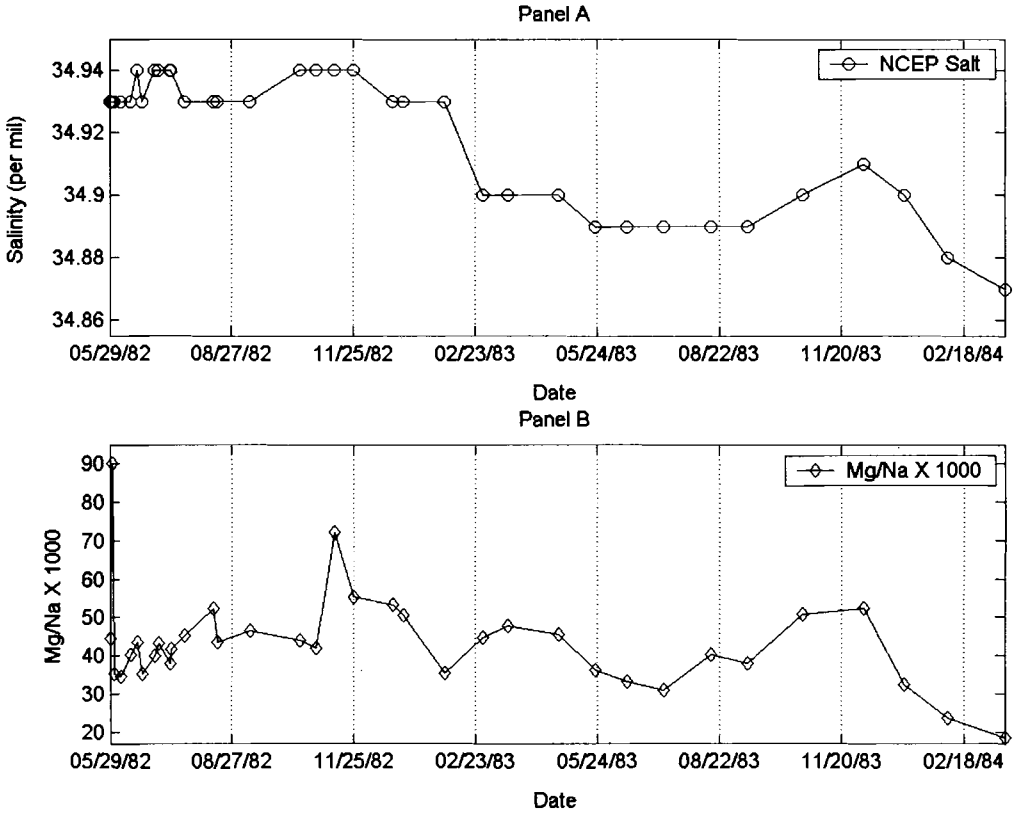

FIGURE 30: Comparative time series of (Mg/Na X 1000) in *T. procerum* TP 1-12 and NCEP salinity. Panel A: NCEP salinity time series. Panel B: (Mg/Na X 1000) time series derived from growth increment counts. Time scales are identical.

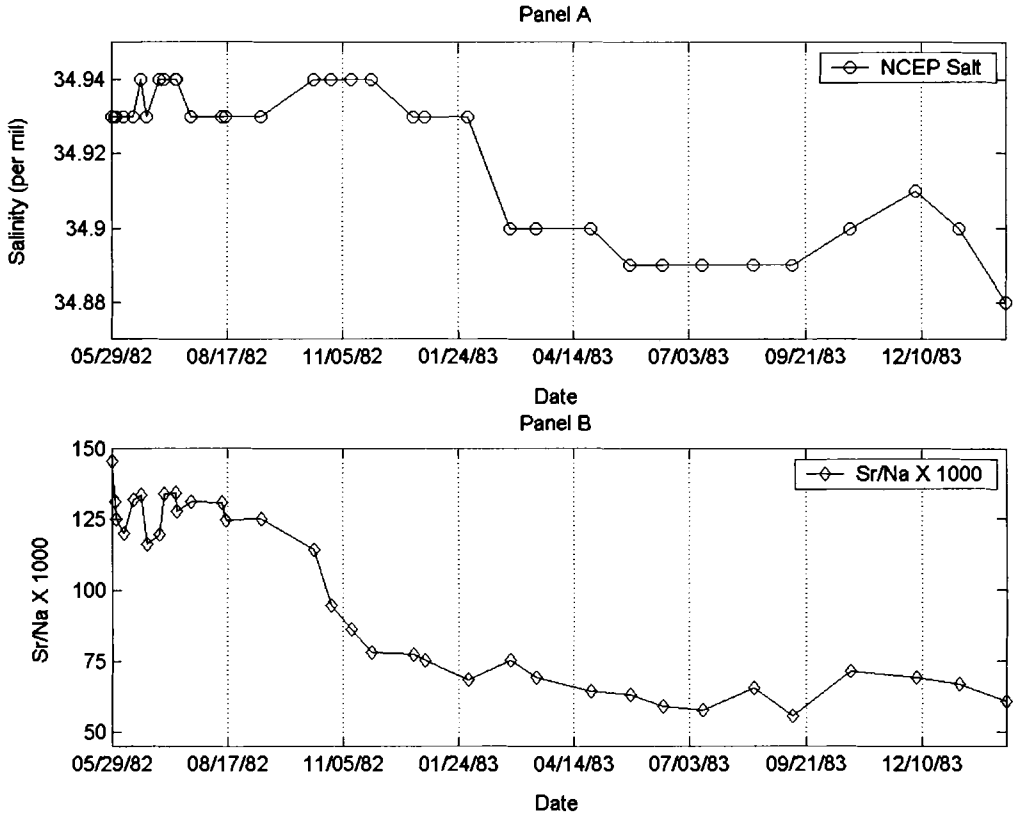

FIGURE 31: Comparative time series of (Sr/Na X 1000) in *T. procerum* TP 1-12 and NCEP salinity. Panel A: NCEP salinity time series. Panel B: (Sr/Na X 1000) time series derived from growth increment counts. Time scales are identical.

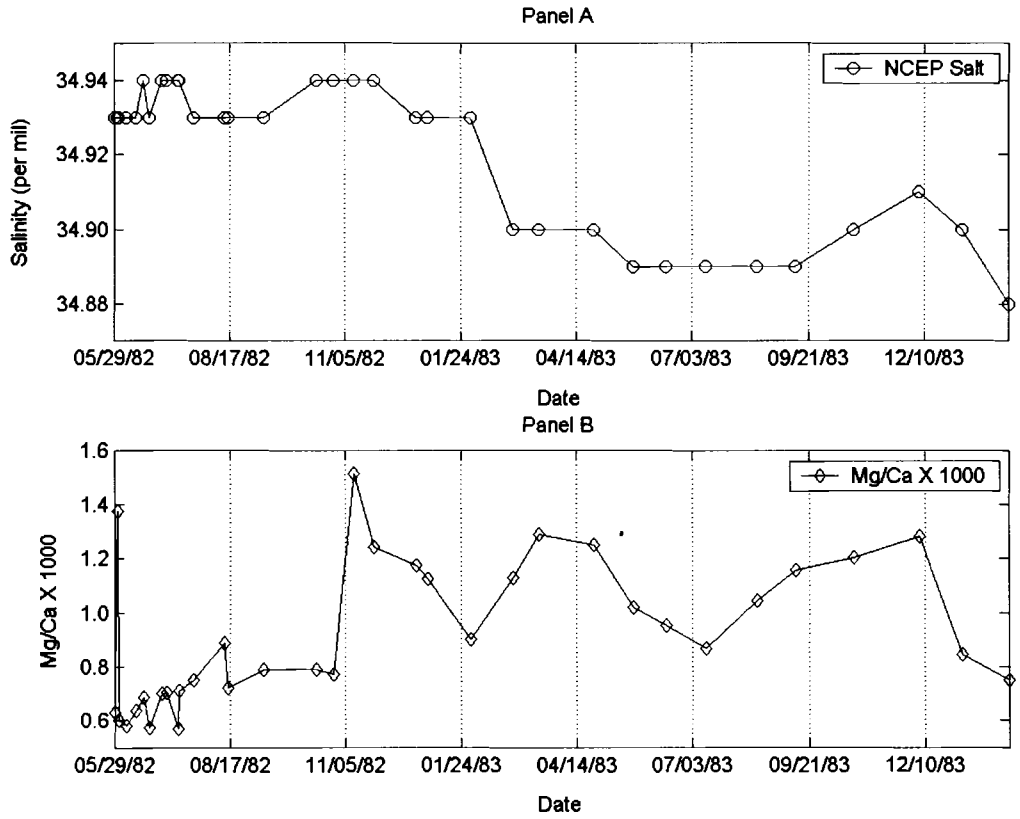

FIGURE 32: Comparative time series of (Mg/Ca X 1000) in *T. procerum* TP 1-12 and NCEP salinity. Panel A: NCEP salinity time series. Panel B: (Mg/Ca X 1000) time series derived from growth increment counts. Time scales are identical.

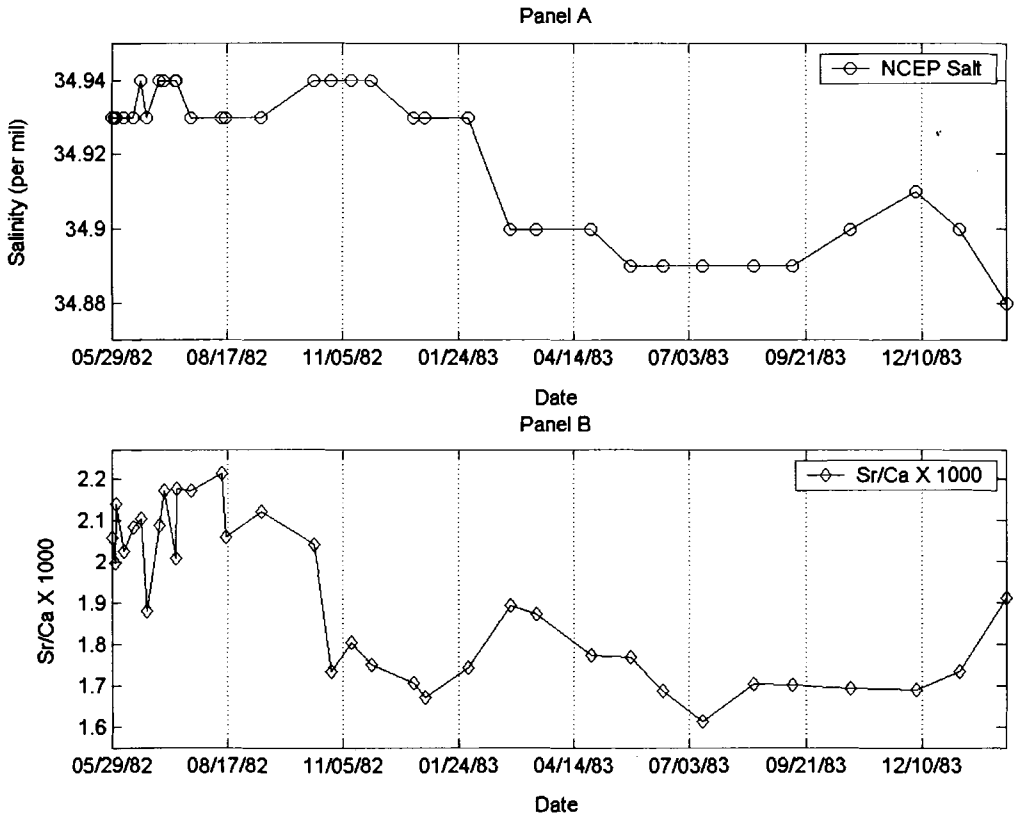

FIGURE 33: Comparative time series of (Sr/Ca X 1000) in *T. procerum* TP 1-12 and NCEP salinity. Panel A: NCEP salinity time series. Panel B: (Sr/Ca X 1000) time series derived from growth increment counts. Time scales are identical.

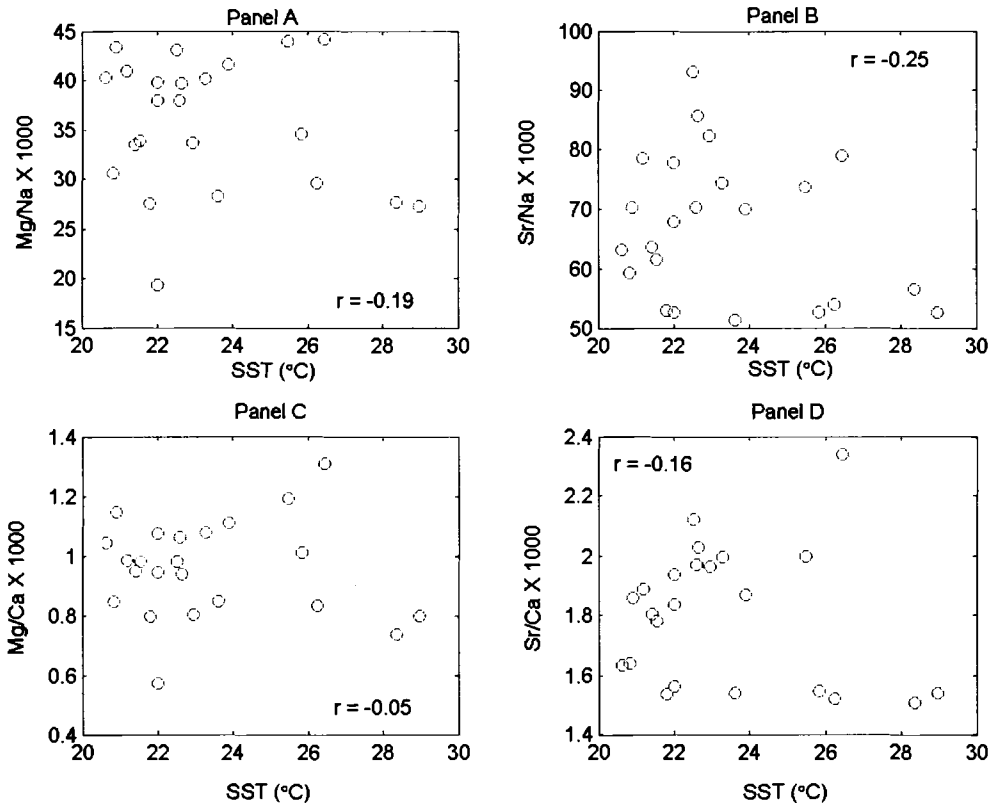

FIGURE 34: NCEP SST versus elemental mole ratios in *C. subrugosa* 2PT1. Panel A: NCEP SST versus (Mg/Na X 1000). Panel B: NCEP SST versus (Sr/Na X 1000). Panel C: NCEP SST versus (Mg/Ca X 1000). Panel D: NCEP SST versus (Sr/Ca X 1000).

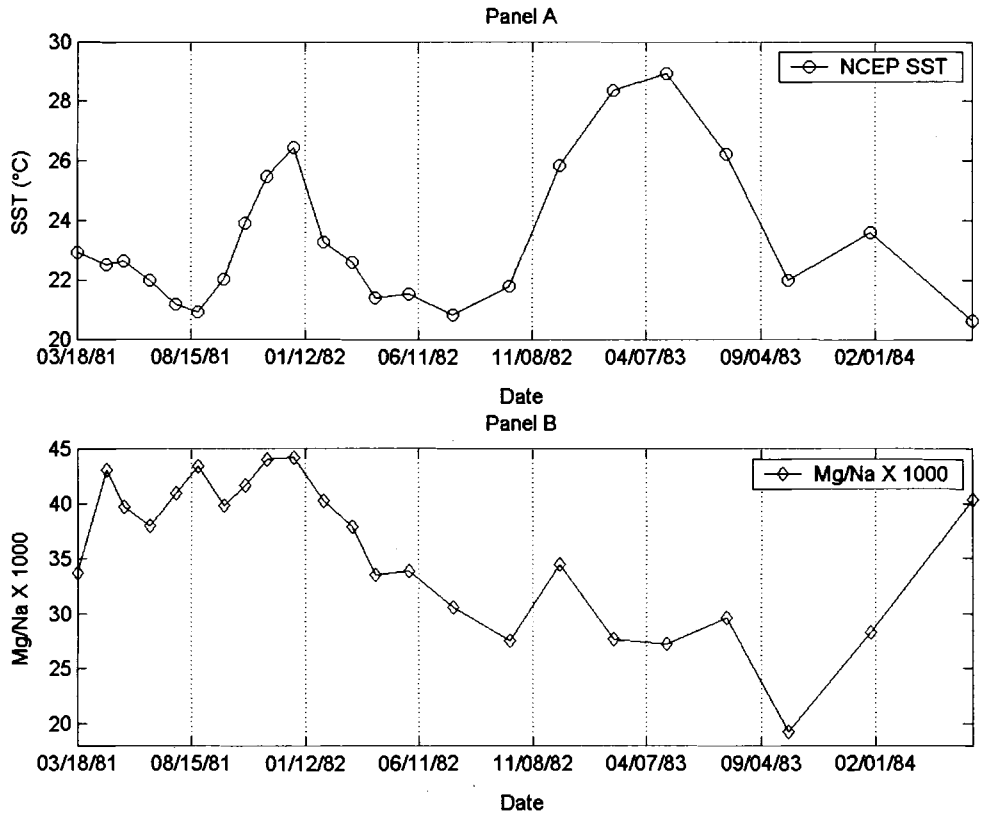

FIGURE 35: Comparative time series of (Mg/Na X 1000) in *C. subrugosa* 2PT1 and NCEP SST. Panel A: NCEP SST time series. Panel B: (Mg/Na X 1000) time series derived from growth increment counts. Time scales are identical.

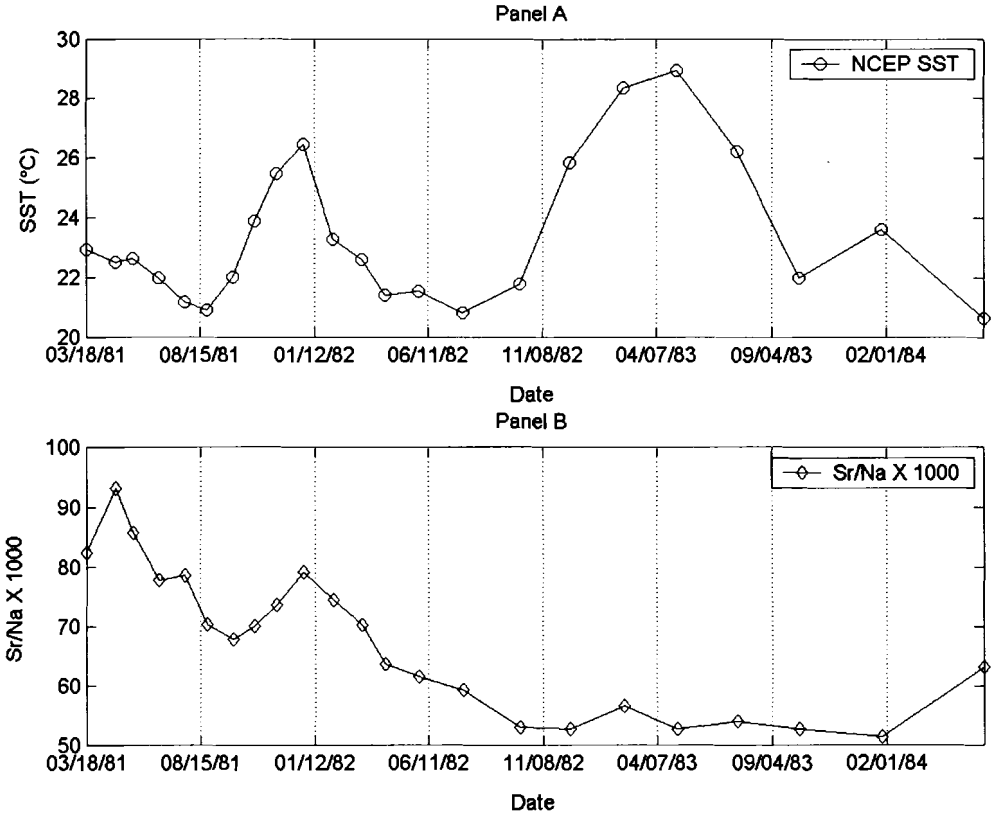

FIGURE 36: Comparative time series of (Sr/Na X 1000) in *C. subrugosa* 2PT1 and NCEP SST. Panel A: NCEP SST time series. Panel B: (Sr/Na X 1000) time series derived from growth increment counts. Time scales are identical.

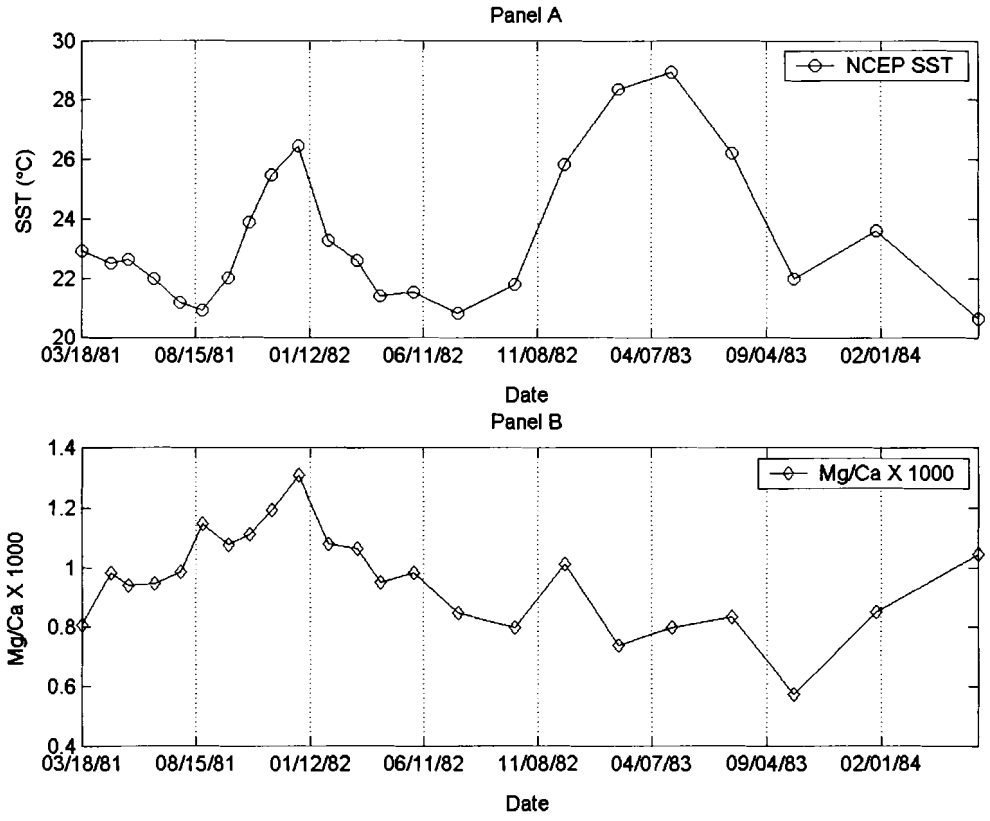

FIGURE 37: Comparative time series of (Mg/Ca X 1000) in *C. subrugosa* 2PT1 and NCEP SST. Panel A: NCEP SST time series. Panel B: (Mg/Ca X 1000) time series derived from growth increment counts. Time scales are identical.

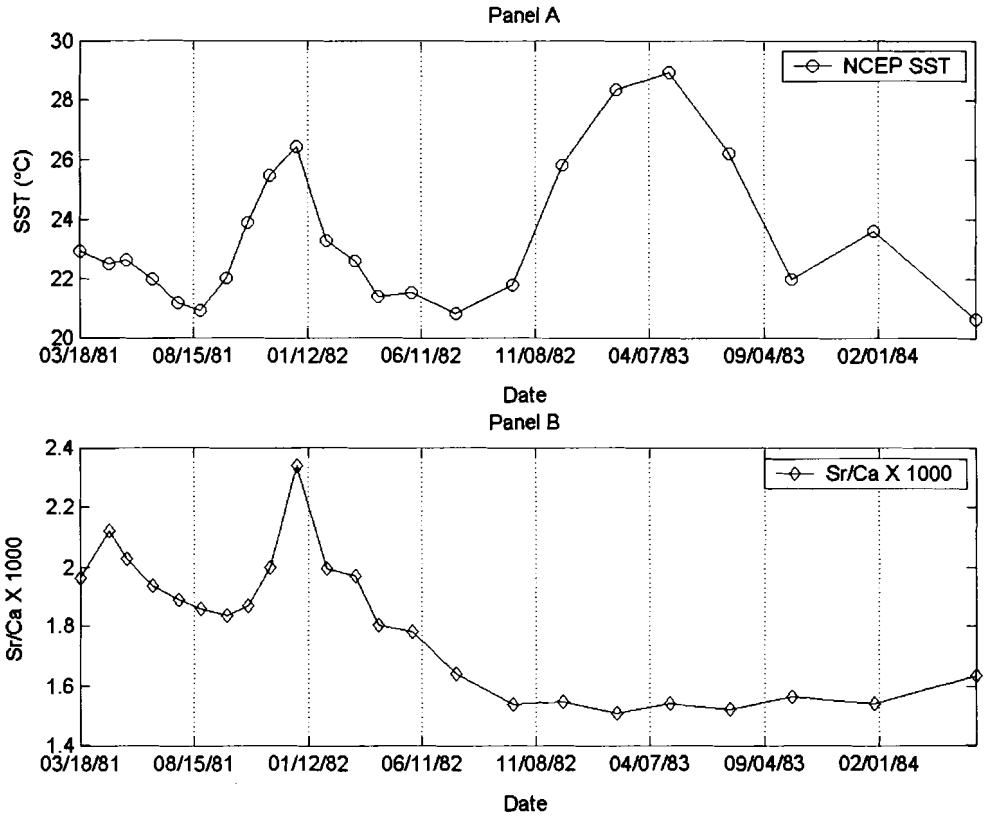

FIGURE 38: Comparative time series of (Sr/Ca X 1000) in *C. subrugosa* 2PT1 and NCEP SST. Panel A: NCEP SST time series. Panel B: (Sr/Ca X 1000) time series derived from growth increment counts. Time scales are identical.

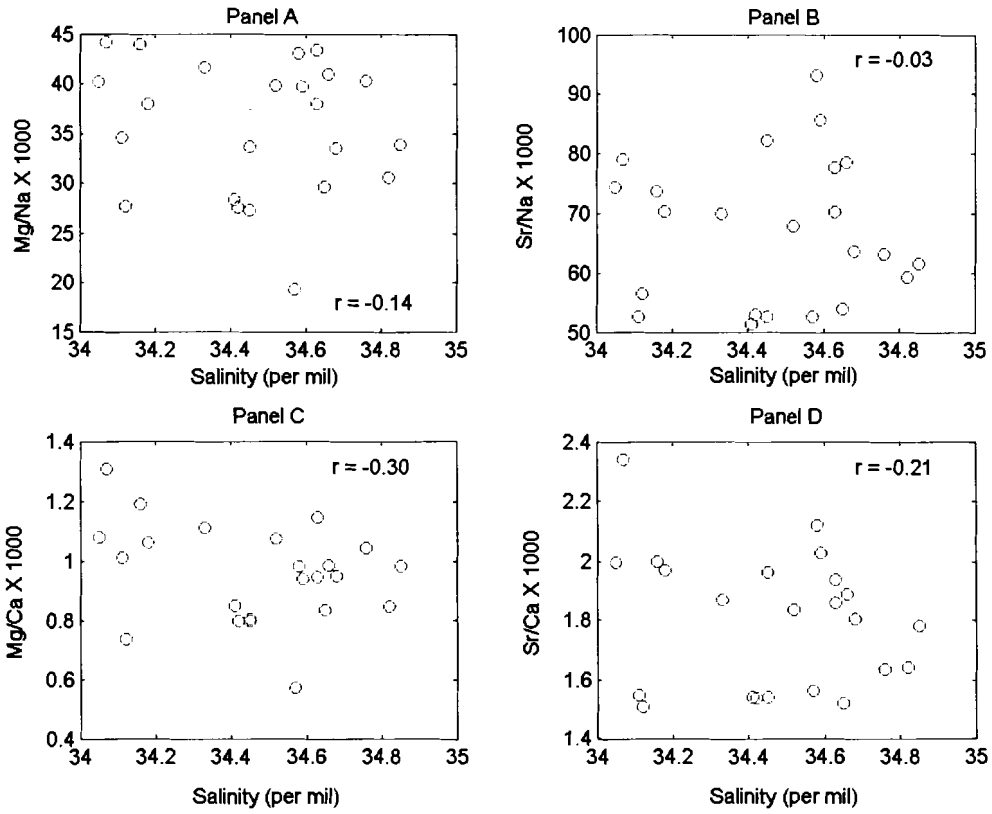

FIGURE 39: NCEP salinity versus elemental mole ratios in *C. subrugosa* 2PT1. Panel A: NCEP salinity versus (Mg/Na X 1000). Panel B: NCEP salinity versus (Sr/Na X 1000). Panel C: NCEP salinity versus (Mg/Ca X 1000). Panel D: NCEP Salinity versus (Sr/Ca X 1000).

These values are also insignificant at the 90% confidence level (df = 21) (Laws 1997, Appendix C). The insignificant covariance of elemental mole ratios and salinity are apparent in the time series of the elemental mole ratios (**FIGURES 40-43**).

4.5. Growth Increment and Stable Isotope Analyses of *C. subrugosa* from the Siches TAMA

Time series for stable oxygen isotope ratios from four archaeological specimens of *Chione subrugosa* were developed in this study. Specimens recovered from levels IB4bi and IB7 at Siches Area I date to the Early Honda component of the site. PV7-19 IB4bi is bracketed by radiocarbon dates of 4930 +/- 80 B.P. (5650 cal yr B.P.) and 5060+/- 80 B.P. (5870-5750 cal yr B.P.). PV 7-19 IB7 is from a context radiocarbon dated at 5060 ± 80 B.P. (5870-5750 cal yr B.P.). Two more specimens from level IIB3, PV7-19 IIB3(a) and PV 7-19 IIB3(b), date to the Siches component of the site. These two specimens are dated by a single radiocarbon date of 6450 ± 80 B.P. (7420-7340 cal yr B.P.).

4.5.1. *C. subrugosa* PV 7-19 IIB3(a) and PV 7-19 IIB3(b) (7420-7340 cal yr B.P.)

Growth increment and stable isotope analyses of *C. subrugosa* PV 7-19 IIB3(a) and PV 7-19 IIB3(b) provided chronologies of 769 days and 762 days from the time of death until the last stable isotope sample near the umbonal region. $\delta^{18}O_{shell}$ values in PV 7-19 IIB3(a) range from –0.41 per mil to –1.86 per mil. The time series of $\delta^{18}O_{shell}$ values in PV 7-19 IIB3(a) is shown in **FIGURE 44**. The $\delta^{18}O_{shell}$ values in PV 7-19 IIB3(b) range from –0.40 per mil to –1.63 per mil. The 762-day time series for $\delta^{18}O_{shell}$ values in PV 7-19 IIB3(b) is shown in **FIGURE 45**.

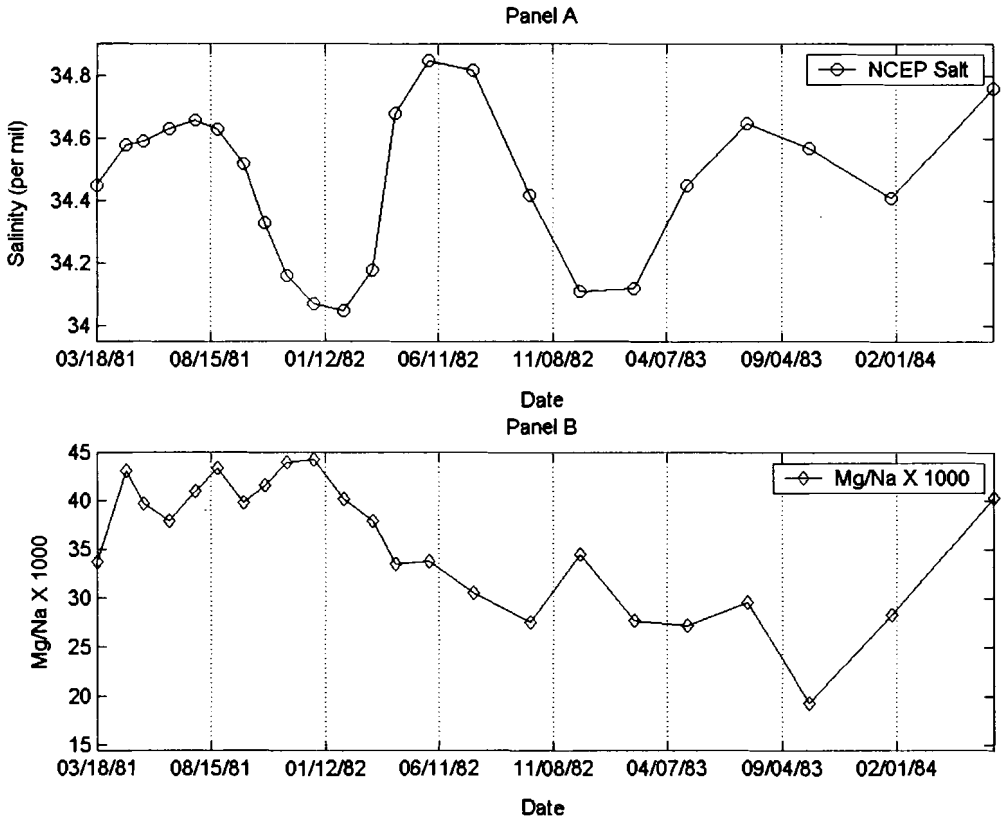

FIGURE 40: Comparative time series of (Mg/Na X 1000) in *C. subrugosa* 2PT1 and NCEP salinity. Panel A: NCEP salinity time series. Panel B: (Mg/Na X 1000) time series derived from growth increment counts. Time scales are identical.

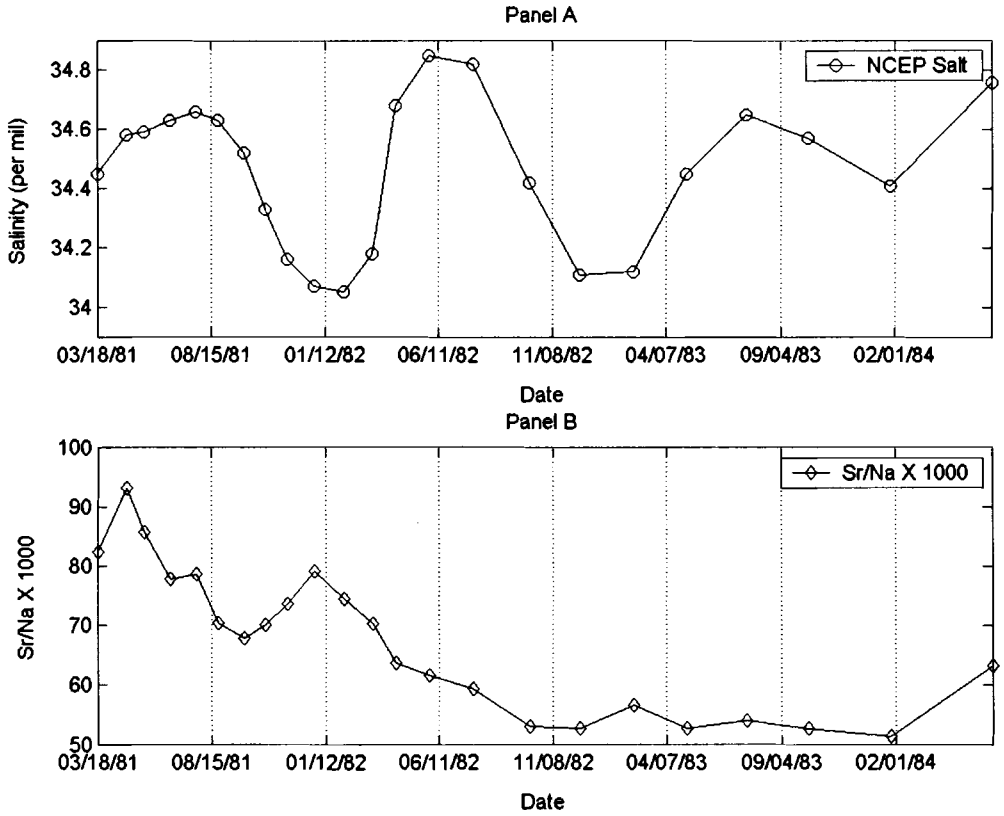

FIGURE 41: Comparative time series of (Sr/Na X 1000) in *C. subrugosa* 2PT1 and NCEP salinity. Panel A: NCEP salinity time series. Panel B: (Sr/Na X 1000) time series derived from growth increment counts. Time scales are identical.

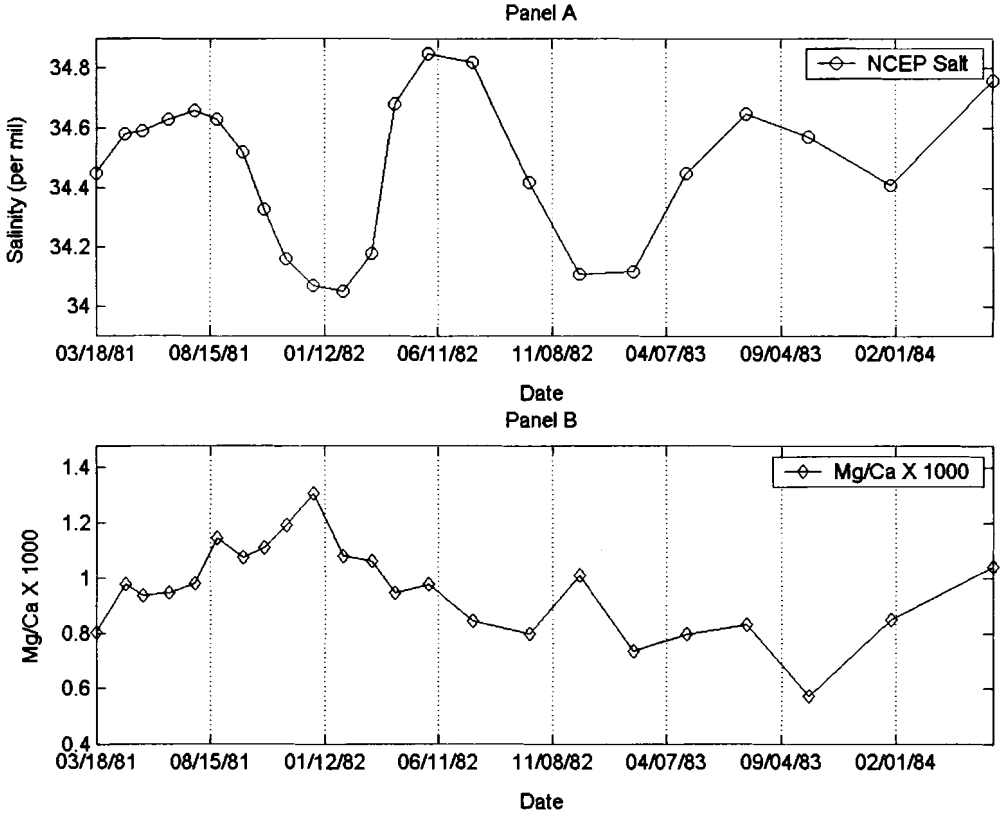

FIGURE 42: Comparative time series of (Mg/Ca X 1000) in *C. subrugosa* 2PT1 and NCEP salinity. Panel A: NCEP salinity time series. Panel B: (Mg/Ca X 1000) time series derived from growth increment counts. Time scales are identical.

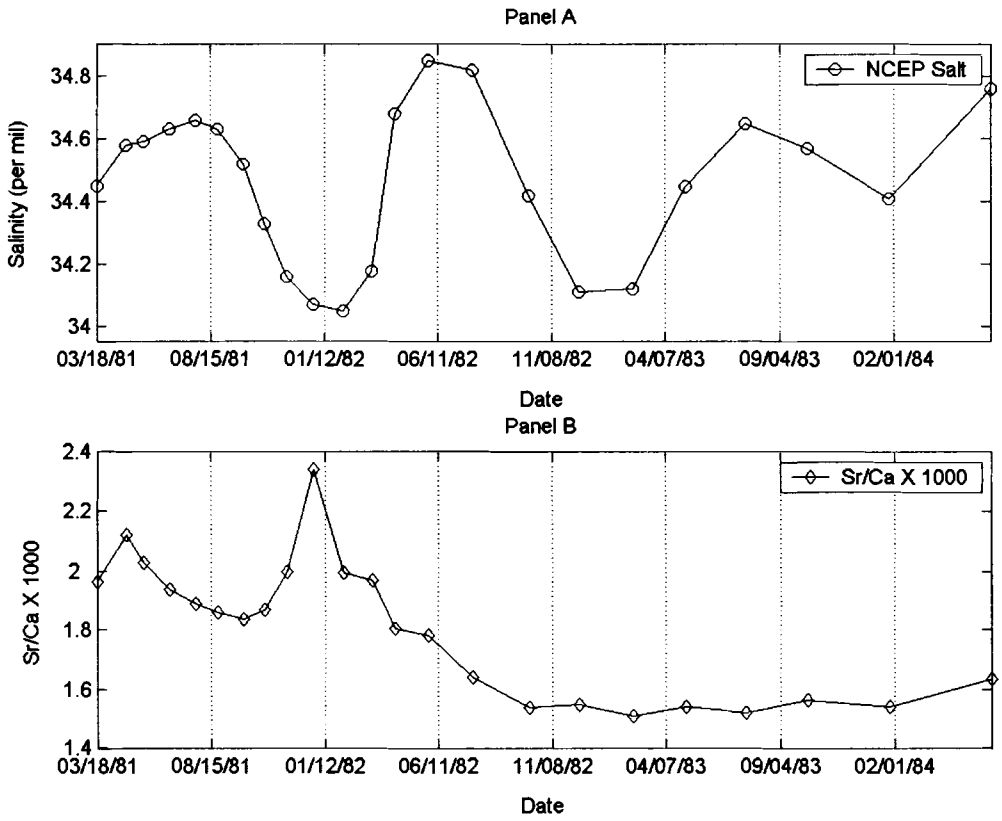

FIGURE 43: Comparative time series of (Sr/Ca X 1000) in *C. subrugosa* 2PT1 and NCEP salinity. Panel A: NCEP salinity time series. Panel B: (Sr/Ca X 1000) time series derived from growth increment counts. Time scales are identical.

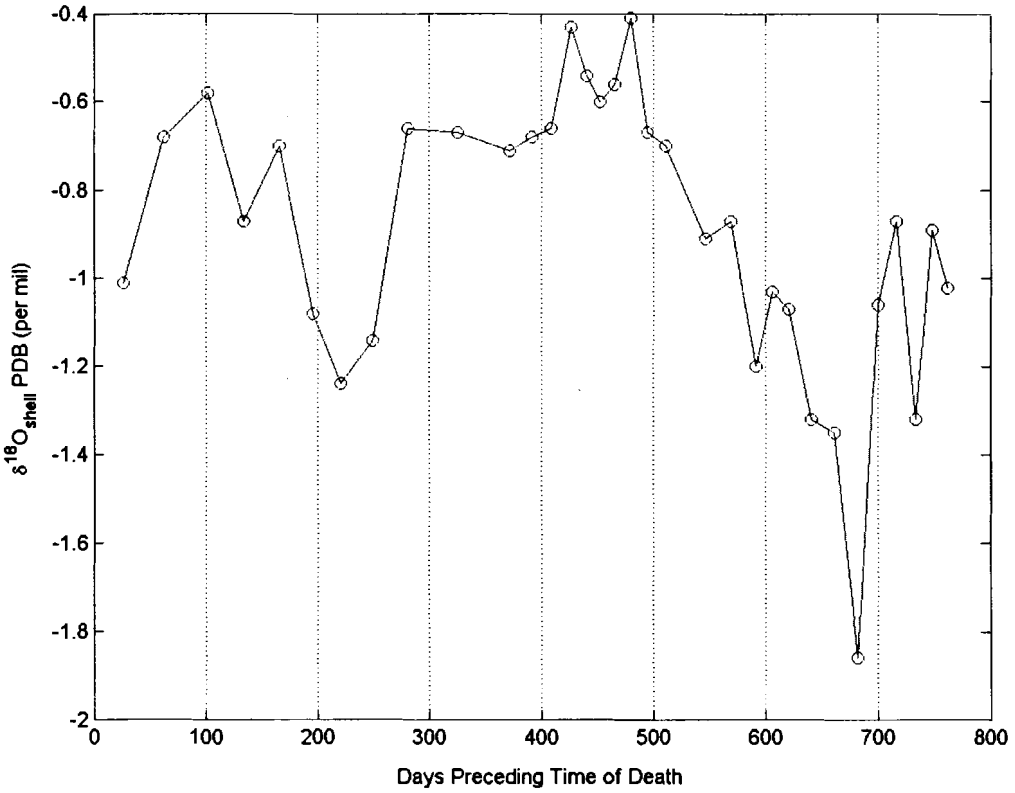

FIGURE 44: Time series of $\delta^{18}O_{shell}$ values in *C. subrugosa* PV 7-19 IIB3(a).

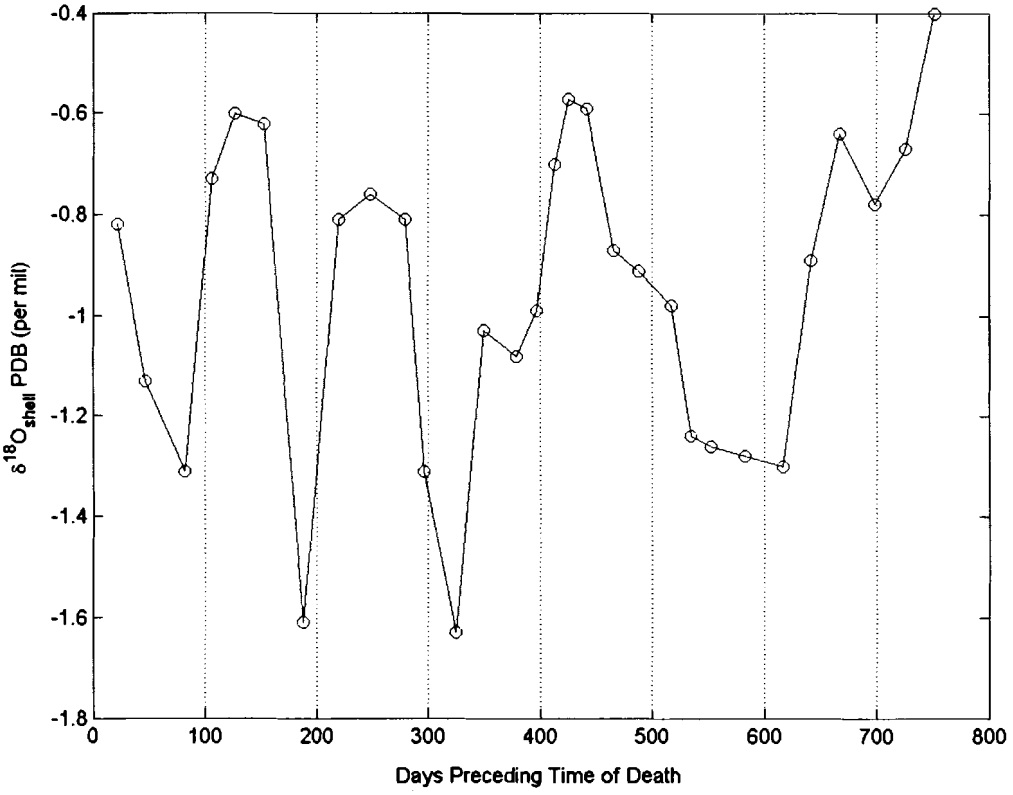

FIGURE 45: Time series of $\delta^{18}O_{shell}$ values in *C. subrugosa* PV 7-19 IIB3(b).

4.5.2. *C. subrugosa* PV 7-19 IB7 (5870-5750 cal yr B.P.) and *C. subrugosa* PV 7-19 IB4bi (5870-5750 to 5650 cal yr B.P.)

Growth increment and stable isotope analyses of PV 7-19 IB7 provided a time series of 844 days (**FIGURE 46**). $\delta^{18}O_{shell}$ values in this shell range from 0.03 per mil to –1.23 per mil. The $\delta^{18}O_{shell}$ values in PV 7-19 IB4bi range from –0.31 per mil to –1.77 per mil. The 670-day time series for $\delta^{18}O_{shell}$ values in PV 7-19 IB4bi is shown in **FIGURE 47**.

4.6. Growth Increment and Stable Isotope Analyses of *A. tuberculosa* from the Siches TAMA

Time series for two specimens of *A. tuberculosa* from the Siches component of site PV 7-19 were developed in this study. Both specimens are associated with a single radiocarbon date of 6450 ± 80 B.P. (7420-7340 cal yr B.P.). The time series $\delta^{18}O_{shell}$ values in *A. tuberculosa* PV 7-19 IIB3(a) is shown in **FIGURE 48**. The time series is 880 days in duration. $\delta^{18}O_{shell}$ values in this time series range from 0.33 per mil to –1.22 per mil. PV 7-19 IIB3(b) provided a chronology of 867 days (**FIGURE 49**). $\delta^{18}O_{shell}$ values for this chronology range from 0.57 per mil to –0.77 per mil.

4.7. Growth Increment and Stable Isotope Analyses of *P. ecuatoriana* from the Siches TAMA

Time series for $\delta^{18}O_{shell}$ values in five specimens of *P. ecuatoriana* from the Siches site were developed in this study. Two specimens, PV 7-19 IIB4(a) and PV 7-19 IIB4(b) are associated with a single radiocarbon date of 6590 +/- 90 B.P. (7470 cal yr B.P.). This date places the two specimens within the Siches component of the site. The

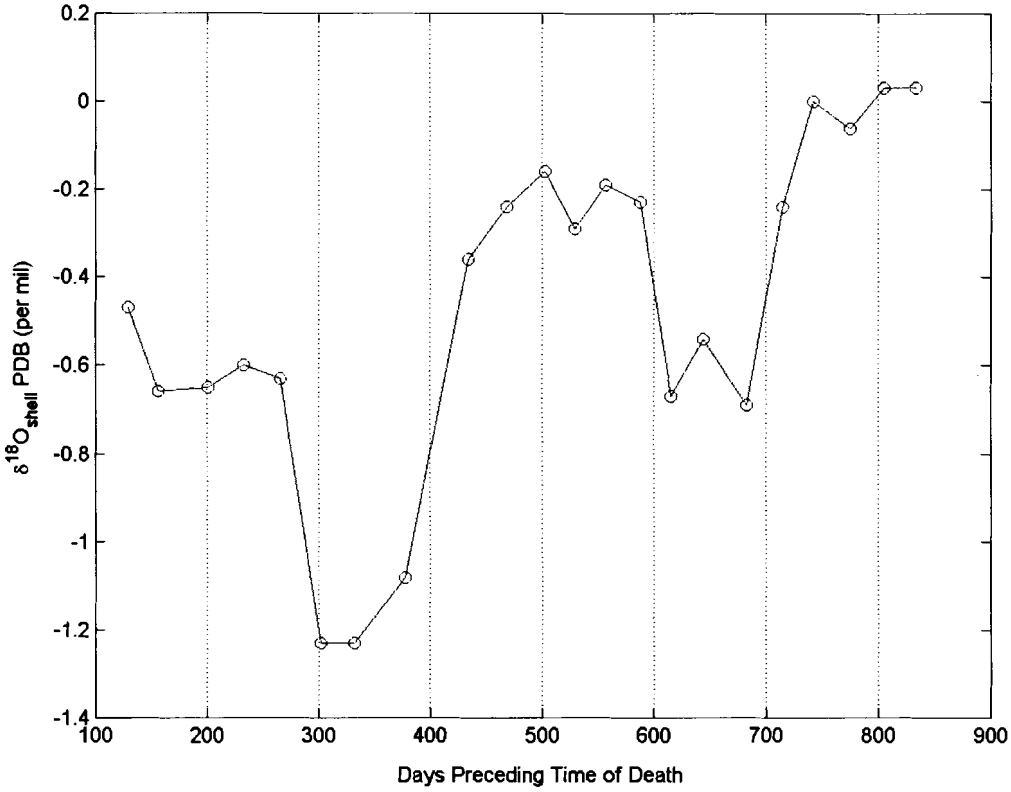

FIGURE 46: Time series of $\delta^{18}O_{shell}$ values in *C. subrugosa* PV 7-19 IB7.

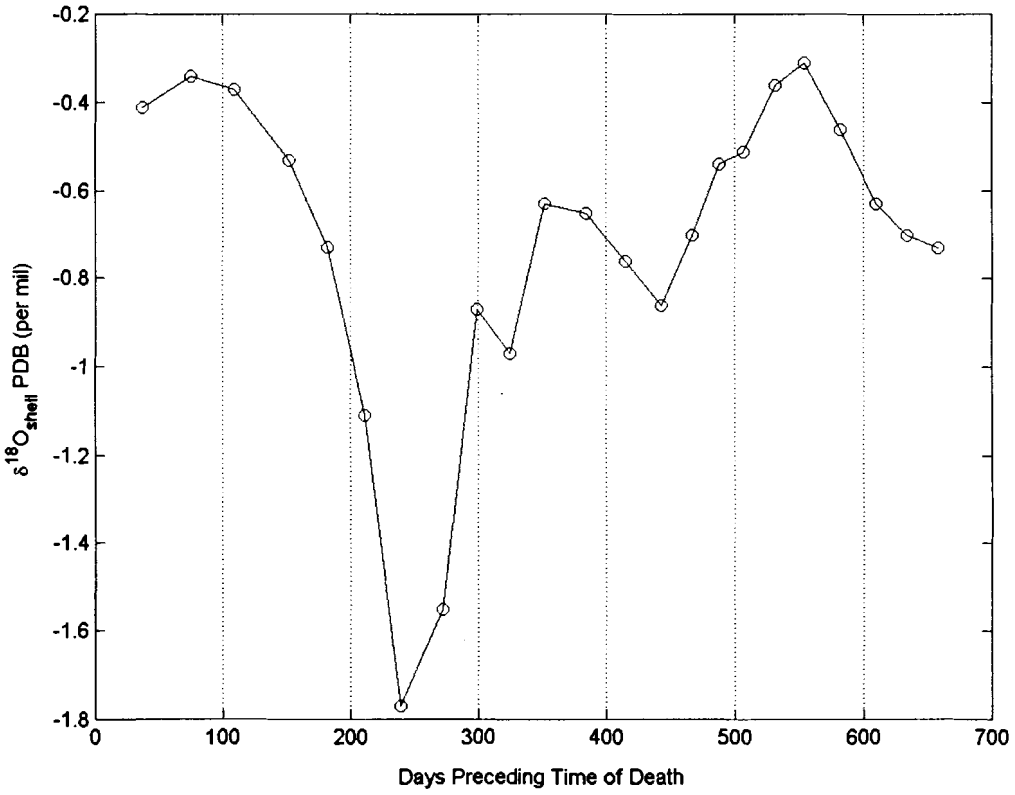

FIGURE 47: Time series of $\delta^{18}O_{shell}$ values in *C. subrugosa* PV 7-19 IB4bi.

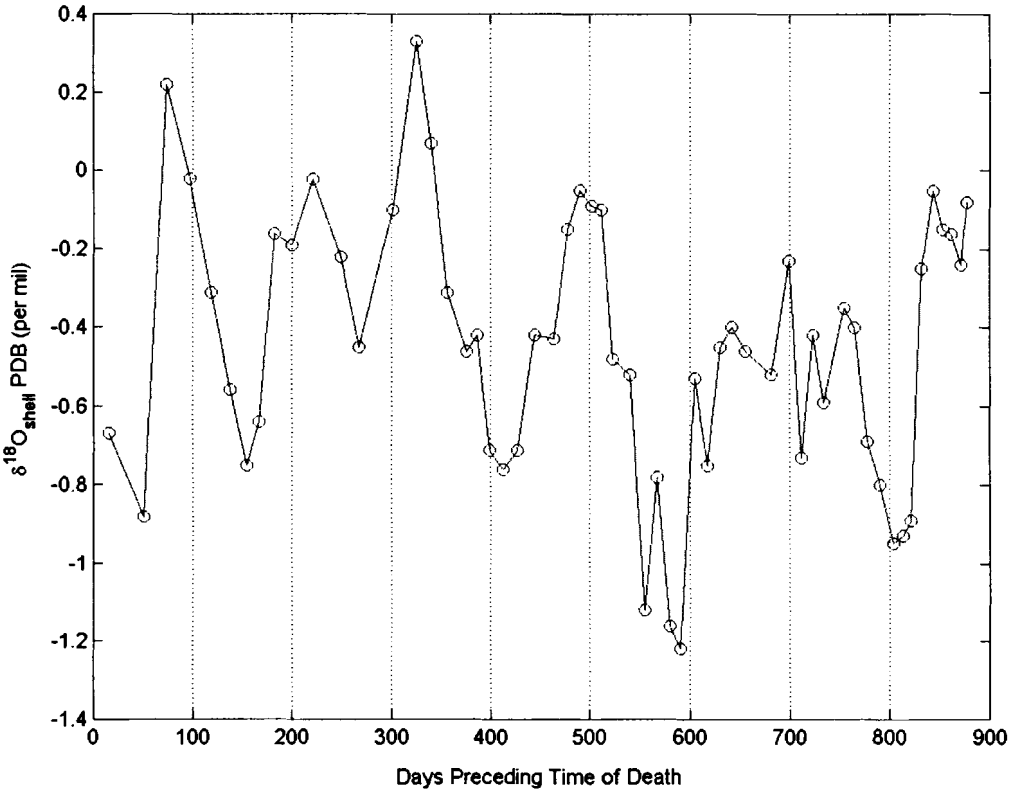

FIGURE 48: Time series of $\delta^{18}O_{shell}$ values in *A. tuberculosa* PV 7-19 IIB3(a).

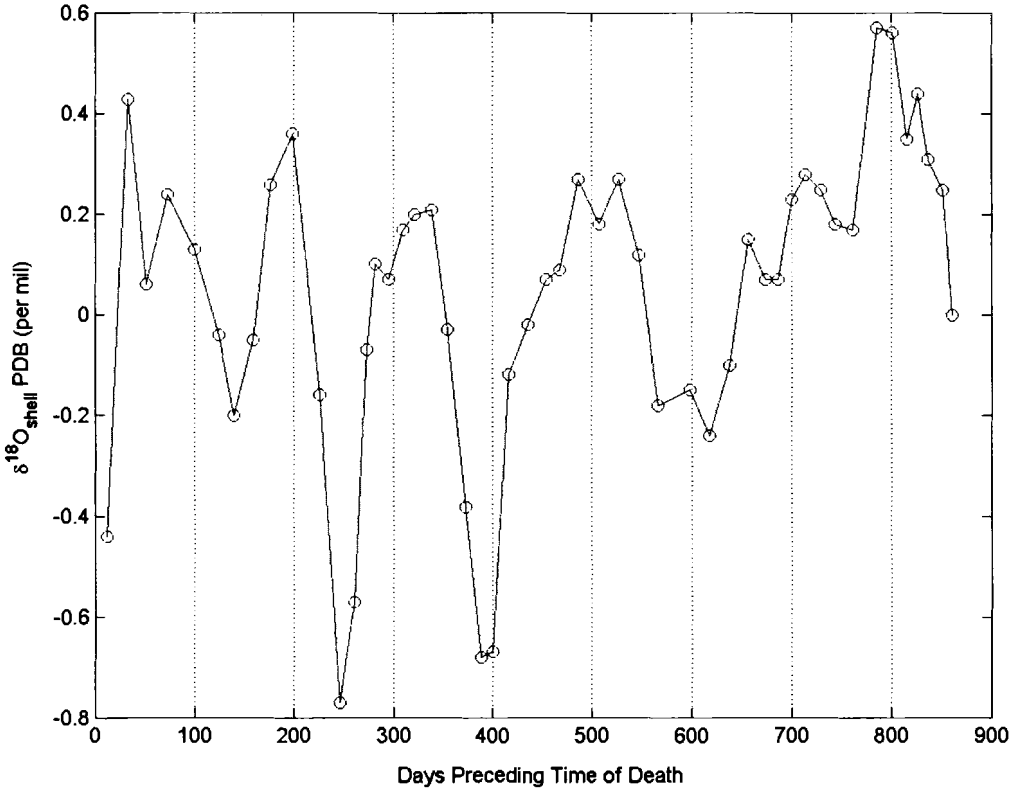

FIGURE 49: Time series of $\delta^{18}O_{shell}$ values in *A. tuberculosa* PV 7-19 IIB3(b).

three remaining specimens are associated with the Early Honda component. Specimens PV 7-19 IB4bi and PV 7-19 IB6b are bracketed by two radiocarbon dates of 4930 +/- 80 B.P. (5650 cal yr B.P.) and 5060 +/- 80 B.P. (5870-5750 cal yr B.P.). Finally, specimen PV 7-19 IB7 is associated with a single radiocarbon date of 5060 +/- 80 B.P. (5870-5750 cal yr B.P.).

4.7.1. *P. ecuatoriana* PV 7-19 IIB4(a) and PV 7-19 IIB4(b) (7470 cal yr B.P.)

Growth increment and stable isotope analyses of *P. ecuatoriana* IIB4(a) provided a time series of 762 days (**FIGURE 50**). $\delta^{18}O_{shell}$ values for this time series range from –0.19 per mil to –1.31 per mil. In addition to the time series of PV 7-19 IIB4(a), growth increment and stable isotope analyses of specimen PV 7-19 IIB4(b) provided a time series of 689 days (**FIGURE 51**). The $\delta^{18}O_{shell}$ values in specimen PV 7-19 IIB4(b) range from –0.11 per mil to –1.23 per mil.

4.7.2. *P. ecuatoriana* PV 7-19 IB7 (5870-5750 cal yr B.P.) and *P. ecuatoriana* PV 7-19 IB4bi and IB6b (5870-5750 to 5650 cal yr B.P.)

Growth increment and stable isotope analyses of *P. ecuatoriana* PV 7-19 IB7 (5870-5750 cal yr B.P.) provided a time series of 743 days in duration (**FIGURE 52**). $\delta^{18}O_{shell}$ values for this time series range from –0.14 per mil to –1.12 per mil. Furthermore, *P. ecuatoriana* PV 7-19 IB4bi and IB6b provided time series of 554 days (**FIGURE 53**) and 532 days (**FIGURE 54**). The $\delta^{18}O_{shell}$ values for the *P. ecuatoriana* PV 7-19 IB4bi time series range from –0.07 per mil to –1.14 per mil, whereas the $\delta^{18}O_{shell}$ values for the *P. ecuatoriana* PV 7-19 IB6b time series range from –0.32 per mil to –1.13 per mil.

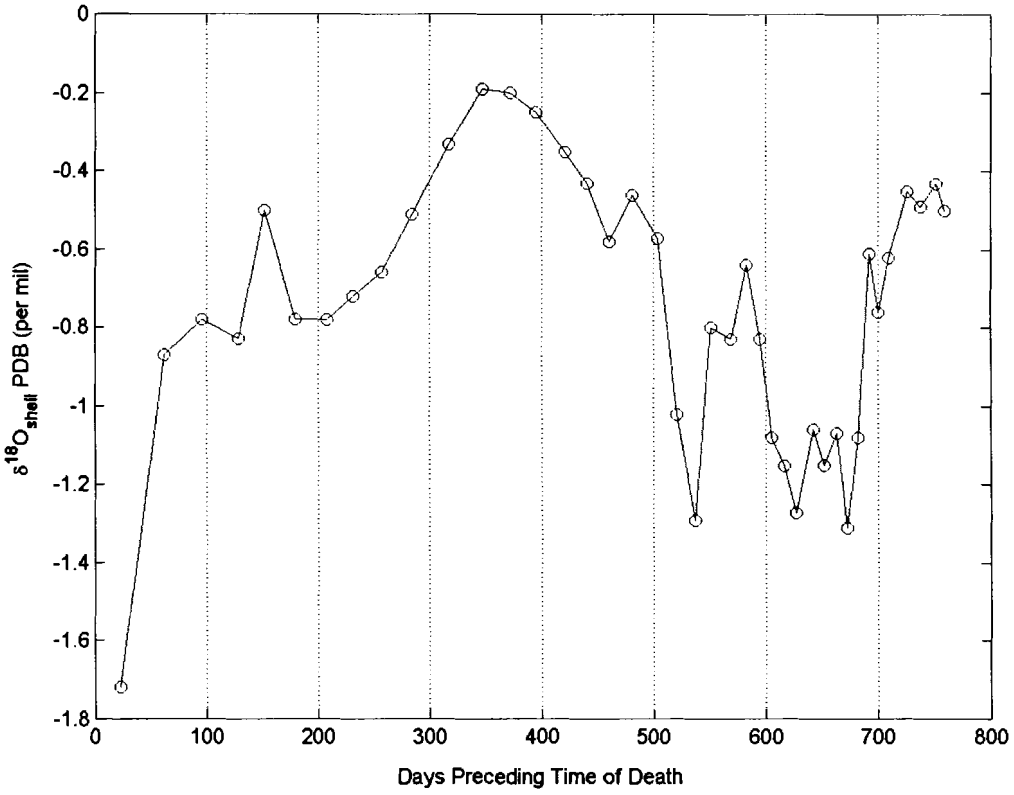

FIGURE 50: Time series of $\delta^{18}O_{shell}$ values in *P. ecuatoriana* PV 7-19 IIB4(a).

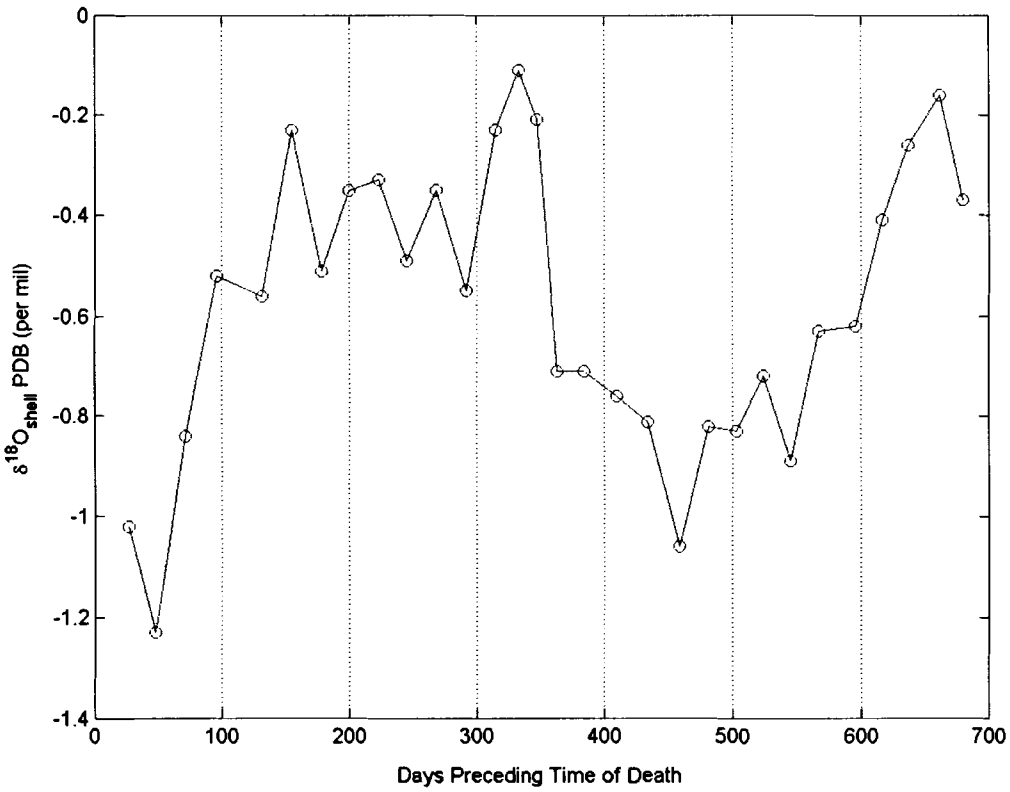

FIGURE 51: Time series of $\delta^{18}O_{shell}$ values in *P. ecuatoriana* PV 7-19 IIB4(b).

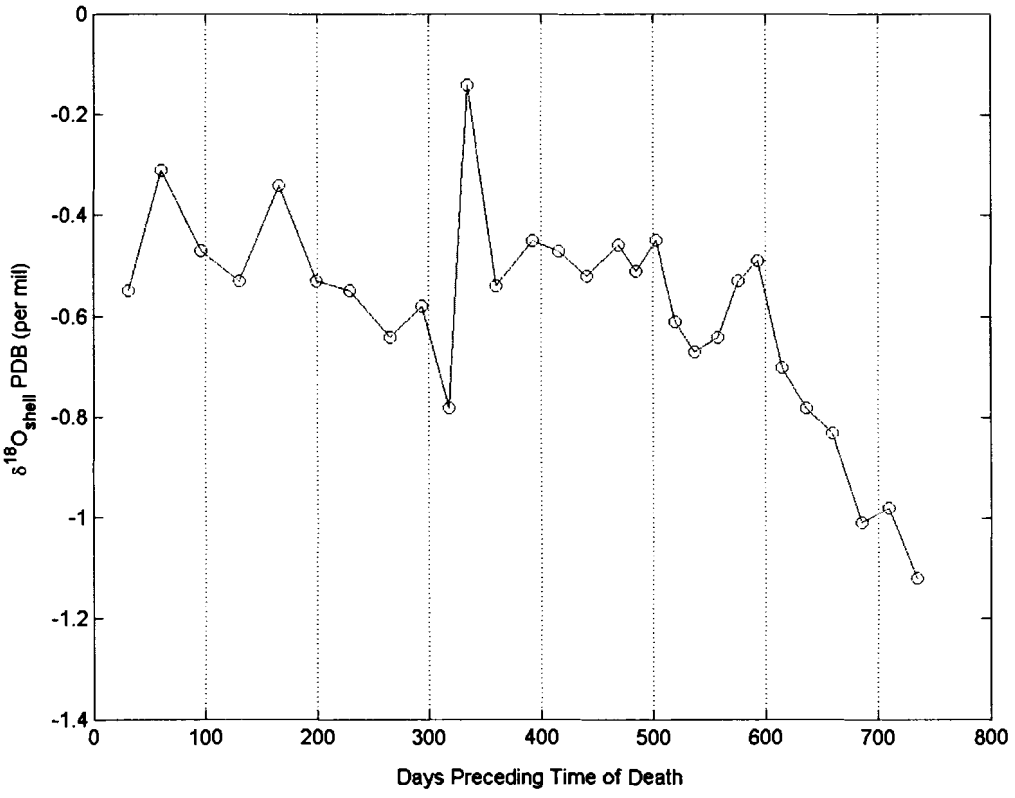

FIGURE 52: Time series of $\delta^{18}O_{shell}$ values in *P. ecuatoriana* PV 7-19 IB7.

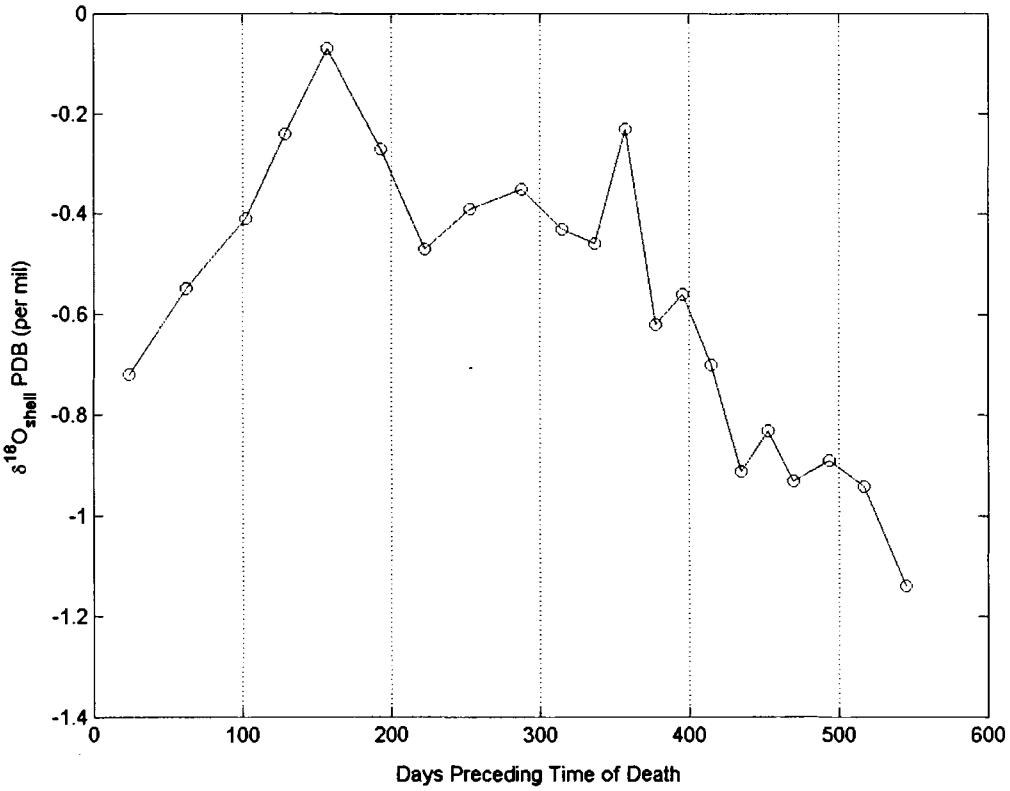

FIGURE 53: Time series of $\delta^{18}O_{shell}$ values in *P. ecuatoriana* PV 7-19 IB4bi.

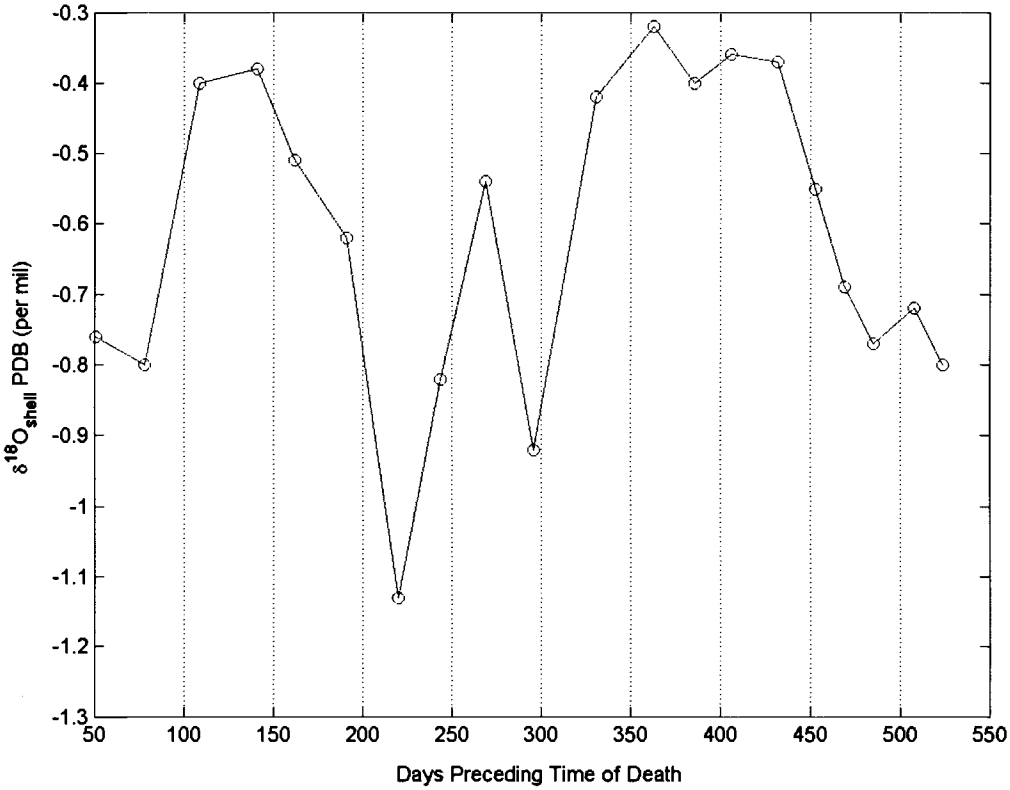

FIGURE 54: Time series of $\delta^{18}O_{shell}$ values in *P. ecuatoriana* PV 7-19 IB6b.

4.8. Growth Increment and Stable Isotope Analyses of *T. procerum* from the Ostra Base Camp

A time series for $\delta^{18}O_{shell}$ values in one *T. procerum* (OBC V-1-C 2i-2ib, El. 2) from Ostra Base Camp was developed using stable isotope and growth increment analyses. The context V-1-C 2i-2ib, El. 2 is not directly dated; however, it is bracketed above and below with coeval radiocarbon dates of 5830 +/- 90 B.P. (6660 cal yr B.P.). The time series for $\delta^{18}O_{shell}$ values in OBC V-1-C 2i-2ib, El. 2 is 748 days in duration (**FIGURE 55**). $\delta^{18}O_{shell}$ values for this time series ranges from 0.50 per mil to –0.01 per mil. In order to estimate ocean temperature at 6660 cal yr B.P. using the Model II regression equation a value for the oxygen isotope content of the water ($\delta^{18}O_{water}$) must be assumed. Based on Sr/Na ratios in a *T. procerum* of mid-Holocene age from OBC, Uwe Brand suggests that salinity at OBC may have been as high as 40 per mil (Sandweiss, personal communication). Moreover, *T. procerum* OBC V-1-C 2i-2ib, El. 2 was probably collected from a depth less than four meters below the surface. Based on analysis of mollusks from another coastal site, four meters was probably the maximum depth at which the prehistoric inhabitants of Ostra Base Camp were able to harvest shellfish (Sandweiss 1982). Thus, *T. procerum* OBC V-1-C 2i-2ib, El. 2 was exposed to surface-level ocean temperature and salinity.

Assuming a constant salinity of 40 per mil for the ocean near OBC (6660 cal yr B.P.), the salinity and $\delta^{18}O_{water}$ relationship established by Nicholas (1996) for the Chira River estuary ($\delta^{18}O_{water} = 0.16*S - 4.99$; where S = salinity) yields a $\delta^{18}O_{water}$ value of 1.41 per mil. If $\delta^{18}O_{water}$ equals 1.41 per mil, then the Model II regression line estimates

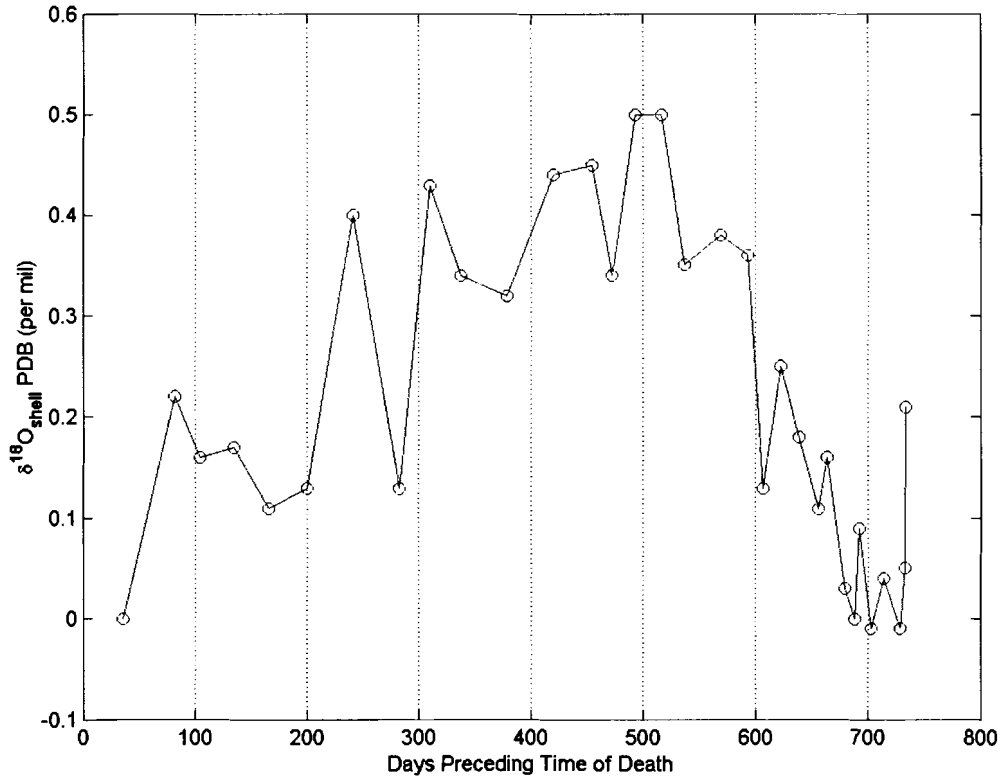

FIGURE 55: Time series of $\delta^{18}O_{shell}$ values in *T. procerum* OBC V-1-C 2i-2ib, Elemento 2.

ocean temperatures for the 748-day time series ranging from 19.00°C to 21.43°C. Nicholas (1996) also sampled a *T. procerum* from OBC context V-1-C 2i-2ib El. 2. That specimen was not available for growth increment analysis; nevertheless, $\delta^{18}O_{shell}$ values in that shell range from 0.74 per mil to –0.58 per mil. The range of stable isotope ratios from Nicholas' analysis of a *T. procerum* from OBC context V-1-C 2i-2ib El. 2 contains negative values which exceed the range of this author's analysis. Thus, ocean temperatures estimated by the Model II regression line for Nicholas' $\delta^{18}O_{shell}$ values range from 17.86°C to 24.14°C.

4.8.1. Elemental Mole Ratios in *T. procerum* OBC V-1-C 2i-2ib, Elemento 2

The time series of the elemental mole ratios of samples drilled from OBC V1C 2i-2ib El. 2 are shown in **FIGURE 56**. As is the case in the modern specimens, the data are difficult to interpret. The data do not reflect a periodicity indicative of seasonality; however, Mg/Na and Mg/Ca ratios indicate a long-term linear trend. Values increase in the time domain with days preceding death or in the space domain with distance from the ventral margin. Sr/Na and Sr/Ca ratios might reflect seasonality; however, the long-term trend is non-linear and increases as days preceding death increases.

4.9. Estimated Temperatures for Middle Holocene *T. procerum* analyzed by Perrier et al. (1994)

Perrier et al. (1994) also conducted stable isotope analyses of *T. procerum*. Those authors collected specimens from behind the Santa beach ridges north of the Santa River in what they describe as a paleolagoon. The associated radiocarbon date for specimens CP-106.1 and CP 106.2 is 5500 +/- 150 B.P. (5600 cal yr B.P.). CP-71 is radiocarbon-dated at 5800 +/- 150 B.P. (5920 cal yr B.P.), and CP-120 is radiocarbon-dated at 6100

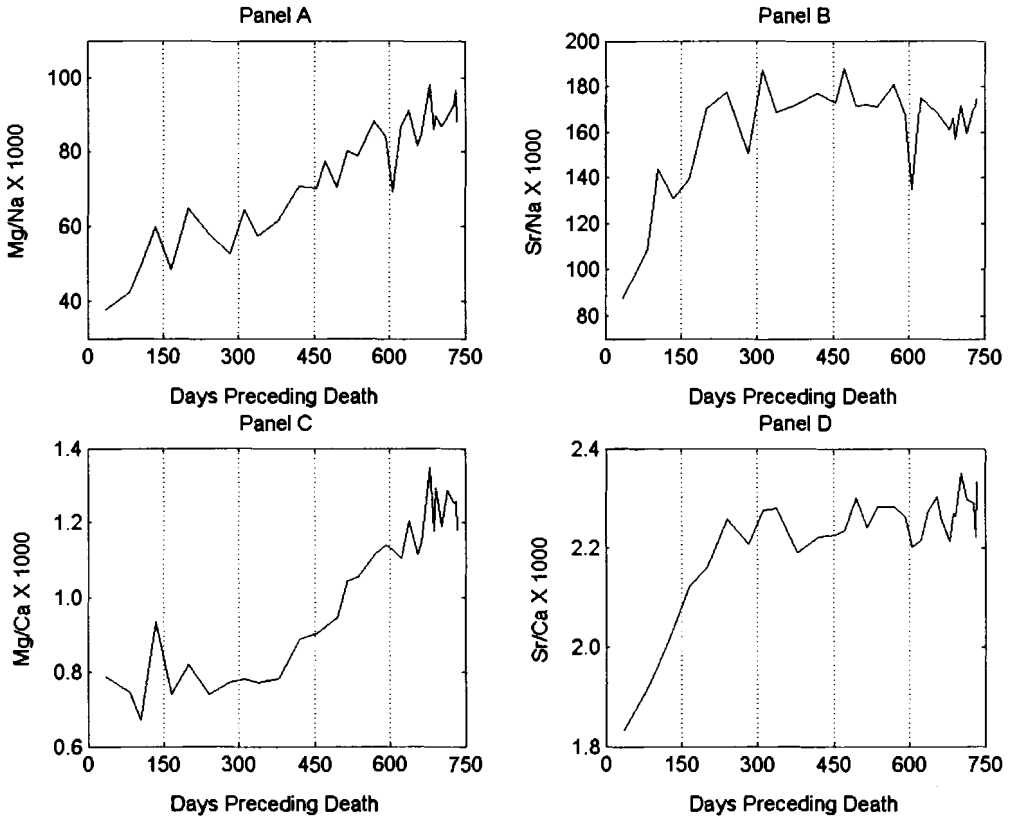

FIGURE 56: Time series of elemental mole ratios in *T. procerum* OBC V-1-C 2i-2ib, Elemento 2. Panel A: Time series of (Mg/Na X 1000). Panel B: Time series of (Sr/Na X 1000). Panel C: Time series of (Mg/Ca X 1000). Panel D: Time series of (Sr/Ca X 1000).

+/- 150 B.P. (6280 cal yr B.P.). Again assuming a salinity of 40 per mil for the mid-Holocene ocean near OBC, the Model II regression line estimates a maximum temperature in CP-106.1 of 25.67°C and maximum temperature in CP 106.2 of 25.67°C as well. Estimated minima for those two specimens are 14.72°C and 18.53°C. In specimen CP-71, the Model II regression line estimates a maximum of 22.33°C and a minimum of 19.48°C. In the final shell, CP-120, the Model II regression line estimates a maximum of 23.76°C and a minimum of 18.05°C. The estimated temperature range from CP-71 (22.08°C to 19.28°C) is similar to the estimated temperature range from OBC V-1-C 2i-2ib, El. 2 (21.43°C to 19.00°C). Though the reported calibrated dates differ, the temperature ranges estimated by the Model II regression line for specimen CP-71 (5920 cal yr B.P.) analyzed by Perrier et al. (1994) and specimen OBC V-1-C 2i-2ib, El. 2 (6660 cal yr B.P.) analyzed by this author are in close agreement.

CHAPTER 5

DISCUSSION

5.1. Intertidal and Mangrove Swamp Bivalves as Sea Surface Temperature Proxies

All modern specimens of *Chione subrugosa* and *Anadara tuberculosa* were collected near Puerto Pizarro, Peru (3.3°S). Puerto Pizarro is located near the southern boundary of the Gulf of Guayaquil in the Panamanian Biogeographic Province. Tropical water, a high number of estuaries, and mangrove swamps are characteristic of this province (Reitz and Sandweiss 2001). Due to these characteristics, the Panamanian Biogeographic Province provides suitable habitats (i.e. lagoons, mudflats, and mangrove swamps near river outlets) for *C. subrugosa* and *A. tuberculosa*. The preferred habitats of these two species suggest that the oxygen isotope ratios measured in their shells might reflect freshening events in the local environment.

The Tumbes River enters the Gulf of Guayaquil near Puerto Pizarro through a web of mangrove islands and swamps (Nicholas 1996). Increased precipitation occurs in the region during the warm season from November to June (Ferdon 1981). A negative correlation, termed the amount effect, has been observed between the amount of precipitation and $\delta^{18}O$ values of precipitation. As precipitation amounts increase, $\delta^{18}O$ values of the precipitation become enriched in the light isotope (Dansgaard 1964). As a result of increased precipitation during the rainy season, the oxygen isotope contents of *C. subrugosa* and *A. tuberculosa* shells probably reflect periodic positive incursions in the value of $\delta^{18}O_{water}$.

In *C. subrugosa* PT 1-14, $\delta^{18}O_{shell}$ values positively covary with NCEP ocean temperatures between September 1981 and September 1982. This positive covariance occurs during a period which should be the rainy season between November 1981 and June 1982; however, CPC Merged Analysis precipitation data show no increase in precipitation levels. Thus, it is difficult to explain the positive covariance in terms of precipitation. September 1982 marks the NCEP ocean temperature increase that accompanies the 1982-83 ENSO. Increased precipitation and flooding which accompanied the 1982-83 event probably affect the isotope content of the shell. $\delta^{18}O_{shell}$ values remain relatively unchanged between December 1982 and February 1983. This plateau in the $\delta^{18}O_{shell}$ curve may result from the interaction between rising ocean temperatures and freshwater flux in the Gulf of Guayaquil. Consequently, it appears that the $\delta^{18}O_{shell}$ values are no more negative during the temperature maximum of the 1982-83 ENSO than they are during seasonal temperature maxima prior to the 1982-83 event.

The chronologies constructed for the $\delta^{18}O_{shell}$ data of both Nicholas (1996) and this author in *C. subrugosa* 2PT1 suggest that oxygen isotope data in this specimen also positively covary with NCEP temperature data. In general, oxygen isotope data from *C. subrugosa* 2PT1 suggest that precipitation levels and freshwater flux strongly affect $\delta^{18}O_{shell}$ values. Oxygen isotope values from both datasets differ in their maximum and minimum values as well as their estimated correlation coefficients with NCEP temperature; nevertheless, both datasets predict the time of the 1982-83 ENSO event. Unfortunately, due to positive covariance between $\delta^{18}O_{shell}$ and ocean temperature, they do not estimate the amplitude of the temperature anomaly.

Given the preferred habitat of *A. tuberculosa*, this species is likely to be exposed to periodic freshening events. Both modern specimens of *A. tuberculosa* exhibit $\delta^{18}O_{shell}$ oscillations consistent with seasonal freshening events. In general, $\delta^{18}O_{shell}$ values in AT 5-1 positively covary with ocean temperature. Warmer ocean temperatures and precipitation levels during January 1993, February 1994, and February 1995 lead to more positive $\delta^{18}O_{shell}$ values. Unfortunately, $\delta^{18}O_{shell}$ values become more negative during periods of cooler ocean temperatures. Due to this positive covariance it is difficult to interpret $\delta^{18}O_{shell}$ values strictly in terms of temperature or salinity.

Unlike specimen AT 5-1, $\delta^{18}O_{shell}$ values in *A. tuberculosa* AT 5-2 are insignificantly correlated with ocean temperature. A negative covariance between $\delta^{18}O_{shell}$ values and ocean temperature during the period June 1994 to October 1994 indicates that the oxygen isotopes in this specimen are affected by temperature. Furthermore, $\delta^{18}O_{shell}$ values in this specimen become more positive after the increase in ocean temperatures and precipitation levels in January 1995. Instead of resulting from precipitation increases in the local environment, $\delta^{18}O_{shell}$ values may become more positive due to increased freshwater flux following increased levels of precipitation. It appears that $\delta^{18}O_{shell}$ values in these specimens of *A. tuberculosa* might be affected by a combination of environmental and physiological factors.

Because intertidal bivalves are prone to periods of valve closure at low tide, one must also consider the effects of shell dissolution. The effect of valve closure on the oxygen isotope content of calcium carbonate shell has not been quantified, but it is reasonable to assume that anaerobic respiration affects oxygen isotope ratios in the extrapallial fluid of the organism and subsequently precipitated carbonates. Furthermore,

lagoonal mud flats, the habitat of *C. subrugosa*, exhibit frequent localized temperature spikes (Rollins et al. 1987). This reinforces the need for local SST and salinity data. Consequently, the relationship between local environmental conditions and open-ocean conditions must ultimately be determined by a program of *in situ* measurement and capture.

5.2. Subtidal Bivalves as Ocean Temperature Proxies

Trachycardium procerum TP 1-12 and 3TP1-1b used in this study were collected near Chimbote, Peru (9°S) in the Peru-Chilean Biogeographic Province. The Peru-Chilean Province is characterized by cold or temperate water with localized upwelling zones. The lack of permanent freshwater streams in the region limits the development of estuarine environments (Reitz and Sandweiss 2001). The port of Chimbote lies south of the mouth of the Santa River, one of the few permanent freshwater streams in the region. The prevailing longshore current moves brackish waters from the estuary north. Thus, the modern specimens of *T. procerum* lie beyond the influence of the Santa River estuary (Nicholas 1996). Furthermore, the subtidal environment of this species minimizes or precludes exposure at low tide. *T. procerum* TP 1-12 $\delta^{18}O_c$ values exhibit a highly significant negative covariance with NCEP SST. Other studies of *T. procerum* suggest that the isotopic compositions of the species reflect the physical and chemical conditions of the ambient seawater (Nicholas 1996, Rollins et al. 1987).

T. procerum TP 1-12 was collected in April 1984 following the 1982-83 ENSO. The shape of the $\delta^{18}O_{shell}$ curve as well as the temperature curve represented by the Model II regression line approximate the curve of NCEP ocean temperatures. $\delta^{18}O_{shell}$ values and the Model II regression line accurately predict the timing of the 1982-83 ENSO

temperature maximum. Considering that $\delta^{18}O_c$ values in the Model II linear regression were corrected for salinity, deviations from the observed NCEP temperature may be explained by a lack of local salinity data, error present in the NCEP salinity data, or vital effect disequilibria. $\delta^{18}O_{shell}$ values in *T. procerum* 3TP 1-1b suggest that an event occurs during the NCEP SST seasonal maximum between November 1993 and April 1994 which affects the oxygen isotope content of the shell and cannot be corrected by the Model II regression line. There is no visible evidence of growth perturbation due to storms, spawning events, or temperature shock.

5.3. Paleoenvironmental Conditions at the Siches site PV 7-19

Shells collected and analyzed from the Siches assemblage include two *A. tuberculosa*, four *C. subrugosa*, and five *P. ecuatoriana*. No modern specimens of *Protothaca ecuatoriana* are available for comparative studies. As a result, it is difficult to determine the significance of $\delta^{18}O_{shell}$ values oscillations in the *P. ecuatoriana* from the Siches assemblage. Nevertheless, its preference for sandy substrates in intertidal environments near river outlets and a temperature tolerance similar to *C. subrugosa* suggest that shell chemistry may behave in ways similar to *C. subrugosa*.

5.3.1. From 7420 cal yr B.P. to 6890-6810 cal yr B.P.

Due to the high number of *P. ecuatoriana* specimens sampled by Nicholas (1996), *P. ecuatoriana* is valuable to a discussion of paleoclimate at Siches PV 7-19 between 7420 cal yr B.P and 6890-6810 cal yr B.P. *P. ecuatoriana* PV 7-19 IIB4(a) and PV 7-19 IIB4(b) (7420 cal yr B.P.) provided time series of 762 days and 689 days, respectively. Other modern intertidal mollusks (i.e. *C. subrugosa*) suggest that $\delta^{18}O_{shell}$ values are an indication of both temperature and salinity fluctuations. Thus, variation of $\delta^{18}O_{shell}$ values

in *P. ecuatoriana* might be affected by both temperature and salinity fluctuations in the local environment. Due to the lack of modern specimens, it is impossible to ascertain if the range of $\delta^{18}O_{shell}$ values in ancient *P. ecuatoriana* is more or less than that of modern specimens.

If strictly interpreted as a measure of freshwater flux, $\delta^{18}O_{shell}$ values in *P. ecuatoriana* PV 7-19 IIB4(a) indicate that freshwater flux into the local environment increased between days 0 and 350. The period between days 350 and 680 is characterized by oscillating wet and dry conditions. *P. ecuatoriana* PV 7-19 IIB4(b) confirms this pattern of wet and dry conditions. PV7-19 IIB4(b) indicates increasingly wetter conditions between days 50 and 330, followed by increasingly drier conditions between days 330 and 460, and a gradual return to wetter conditions from 460 days to 660 days. Currently, there are no sources of freshwater flux near the Siches site. Thus, any indication of freshwater flux in the isotope data of these specimens also implies the existence of a paleoestuary near the site.

Data from *Anadara tuberculosa* PV 7-19 IIB3(a) and PV 7-19 IIB3(b) (7420-7340 cal yr B.P.) are difficult to interpret because $\delta^{18}O_{shell}$ values in modern *A. tuberculosa* may covary both negatively and positively with ocean temperature; however, higher NCEP ocean temperatures often coincide with the rainy season at 3°S81°W, which possibly contributes to the positive covariance. Because of the relationship between ocean temperature and precipitation levels, positive incursions of $\delta^{18}O_{shell}$ values can be cautiously interpreted as indications of elevated freshwater flux.

If $\delta^{18}O_{shell}$ values in *A. tuberculosa* PV 7-19 IIB4(a) and PV 7-19 IIB4(b) are interpreted as indications of freshwater flux, then $\delta^{18}O_{shell}$ values in these specimens

indicate multiple freshening events per annual cycle. These multiple freshening events may represent salinity fluctuations in the brackish water of the mangrove swamp habitat preferred by *A. tuberculosa*. No mangrove swamp habitat currently exists near the Siches site. The presence of *A. tuberculosa* in the Siches component further supports the conclusion that a paleoestuary exists near the site.

Chione subrugosa specimens PV 7-19 IIB3(a) and PV 7-19 IIB3(b) (6890-6810 cal yr B.P.) provide a 769-day time series and a 762-day time series, respectively. If $\delta^{18}O_{shell}$ values are interpreted as indicators of salinity, then two consecutive annual cycles in PV 7-19 IIB3(a) show a single dry period per annual cycle. The time series of $\delta^{18}O_{shell}$ values in *C. subrugosa* PV 7-19 IIB3(b) indicates multiple wet and dry periods within the first annual cycle. The second annual cycle exhibits a single wet period followed by a single dry period. Because $\delta^{18}O_{shell}$ values in modern *Chione subrugosa* are not reliable indicators of ocean temperature it is difficult to interpret seasonal oscillations in the ancient shells in terms of temperature. Regardless, wetter conditions probably accompany warmer ocean temperatures. Warmer ocean temperatures would lead to increased evaporation and precipitation as a result of adiabatic cooling in the air column. This would in turn lead to increased freshwater influx into the local environment. The effects of this freshwater influx are evident in the modern shells.

5.3.2. 5880-5750 cal yr B.P.

P. ecuatoriana PV 7-19 IB7 (5880-5750 cal yr B.P.) provided a time series of 743 days. $\delta^{18}O_{shell}$ values are difficult to interpret, as already stated. The chronology contains two annual cycles. The first annual cycle may be characterized as a low amplitude

oscillation between wet and dry conditions. The second consecutive annual cycle trends toward increasingly wetter conditions.

C. subrugosa PV 7-19 IB7 (5880-5750 cal yr B.P.) provided a time series of 844 days. Two annual cycles are present with both cycles exhibiting $\delta^{18}O_{shell}$ minima interpreted to indicate drier conditions. Due to the positive covariance between ocean temperature and $\delta^{18}O_{shell}$ values in modern *C. subrugosa* specimens it is difficult to interpret $\delta^{18}O_{shell}$ values in terms of temperature. Because temperature-$\delta^{18}O_{shell}$ correlation coefficients dramatically differ among *C. subrugosa* 2PT1 datasets and the *C. subrugosa* PT 1-14 dataset, it will be necessary to expand the modern sample size of future analyses involving this species.

5.3.3. From 5880-5750 cal yr B.P. to 5650 cal yr B.P.

Two specimens of *P. ecuatoriana* date to the interval 5880-5750 cal yr B.P. to 5650 cal yr B.P. *P. ecuatoriana* PV 7-19 IB6b provided a 532-day time series, and PV 7-19 IB4bi provided a time series 554 days long. One complete annual cycle in PV 7-19 IB6b shows two $\delta^{18}O_{shell}$ maxima suggestive of wet conditions. One complete annual cycle in *P. ecuatoriana* PV 7-19 IB4bi indicates a low-amplitude oscillation between wet and dry periods. After the first annual cycle, the remainder of the *P. ecuatoriana* PV 7-19 IB4bi chronology is approximately 6 months in duration and indicates an increasingly dry period. In addition to the two specimens of *P. ecuatoriana*, a single *C. subrugosa* from context PV 7-19 IB4bi also dates to this time interval. *C. subrugosa* PV 7-19 IB4bi provided a 670-day time series that indicates increasingly drier conditions for the first 230 days of the chronology. This period is followed by increasingly wet conditions and a low-amplitude oscillation between wet and dry periods. Based on the small number of

shell analyzed, this low-amplitude oscillation between wet and dry periods appears to characterize climate conditions at Siches PV 7-19 between 5880-5750 cal yr B.P. and 5650 cal yr B.P. In order to fully understand $\delta^{18}O_{shell}$ variations in *P. ecuatoriana* and *C. subrugosa*, it is necessary to increase the sample size of modern *C. subrugosa* and initiate a study of modern *P. ecuatoriana*.

5.4. Paleoenvironmental Conditions at Ostra Base Camp (6660 cal yr B.P.)

Trachycardium procerum OBC V1C 2i-2ib El. 2 (Houk) provides a 748-day time series. The two annual cycles show low-amplitude $\delta^{18}O_{shell}$ oscillations. Assuming a salinity of 40 per mil, the Model II regression line predicts a mean temperature of 19.70°C. According to NCEP ocean temperature data, the mean surface temperature (-5 m) at Chimbote (9°S 80°W) from January 1980 to March 2000 was 20.5°C. Thus, the Model II regression line estimates a cooler mean surface temperature for the ocean near Ostra Base Camp (6660 cal yr B.P.).

Reasons for a cooler mean estimated temperature at OBC might lie in the oxygen isotope data and the temperature equation. The Model II regression line establishes the species-specific relationship between $\delta^{18}O_c$ and temperature in *T. procerum*. The small number of individuals included in the pooled sample certainly reinforces the need for an expanded sample size and further work. It has been shown that the oxygen isotope contents of individuals of the same species vary by as much as 1-2 per mil at a given temperature (Grossman 1982). Furthermore, individual temperature equations predict $\delta^{18}O_{shell}$ values that differ by as much as 1.3 per mil for a given temperature (McConnaughey 1986).

It is also difficult to accurately estimate temperature at Ostra Base Camp without a high-resolution salinity proxy to estimate $\delta^{18}O_{water}$ values. Uwe Brand, based on experimental results, suggests that mid-Holocene salinities at OBC reached 40 per mil. This value further suggests that the existence of a shallow embayment near the OBC site was likely (Sandweiss, personal communication). Regardless, it is apparent from the data that assuming constant evaporative conditions (40 per mil) biases the temperature equation for warmer ocean temperature.

According to the Model II regression line, the raw data from Nicholas' (1996) analysis of a *T. procerum* from context OBC V1C 2i-2ib El. 2 and some of the archaeological specimens of *T. procerum* analyzed by Perrier et al. (1994) also indicate decreased mean mid-Holocene SST at the Ostra site. Assuming a constant salinity of 40 per mil, the Model II regression line estimates a mean ocean temperature of 19.57°C for the raw data collected by Nicholas (1996). Further, $\delta^{18}O_{shell}$ values from *T. procerum* specimen CP 106.1 (6290 cal yr B.P.) analyzed by Perrier et al. (1994) yields a mean estimated ocean temperature of 19.25°C. Other *T. procerum* analyzed by Perrier et al. (1994) yield estimated mean ocean temperatures that equal or exceed the modern mean. $\delta^{18}O_{shell}$ values from CP 106.2 (6290 cal yr B.P.) yield a mean estimated ocean temperature of 21.27°C, and $\delta^{18}O_{shell}$ values from CP-71 (6640-6570 cal yr B.P.) and CP 120 (6950 cal yr B.P.) yield mean estimated ocean temperatures equal to the modern value. Without time constraints for the oxygen isotope data in these specimens, it is difficult to determine the presence of annual cycles.

There is inherent uncertainty regarding the location from which archaeological specimens of *T. procerum* were originally harvested. Modern specimens indicate that the

species records ambient water conditions; however, the original location and proximity to the Santa River estuary are unknown for the archaeological specimens. It is likely that archaeological specimens were collected from depths of no greater than four meters below the surface, which is near the current upper depth limit where *T. procerum* can be found. Moreover, it is also possible that the archaeological specimens were collected from outside the Ostra embayment (Nicholas 1996).

The Early to Middle Holocene environment at Ostra was characterized by a large, shallow, arcuate bay with warm water in the Santa River estuary and the adjacent open coast (Sandweiss et al. 1983, 1996). The significant numbers of warm-tropical species at Ostra confirm this interpretation (Reitz and Sandweiss 2001); however, some oxygen isotope data from archaeological specimens of *T. procerum* conflict. The low number of *T. procerum* found in the Ostra molluscan assemblage suggests that the species did not inhabit the embayment in large numbers. Thus, the shells may come from locations outside the embayment or areas influenced by discharge from the Santa River (Nicholas 1996). Such river discharge would lead to a lower $\delta^{18}O_{water}$ value and result in cooler estimated temperatures.

5.5. Conclusions

Stable oxygen isotope ratios in the subtidal bivalve *Trachycardium procerum* are indicative of ambient water conditions (i.e. temperature or salinity). The subdaily growth period of this species accommodates the construction of proxy data time series for the life of the organism. The high correlation between $\delta^{18}O_c$ ($\delta^{18}O_{shell} - \delta^{18}O_{water}$) and ocean temperature in the modern specimens of *T. procerum* also provides opportunities for constructing a species-specific temperature equation. The Model II regression method

employed in this study has no procedure for minimization of the variance due to vital disequilibria; nevertheless, a temperature equation developed from $\delta^{18}O_c$ values in *T. procerum* is likely to approximate ocean temperatures in the subtidal or open ocean environment.

$\delta^{18}O_{shell}$ values in archaeological specimens of *T. procerum* from the Ostra Base Camp site indicate that a larger sample size and further stable isotope analyses are required in order to estimate mid-Holocene (6660 cal yr B.P.) ocean temperatures near the site. Recently, oxygen isotope samples extracted from another *T. procerum* in the OBC molluscan assemblage yielded oxygen isotope ratios more negative than those of either Nicholas (1996) or *T. procerum* OBC V-1-C 2i-2ib El. 2 in this study, which further supports an interpretation of warmer ocean temperatures (Andrus, personal communication). Warmer ocean temperatures near OBC are further supported by high numbers (53 %) of warm-tropical species present in the site's faunal assemblage prior to 5730 cal yr B.P. (5000 ^{14}C B.P.) (Reitz and Sandweiss 2001), the presence of warm-tropical mollusks in living position on the Ostra fossil beach (Rollins et al. 1986, Sandweiss et al. 1983, 1996), and otolith records, which indicate mean SST at OBC approximately 2-3°C higher than present (Andrus et al. 2001).

A cooler mean temperature estimated by the Model II regression line argues for the development of a high-resolution salinity proxy. The reason for cooler predicted temperatures may lie in the unknown values of $\delta^{18}O_{water}$. If, as faunal and otolith evidence suggest, ocean temperatures at Ostra prior to 5730 cal yr B.P. (5000 ^{14}C B.P.) were warmer than modern values, then higher levels of regional precipitation may contribute to cooler estimated temperatures.

Analyses of modern specimens of *C. subrugosa* and *A. tuberculosa* indicate that $\delta^{18}O_{shell}$ values in these species are influenced by erratic temperature and salinity changes in the local environment. To interpret the isotope data from the archaeological specimens of these species in terms of absolute temperature requires a high-resolution salinity proxy as well. Otherwise, $\delta^{18}O_{shell}$ values are reduced to indicators of relative changes in salinity. Some archaeological specimens from the Siches and Early Honda components of the Siches site (4.5°S) indicate multiple freshening events (e.g. increased precipitation or freshwater flux in estuaries) per annual cycle. These events imply a climate regime wetter than the modern climate regime at 4.5°S. According to otolith records from the Siches site, mean SST at Siches prior to 5000 ^{14}C B.P. (5730 cal yr B.P.) was approximately 2-3°C warmer than the modern value (Andrus et al. 2001). The warmer mean SST could have resulted in increased evaporation and precipitation, which explains the frequent freshening events in some of the Siches specimens.

As stated previously, *in situ* measurement of environmental conditions and specimen collection is necessary in order to accurately interpret $\delta^{18}O_{shell}$ values in some of these species. The NCEP ocean temperature and salinity data employed in this study are resolved by a grid system in increments no smaller than 1°. This spatial resolution is not sufficient to resolve temperature and salinity fluctuations in small onshore microenvironments. Moreover, knowledge of offshore mid-Holocene ocean temperatures is required in order to address the question of mid-Holocene ocean circulation change; therefore, the connection between offshore temperatures and onshore microenvironments must be established.

It is also apparent that the sample of modern specimens must be expanded to include *P. ecuatoriana* as well as more specimens of each species. Examination of the $\delta^{18}O_{shell}$ time series for ancient *P. ecuatoriana* suggests that this species may actually exhibit a subdaily growth period rather than a daily period. Further experimentation is required to address that question. Also, the $\delta^{18}O_{shell}$ values in ancient *A. tuberculosa* exhibit high-frequency oscillations that are not easily explained by environmental fluctuations (Chai, personal communication); therefore, it may be necessary to cultivate the species *in vitro* in order to separate environmental variability from physiological variability.

Finally, growth increment analysis can be difficult, and some acetate peels or photomosaics exhibit only the most prominent growth lines. In some species, subdaily growth patterns may appear and disappear abruptly (Kennish and Olsson 1975). *C. subrugosa* can also exhibit tridaily growth lines during periods of rapid growth (Pallant 1990). Furthermore, *C. subrugosa* PT 1-14 and *T. procerum* TP 1-12 exhibit growth perturbations associated with the temperature maximum of the 1982-83 ENSO. These growth perturbations can result in a short-term growth hiatus that affects growth increment counts. Further analysis of the relationship between growth rate variability and environmental factors can supplement interpretations based on stable isotope analyses.

BIBLIOGRAPHY

Alamo, V.V., and Valdivieso, M.V., 1987: Lista sistemática del moluscos marinos del Peru, *Boletín: Volumen Extraordinario.* Callao, Peru: Instituto del Mar del Peru.

Andrus, C.F.T., Crowe, D.E., Sandweiss, D.H., Reitz, E.J., and Romanek, C.S., 2001: Otolith delta ^{18}O record of mid-Holocene sea surface temperatures in Peru, *Science*, **295**, 1508-1511.

Arntz, W.E., and Valdivia, E., 1985: Incidencia del fenómeno "El Niño" sobre los mariscocos en el litoral peruano. *In* Arntz, W. et al. (eds.), *"El Niño": Su impacto en la fauna marina.* Callao, Peru: IMARPE, Boletín Extraordinario, 91-101.

Bailey, G.N., Deith, M.R., and Shackleton, N.J., 1983: Oxygen isotope analysis and seasonality determinations: limits and potentials of a new technique, *American Antiquity*, **48**(2), 390-398.

Barber, R.T., and Chavez, F.P., 1983: Biological Consequences of El Niño, *Science*, **222**, 1203-1210.

Bernard, F.R., 1983: *Catalog of the living Bivalvia of the eastern Pacific Ocean: Bering Strait to Cape Horn.* Canadian Special Publication of Fisheries and Aquatic Sciences, **61**.

Betancourt, J.L., Latorre, C., Rech, J.A., Quade, J., and Rylander, K.A., 2000: A 22,000-Year Record of Monsoonal Precipitation from Northern Chile's Atacama Desert, *Science*, **289**, 1542-1546.

Cane, M.A., 1983: Oceanographic Events during El Niño, *Science*, **222**, 1189-1195.

Clement, A.C., Seager, R., and Cane, M.A., 2000: Suppression of El Niño during the mid-Holocene by changes in the Earth's orbit, *Paleoceanography*, **15**, 731-737.

Dansgaard, W., 1964: Stable Isotopes in Precipitation, *Tellus*, **16**, 436-468.

DeVries, T.J., Ortlieb, L., Diaz, A., Wells, L., and Hillaire-Marcel, C., 1997: Determining the early history of El Niño, *Science*, **276**, 965-966.

DeVries, T.J., and Wells, L., 1990: Thermally-anomalous Holocene molluscan assemblages from coastal Peru: Evidence for paleogeographic, not climatic change, *Palaeogeography, Palaeoclimatology, and Palaeoecology*, **81**, 11-32.

Dieth, M.R., 1983: Molluscan calendars: the use of growth-line analysis to establish seasonality of shellfish collection at the Mesolithic site of Morton, Fife, *Journal of Archaeological Science*, **10**, 423-440.

Faure, G., 1977: *Principles of Isotope Geology*. New York: John Wiley and Sons.

Ferdon, E.N., 1981: Holocene mangrove formations on the Santa Elena Peninsula, Ecuador: pluvial indicators or ecological response to physiographic changes, *American Antiquity*, **46**(3), 619-626.

Fontugne, M., Usselmann, P., Lavallée, D., Julien, M., and Hatté, C., 1999: El Niño variability in the Coastal Desert of Southern Peru during the Mid-Holocene, *Quaternary Research*, **52**, 171-179.

Gagan, M.K., Ayliffe, L.K., Hopley, D., Cali, J.A., Mortimer, G.E., Chappell, J., McCulloch, M.T., and Head, M.J., 1998: Temperature and surface-ocean water balance of the mid-Holocene tropical western Pacific, *Science*, **279**, 1014-1018.

Glassow, M.A., Kennet, D.J., Kennett, J.P., and Wilcoxon, L.R., 1994: Confirmation of middle Holocene ocean cooling inferred from stable isotopic analysis of prehistoric shells from Santa Cruz Island, California. *In* Halvorson, W.L. and Maender, G.J. (eds.) *The Fourth California Islands Symposium: update on the state of resources*. Santa Barbara: Santa Barbara Museum of History, 223-232.

Grossman, E.L., 1982: Stable isotopes in live benthic foraminifera from the Southern California Borderland, Ph.D. dissertation, University of Southern California, Los Angeles, California.

Grossman, E.L. and Ku, T., 1986: Oxygen and carbon isotope fractionation in biogenic aragonite: temperature effects, *Chemical Geology (Isotope Geoscience Section)*, **59**, 59-74.

Horibe, Y., and Oba, T., 1972: Temperature scales of aragonite-water and calcite-water systems, *Fossils*, **23/24**, 69-79.

Hutchings, P., and Saenger, P., 1987: *Ecology of Mangroves*. New York: University of Queensland Press.

Keefer, D.K., de France, S.D., Moseley, M.E., Richardson, J.B., III, Satterlee, D.R., and Day-Lewis, A., 1998: Early maritime economy and El Niño events at Quebrada Tacahuay, Peru, *Science*, **281**, 1833-1835.

Kennett, D., and Voorhies, B., 1995: Middle Holocene periodicities in rainfall inferred from oxygen and carbon isotopic fluctuations in prehistoric tropical estuarine mollusk shells, *Archaeometry*, **37**(1), 157-170.

Kennish, M.J., Lutz, R.A., and Rhoads, D.C., 1980: Preparation of Acetate Peels and Fractured Sections for Observation of Growth Patterns within the Bivalve Shell. *In* Rhoads, D.C. and Lutz, R.A. (eds.) *Skeletal Growth of Aquatic Organisms*, Appendix 1. New York: Plenum, 597-601.

Kennish, M.J., and Olsson, R.K., 1975: Effects of Thermal Discharges on the Microstructural Growth of Mercenaria mercenaria, *Environmental Geology*, **1**, 41-64.

Killingley, J.S., 1981: Seasonality of mollusk collecting determined from O-18 profiles of midden shells, *American Antiquity*, **46**(1), 152-158.

Killingley, J.S., and Berger, W.H., 1979: Stable isotopes in a mollusk shell: detection of upwelling events, *Science*, **205**, 186-188.

Koike, H., 1980: Seasonal dating by growth-line counting of the clam, *Meretrix lusoria*: Toward a reconstruction of prehistoric shell-collecting activities in Japan. *University of Tokyo Museum Bulletin*, **18**, 104 pp.

Koike, H., 1979: Seasonal dating and the valve-pairing technique in shell-midden analysis, *Journal of Archaeological Science*, **6**, 63-74.

Laws, E., 1997: *Mathematical Methods for Oceanographers*. New York: John Wiley and Sons.

Lindzen, R.S., and Nigam, S., 1987: On the role of sea surface temperature gradients in forcing low-level winds and convergence in the tropics, *Journal of the Atmospheric Sciences*, **44**, 2418-2436.

Lutz, R.A., and Rhoads, D.C., 1977: Anaerobiosis and a theory of growth line formation, *Science*, **198**, 1222-1227.

Markgraf, V., and Diaz, H.F., 2000: The Past ENSO Record: A Synthesis. *In* Diaz, H.F. and Markgraf, V. (eds.), *El Niño and the Southern Oscillation: Multiscale Variability and Global and Regional Impacts.* Cambridge: Cambridge University Press, 465-488.

McConnaughey, T., 1986: *Oxygen and Carbon Stable Isotope Disequilibria in Galápagos Corals: Isotopic Thermometry and Calcification Physiology*, Ph.D. Dissertation, University of Washington.

Nicholas, S.L., 1996: *Implications of the Stable Isotopes from Marine Shells for the Mid-Holocene Paleoclimate of the North Coast of Peru*, Unpublished thesis, University of Maine.

Olsson, A.A., 1961: *Mollusks of the tropical eastern Pacific, particularly from the southern half of the Panamic-Pacific faunal province (Panama to Peru).* Ithaca: Paleontological Research Institution.

Pallant, Eric, 1990: Applications of molluscan microgrowth analysis to geoarchaeology; A case study from Costa Rica. *In* (Lasca, N.P., and Donahue, J., (eds.), *Archaeological Geology of North America.* Boulder, Colorado: Geological Society of America Centennial Special, **4**, 421-430.

Pannella, G., and MacClintock, C., 1968: Biological and environmental rhythms reflected in molluscan shell growth, *Journal of Paleontology, Paleontological Society Memoir*, **2**, 64-79.

Perrier, C., Hillaire-Marcel, C., and Ortlieb, L., 1994: Paléogéographie Littorale et Enregistrement Isotopique (^{13}C, ^{18}O) D'Événements de Type El Niño par les Mollusques Holocènes et Récents du Nordouest Péruvien, *Géographie Physique et Quaternaire*, **48**, 23-28.

Rasmusson, E.M., and Wallace, J.M., 1983: Meteorological Aspects of the El Niño/Southern Oscillation, *Science*, **222**, 1195-1202.

Reitz, E.J. and Sandweiss, D.H., 2001: Environmental Change at Ostra Base Camp, a Peruvian Pre-Ceramic Site, *Journal of Archaeological Science*, **28**, 1085-1100.

Richardson III, J.B., 1992: Early Hunters, Fishers, Farmers, and Herders: Diverse Economic Adaptations in Peru to 4,500 B.P., *Revista de Arqueología Americana*, **6**, 71-90.

Richardson III, J.B., 1981: Modeling the development of sedentary maritime economies on the coast of Peru: a preliminary statement, *Annals of the Carnegie Museum*, **50**, 139-150.

Richardson III, J.B., 1978: Early man on the Peruvian north coast, early maritime exploitation and Pleistocene and Holocene environment. *In* Bryan, A.L. (ed.), *Early Man in America from a Circum-Pacific Perspective.* Edmonton: Archaeological Researches International, 274-289.

Richardson III, J.B., 1973: The Preceramic Sequence and the Pleistocene and Post-Pleistocene Climate of Northwest Peru. *In* Lathrap, D., and Douglas, J. (eds.), *Variation in Anthropology.* Urbana: Illinois Archaeological Survey, 199-211.

Richardson III, J.B., Sandweiss, D.H., and Paredes E., R., 1996: *Informe: Proyecto Arqueológico Siches.* Unpublished report. Submitted to the Instituto Nacional de Cultura, Lima, Peru.

Rodbell, D.T., Seltzer, G.O., Anderson, D.M., Abbott, M.B., Enfield, D.B., and Newman, J.H., 1999: An ~15,000-Year Record of El Niño-driven Alluviation in Southwestern Ecuador, *Science*, **283**, 516-520.

Rollins, H.B., Sandweiss, D.H., Brand, U., and Rollins, J.C., 1987: Growth Increment and Stable Isotope Analysis of Marine Bivalves: Implications for the Geoarchaeological Record of El Niño, *Geoarchaeology: An International Journal*, **2**, 181-197.

Rollins, H.B., Richardson III, J.B., and Sandweiss, D.H., 1986: The Birth of El Niño: Geoarchaeological Evidence and Implications, *Geoarchaeology: An International Journal*, **1**, 3-15.

Sandweiss, D.H., 1996a: Mid-Holocene Interaction between the North coast of Peru and Ecuador, *Latin American Antiquity*, **7**(1), 41-50.

Sandweiss, D.H., 1996b: Environmental Change and Its Consequences for Human Society on the Central Andean Coast: A Malacological Perspective. *In* Reitz, E.J., Newsom, L.A., and Scudder, S.J. (eds.), *Case Studies in Environmental Archaeology*. New York: Plenum Press, 127-146.

Sandweiss, D.H., 1986: The Beach Ridges at Santa, Peru: El Niño, Uplift, and Prehistory, *Geoarchaeology: An International Journal*, **1**, 17-28.

Sandweiss, D.H., 1982: Materiales Arqueológicos de Garagay: IV. Material Malacológico, *Revista del Museo Nacional* (Lima), **XLVI**, 212-224, 228-229.

Sandweiss, D.H., Maasch, K.A., Burger, R.L., Richardson III, J.B., Rollins, H.B., and Clement, A., 2001: Variation in Holocene El Niño frequencies: Climate records and cultural consequences in ancient Peru, *Geology*, **29**, 603-606.

Sandweiss, D.H., Richardson III, J.B., Reitz, E.J., Rollins, H.B., and Maasch, K.A., 1997: Determining the early history of El Niño: Response, *Science*, **276**, 966-967.

Sandweiss, D.H., Richardson III, J.B., Reitz, E.J., Rollins, H.B., and Maasch, K.A., 1996: Geoarchaeological Evidence from Peru for a 5000 Years B.P. Onset of El Niño, *Science*, **273**, 1531-1533.

Sandweiss, D.H., Richardson III, J.B., Reitz, E.J., Hsu, J.T., and Feldman, R.A., 1989: Early maritime adaptations in the Andes: Preliminary studies at the Ring Site, Peru. *In* Rice, D.S., Stanish, C., and Scarr, P.R. (eds.), *Ecology, Settlement and History in the Osmore Drainage, Peru*. Oxford: BAR International Series, **545 I**, 35-84.

Schulmeister, J., and Lees, B.G., 1995: Pollen evidence from tropical Australia for the onset of an ENSO-dominated climate at *c.* 4000 B.P., *The Holocene*, **5**, 10-18.

Shackleton, N.J., 1973: Oxygen isotope analysis as a means of determining season of occupation of prehistoric midden sites, *Archaeometry*, **15**(1), 133-141.

Sun, D., 2000: Global Climate Change and El Niño: A Theoretical Framework. *In* Diaz, H.F. and Markgraf, V. (eds.), *El Niño and the Southern Oscillation: Multiscale Variability and Global and Regional Impacts.* Cambridge: Cambridge University Press, 443-463.

Tomlinson, P.B., 1986: *The botany of mangroves*. New York: Harvard University Press.

Valero-Garcés, B.L., Grosjean, M., Schwalb, A., Geyh, M., Messerli, B., and Kelts, K., 1996: Limnogeology of Laguna Miscanti: evidence for mid to late Holocene moisture changes in the Atacama Altiplano (Northern Chile), *Journal of Paleolimnology*, **16**, 1-21.

Wells, L.E., 1990: Holocene history of the El Niño phenomenon as recorded in flood sediments of northern coastal Peru, *Geology*, **18**, 1134-1137.

Wells, L.E., and Noller, J.S., 1997: Determining the early history of El Niño, *Science*, **276**, 966.

Whyte, M.A., 1975: Time, tide, and the cockle. *In* Rosenberg, G. D. and Runcorn, S.K. (eds.) *Growth rhythms and the history of the earth's rotation.* London: John Wiley and Sons, 177-189.

Wilbur, K.M., 1972: Shell Formation in Mollusks. *In* Florkin, M. and Scheer, B.T. (eds.) *Chemical Zoology*, **VII**. New York: Academic Press, 103-142.

Appendix A

GROWTH INCREMENT ANALYSIS AND CORRELATION OF TEMPERATURE AND STABLE ISOTOPE DATA

Acetate Peels. The preparation of acetate peels is outlined in Kennish et al. (1980). One deviation from the Kennish et al. outline should be noted. Because a single archaeological bivalve specimen will be used repeatedly in further analyses, no specimens should be embedded in epoxy resin. Many of the archaeological specimens are well preserved and should not fracture under the saw. Regardless, one must be cautious while cutting the specimens. One should align the shell with the saw blade so the blade follows the transect of stable isotope samples. The goal is to show the stable isotope samples in the cross-section and the acetate peel. The acetate used in this study was purchased at Structure Probe, Inc. Combinations of both thick (product #1857) and thin (product #1856) sheets were used.

Digital Photomosaics. The acetate peels should be placed between two glass microscope slides and photographed using an incident light microscope with a digital camera attached. Magnification up to 100X is sufficient. Magnifications greater than 100X will resolve shell microstructures finer than subdaily growth lines; however, this results in a large number of images, which can be difficult to manage. Use digital imaging software to stamp the images with a scale, and ensure that the images overlap while photographing the acetate peels.

Once the images have been collected, use Photoshop 6.0 or a similar application to merge them into a single photomosaic for each shell. In Photoshop 6.0, open the first

image at the ventral margin and convert it to a Photoshop layer (layer 1). Next, open the second contiguous image and convert it to a Photoshop layer (layer 2). Drag layer 2 into layer 1. Adjust the layers so layer 2 lies over layer 1. Now, adjust the opacity of layer 2 to 60% or less. Find a structure that is common to both layers. Move layer 2 until that structure in layer 2 lies over that structure in layer 1. Lock the layers. Adjust the opacity of layer 2 to 100%, and merge the two layers. Repeat this process for each subsequent image until the photomosaic is complete. If the orientation of the images relative to each other is different, then rotate the images in incremental degree units until they match.

Photoshop 6.0 is equipped with an X-Y coordinate system that facilitates measurement of the shell. In order to calibrate the ruler tool, the image size of the photomosaic should be adjusted until one unit in Photoshop's coordinate system equals one unit on the image scale.

Growth Increment Counts. All growth increment counts begin at the first growth increment in the ventral margin. For archaeological specimens this increment equals day 0, but for modern specimens this increment equals the date of death. Depending on the species, one daily increment will equal one dark line and one light line (*C. subrugosa* and *P. ecuatoriana*) or one dark line, one light line, one dark line, and one light line (*A. tuberculosa* and *T. procerum*). Due to a CO_2 gradient between the umbo and the ventral margin, some dissolution may take place in this area. Thus, sometimes it is difficult to identify the first daily growth increment.

Once the first daily increment is identified, count daily increments from the ventral margin to the beginning of the first stable isotope sample on the acetate peel. Record this

time interval. Now, count the number of daily increments from the beginning to the end of the stable isotope sample, and record that time interval. Repeat this process until the time intervals between and within each stable isotope sample in the photomosaic are recorded.

Correlating Stable Isotope Data with Ocean Temperature and Salinity Data.

NCEP ocean temperature and salinity data are available from the NOAA-CIRES Climate Diagnostics Center, Boulder, Colorado, USA. NCEP Pacific Ocean temperatures are weekly means at multiple levels for a 1°x1° grid. NCEP Pacific Ocean salinities are monthly means at multiple levels for a 1°x1° grid. For modern shell specimens the growth increment counts provide a date interval for each stable isotope value. Thus, in order to correlate the stable isotope value with temperature and salinity it is necessary to average the mean weekly temperature and mean monthly salinity values during those date intervals. Each stable isotope value is now correlated with a single average temperature and salinity value. Without daily *in situ* measurements of temperature and salinity, an average of weekly and monthly mean values is the best one can achieve.

Developing the Temperature Equation for *Trachycardium Procerum*.

The temperature equation for *T. procerum* was developed by Model II linear regression (Reduced Major Axis) of $\delta^{18}O_c$ values in a pooled sample of all modern specimens and correlated NCEP ocean temperatures. $\delta^{18}O_c$ values represent the difference between the oxygen isotope content of the shell ($\delta^{18}O_{shell}$) and the oxygen

isotope content of the water in which the organism lived ($\delta^{18}O_{water}$). Thus, $\delta^{18}O_c = \delta^{18}O_{shell} - \delta^{18}O_{water}$, where $\delta^{18}O_{water} = 0.16(\text{Salinity}) - 4.99$. This relationship between $\delta^{18}O_{water}$ and salinity was established by analysis of water samples from the Chira River estuary (Nicholas 1996). Salinity values are based on NCEP monthly mean salinities correlated with stable isotope samples as described above.

BIOGRAPHY OF THE AUTHOR

Stephen D. Houk was born at Fort Belvoir, Virginia on June 19, 1973. He graduated from John F. Kennedy High School in Denver, Colorado in 1991. He attended Colorado State University and graduated in 1998 with a Bachelor's degree in Anthropology. Following graduation, Stephen worked as an archaeologist first in Wyoming and later in New York. He entered the Institute for Quaternary and Climate Studies graduate program at the University of Maine in the fall of 1999.

After receiving his degree, Stephen will attend Johann Wolfgang Goethe University, Frankfurt am Main, Germany, to pursue a Ph.D. in geology. Stephen is a candidate for the Master of Science degree in Quaternary and Climate Studies from The University of Maine in December 2002.